SOME EXPERIMENTS IN PULSED MAGNETIC FIELDS

INSTITUUT-LORENTZ
voor theoretische natuurkunde
Nieuwsteeg 18-Leiden-Nederland

J. C. A. VAN DER SLUIJS

SOME EXPERIMENTS IN PULSED MAGNETIC FIELDS

2 OKT. 1967

PROEFSCHRIFT

TER VERKRIJGING VAN DE GRAAD VAN DOCTOR IN DE WISKUNDE EN DE NATUURWETENSCHAPPEN AAN DE RIJKSUNIVERSITEIT TE LEIDEN OP GEZAG VAN DE RECTOR MAGNIFICUS DR P. MUNTENDAM, HOOGLERAAR IN DE FACULTEIT DER GENEESKUNDE TEN OVERSTAAN VAN EEN COMMISSIE UIT DE SENAAT TE VERDEDIGEN OP MAANDAG 2 OCTOBER 1967 TE 16 UUR

DOOR

JAN CHRISTIAAN ALEXANDER VAN DER SLUIJS
GEBOREN TE AVEREEST IN 1936

kast dissertaties

1967
V.R.B. — GRONINGEN

PROMOTOR: PROF. DR C. J. GORTER

Dit proefschrift is bewerkt onder toezicht van dr D. de Klerk.

Aan mijn ouders
Aan Marijke

Het in dit proefschrift beschreven onderzoek werd uitgevoerd als onderdeel van het programma van de werkgroep VSL van de stichting voor Fundamenteel Onderzoek van de Materie en is mogelijk gemaakt door financiële steun van de Nederlandse organisatie voor Zuiver Wetenschappelijk Onderzoek.

CONTENTS.

A. THE GENERATION OF PULSED MAGNETIC FIELDS.

I. INTRODUCTION.

Before going into the discussion of the generation of pulsed magnetic fields, we shall give a short sketch of the historical framework in which magnetism and magnets develop [1,2].

The remark that Thales of Milete (ca 600 B.C.) knew about natural magnets is a commonplace and it is probable that he has not been the first to do so.

However, magnetism is distinguished from subjects such as mechanics in that its description depends strongly upon microscopic models, and it should not be surprising that progress has been slow in a thinking framework based upon observations only. A successful attack is only possible starting from the abstract empiricism, which was introduced by Newton (1643 - 1727).

The traces of this approach go back as far as Plato (428 - 347 B.C.) but initially the development went in the direction of observational empiricism, as it has been developed further by Aristotle (384 - 322 B.C.). The line which eventually resulted in Newton's ideas has been continued e.g. by Archimedes (287 - 212 B.C.) and Heron (ca 130 B.C.).

In the middle ages the Aristotelian ideas prevailed, although alternative views were promoted by Roger Bacon (1214 - 1284). In this period Peter Peregrinus (ca 1250) wrote his book: "De magnete", which was an important step ahead in magnetism. In his book he described experiments which revealed the repulsion between like poles and the fact that a split magnet gives two new magnets. He also made some correct suggestions on a model for the earth's magnetic field.

The change to a more abstract empiricism, which culminated in Newton's ideas, commenced with the translation into Latin of the works written by Archimedes and Heron by Nicholas of Cusa in 1448.

William Gilbert (1540 - 1603), a contemporary of Galilei and Keppler, took up the ideas of Peregrinus and formulated the concepts of field lines, induction, and magnetic conductivity.

However, in the next two centuries the progress in magnetism did not go beyond the discovery of the second power law of the magnetic forces by John Michell (1724 - 1794) and its confirmation by Coulomb (1736 - 1806).

The rapid progress started with the work by Oersted, who in 1820 published his research on the magnetic field of currents. This led to the construction of the first electromagnets by Sturgeon in 1825. The electromagnet turned out to be one of the important tools for the study of magnetic phenom-

ena. These tools made possible part of the work by Faraday and Weber.

During the 19th and the first part of the 20th century most magnets were iron magnets. The range of efficient use of iron magnets is limited by the saturation magnetisation of iron to about 30 k0e. The use of solenoid magnets was expensive because of the limited capacities of the electrical generators.

With the construction of large power sources the development of magnets without iron cores, the solenoid magnets, could be commenced. However, now the problem of obtaining the required amounts of energy was replaced by the difficulty of removing the heat which is dissipated in the magnet coil. In a magnet coil in which a constant field is maintained all power from the power source is converted into heat. The amount of heat is equal to $\int I^2R\ dt$.

Three lines of approach have been made to obtain still higher magnetic fields.

Firstly one builds large installations with sufficient cooling capacities. The power dissipations are up to 32 MW. Up to now this approach has resulted in magnetic fields up to 250 k0e in spaces of several centimeters diameter [9]. These installations are quite expensive.

In the second place one can reduce the resistivity of the conductor material by cooling down the magnet, the cryogenic magnets. The most successful approach on this line is the superconducting magnet which is based on the property that some metals and alloys obtain zero resistance below a certain critical temperature. Recently the development of alloys led to materials for magnets which are able to sustain currents of several hundred amperes in the presence of magnetic fields of the order of magnitude of 100 k0e. With these materials, mainly Nb25%Zr and Nb_3Sn, one succeeds in constructing magnets which produce magnetic fields up to 70 and 150 k0e [10], respectively, with little or no energy dissipation.

Thirdly one can reduce the heat development by decreasing the time during which the magnetic field is switched on: the pulsed magnet. In these short times one allows the magnet to heat up, and after the duty cycle one waits until the initial temperature has been reached again, before one generates another magnetic field pulse.

In this way a reasonable efficiency is reached, which is the better the shorter the pulse time. In the experiments which we shall describe, the efficiency as defined in chapter II goes up to 60%. The pulse times vary between 10^{-6} and 1 second, in our case we have a pulse time of 2×10^{-2} second.

Work on pulsed magnets was started by Kapitza[3,4,5,6]. Initially he worked with accumulator cells and obtained 500 k0e occasionally, but later he used a motor generator set and obtained 320 k0e regularly.

At present the most frequently used method is the discharge of a capacitor bank.

We shall not go into literature references in much detail,

because good review articles have been published recently by de Klerk [7], by Strachovskii and Kvartsov [8], and by Kolm and Freeman [9].

The coil design depends upon field strength and pulse duration. Most design data are based on the work by Champion [11].

Generally the magnet coils can be made stronger if the pulse duration is shortened. We refer to the single-turn coils constructed by Furth, Levine and Waniek [12] and to the helix coils constructed by Foner and Kolm [13,14]. In both cases the material has been a beryllium-copper alloy.

For pulse durations of more than a millisecond, wire-wound or disc-wound coils have to be used to obtain the required self inductance. This type of coil is essentially weaker than the single-turn or helix type.

If one uses the coil at room temperature the efficiency is rather poor, because of the high resistivity of the materials. The efficiency can be improved by immersing the coil in liquid nitrogen [15,16,17,18,19], liquid hydrogen [15,20], or liquid helium [21]. However, to make the gain in efficiency considerable, one has to use pure metals as conductor materials because of their low residual resistivity. This decreases the coil strength. To improve the strength, reinforcements of non-conducting materials have to be used.

The maximum fields which have been obtained depend on the pulse duration. The strongest magnetic fields, at present up to 15 M0e [23], have been obtained by the method of implosion coils. In this method, chemical energy of an explosive material is converted into magnetic energy [24]. Single turn coils have generated up to 1.6 M0e.

In fig. I.1, which has been copied from Kolm and Freeman [9], we have inserted some recent improvements since the publication of that paper in 1965, obtained by several research groups in the region between 10^{-3} and 10^{-1} second pulse duration.

However, the pulsed field method suffers from heavy drawbacks if applied for instrumental use in experimental physics. Phenomena with long relaxation times cannot be studied, e.g. thermal effects, and one has to be careful not to be confused by one of the spurious effects which can be caused by the dynamical character of the field, e.g. eddy currents in metals. Moreover the method introduces large disturbances which limit the sensitivity in some cases.

In this thesis we describe the design and construction of a pulsed magnetic field device and some experiments we performed with it.

In part A (chapters I, II, III, and IV) we give, after a short introduction in chapter I, an analysis of some problems we met in the construction of pulsed magnets (chapter II). In chapters III and IV the magnet coils and the current generator are discussed.

An introduction to the contents of part B (chapters V, VI, and VII) is presented in chapter V.

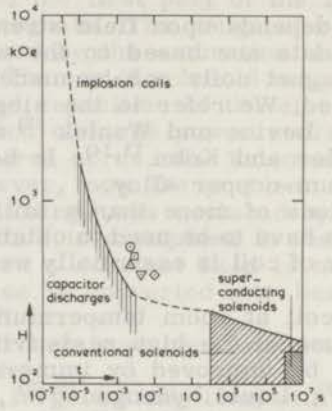

Fig. I. 1. Survey of magnetic fields generated by several methods with some improvements since 1965[9].
O van Itterbeek c.s.[19], incidentally.
□ Kapitza[1,2,3,4].
△ van Itterbeek c.s.[19].
▽ present work.
◇ Gersdorf c.s.[22].

The apparatus consists of a capacitor bank of 3×10^{-2} F and 3.5 kV, which is short circuited over a magnet coil of 1.3 mH. We obtained magnetic fields of half sine-wave shape, a duration of 20 msec, and a maximum field strength of 40 k0e.

The magnet coil has about 250 turns, an inner diameter which ranges between 6 and 20 mm, and an outer diameter between 40 and 90 mm. The length of the useful space is about 2 cm.

The magnet coil is immersed in liquid nitrogen to keep the resistive losses low.

The capacitors are standard paper capacitors and the control circuits presented only those difficulties which are characteristic for experimental electronics. They are discussed in chapter IV.

The main problem in obtaining high pulsed magnetic fields is presented by the magnet coil itself and the larger part of the discussion is devoted to this subject (chapters II and III).

In chapter II we discuss some properties of the coil from a physical point of view, both by theoretical and experimental analysis.

In chapter III we show which type of compromise we made to achieve our aims. However, we intend to improve the results by 10 to 25%.

Up to now we concentrated on simple coils with small ex-

perimental volumes, because they are easy to understand from a constructional point of view. This type of coil does not need the total amount of energy which is available. The total amount of energy is expected to be necessary when using other coil types, e.g. for microwave experiments, which require larger experimental spaces.

References.

1). E.Hoppe, Handbuch der Physik, Berlin, 1926, pt.1, p.1.
2). P.Feyerabend, Essays in contemporary science and philosophy, R.Colodny ed., Englewood Cliffs, 1965, p.145.
3). P.L.Kapitza, Proc.Roy.Soc. A 105 (1924), 691.
4). P.L.Kapitza, Proc.Roy.Soc. A 109 (1925), 224.
5). P.L.Kapitza, Proc.Roy.Soc. A 115 (1927), 658.
6). P.L.Kapitza, Proc.Phys.Soc. 42 (1930), 425.
7). D.de Klerk, Construction of electromagnets, Newport Pagnell, 1964. Ned. T.Natuurk. 27 (1961), 352.
8). H.M.Strachovskii and N.V.Kvartsov, Usp.Phys.Nauk, 70 (1960), 693.
9). H.H.Kolm and A.J.Freeman, Scient.Amer. 212 (1965), 66.
10). RCA, priv.comm. 1966.
11). K.S.W.Champion, Proc.Phys.Soc. B 63 (1950), 795.
12). H.P.Furth, M.A.Levine and R.W.Waniek, Rev.Scient.Instr. 28 (1957), 949.
13). S.Foner and H.H.Kolm, Rev.Scient.Instr. 27 (1956), 547.
14). S.Foner and H.H.Kolm, Rev.Scient.Instr. 28 (1957), 799.
15). J.C.A.van der Sluijs, High Magnetic Fields, Boston, 1961, p.290.
16). J.C.A.van der Sluijs, D.de Klerk and C.J.Gorter, Conf.High Magnetic Fields, Oxford, 1963, unpubl.
17). J.C.A.van der Sluijs, H.R.de Beun, B.A.Zweers and D.de Klerk, Bull.Belg. Phys. Soc.V, no 2-3 (1966), 165.
18). P.Cotti, Z.ang.Math.Phys. 11 (1960), 17.
19). A.A.van Itterbeek, W.van Driessche, I.de Grave and H.Myncke, Bull.Belg. Phys. Soc.V, no 2-3 (1966), 188.
20). W.J.de Haas and J.B.Westerdijk, Nature 158 (1946), 271.
21). J.L.Olsen, Helv.Phys.Acta 26 (1953), 798.
22). R.Gersdorf, F.A.Muller and L.W.Roeland, Rev.Scient.Instr. 36 (1965), 1100.
23). C.M.Fowler, W.B.Gairn and R.S.Caird, J.Appl.Phys. 31 (1960), 588.
24). F.Herlach, H.Knoepfel, R.Luppi and J.van Montfoort, Bull.Belg.Phys.Soc. V, no 2-3 (1966), 179.

II. ON THE BEHAVIOUR OF PULSED MAGNET COILS IN THE MILLISECOND RANGE.

Index of symbols.

The number indicates the section where the symbol is used for the first time.

B Magnetic induction. (3)
B_{br} Break induction. (5)
C Capacity. (2)
D_u Outer diameter of magnet coil. (3)
D_i Inner diameter of magnet coil. (3)
$\bar{D}$ Average diameter conductor winding magnet coil. $\bar{D} = \frac{1}{2}(D_u + D_i)$. (3)
E Energy. (3)
E_f Energy of magnetic field. (3)
E_h Thermal energy loss. (3)
F Mechanical force. (5)
F_r Radial force component per unit volume. (5)
F_z Axial force component per unit volume. (5)
G Fabry geometrical factor. (4)
H Magnetic field strength. (4)
I Current strength. (2)
I_o Maximum current strength. (3)
J Current density. (3)
K Stray factor. (4)
K_o, K_1 Constants defined in (II, 59) and (II, 63). (5)
L Self-inductance. (2)
M Coil mass. (3)
P Mechanical pressure. (5)
R Resistance. (2)
S Stray factor as used by Cotti. (4)
T Temperature. (3)
V Voltage. (3)
V_o Initial voltage of capacitor bank. (2)
V_m Mechanical potential. (5)
W Power.

c_p Specific heat. (3)
f Conductor cross section. (3)
l Length of magnet coil. (4)
n Number of turns. (3)
r Radial variable. (5)
r_u Outer radius of magnet coil. (5)
r_i Inner radius of magnet coil. (4)
t Time. (2)
t_p Pulse duration. (2)

v Volume. (5)
z Axial variable. (5)

α D_u/D_i. (3)
β $1/D_i$. (4)
γ, δ, ϵ Constants, defined in (II, 15)
γ r/r_i. (5)
η Efficiency. (3)
Θ Reduced temperature. (3)
θ Polar angle. (5)
λ Filling factor of magnet coil. (4)
Λ Geometrical factor of inductance. (4)
μ_o Permeability vacuum. (4)
ν Poisson's modulus. (5)
ρ_m Specific mass. (3)
ρ_{el} Specific resistivity. (3)
σ_r Radial stress component. (5)
σ_z Axial stress component. (5)
σ_t Tangential stress component. (5)
τ Reduced time. (3)
τ_{rt}, τ_{rz}, τ_{tz} Components of shearing stress. (5)
ϕ Stress function. (5)
Φ Geometrical factor of field distribution. (5)
ω Frequency in radians per second. (2)

§ 1. *Introduction.*

In this chapter we consider some aspects of the behaviour of pulsed magnets operated in the millisecond range. The choice of the problems is determined by the practical difficulties which we had to solve in designing our magnets.

After a presentation of the limiting factors of the magnetic field generated by a pulsed magnetic field device (§ 2) we analyse the Joule losses in the magnet coil, under the assumption of a fixed inductance L. As should be expected the copper cross section turns out to be the important quantity, together with the current density. An experimental example of coil efficiency is given. Because this efficiency only decribes the total amount of magnetic energy we discuss in § 4 the distribution of the magnetic energy in space as a function of coil geometry.

Another main problem in coil design is presented by the Lorentz forces. (§ 5). The problem is analysed by the standard methods of elasticity theory in a statical approach[1]. The problem of the boundary conditions is considered in some detail. It is shown that in practical coil design the validity of the standard approach is questionable. For the type of coil we used, we calculate the axial and the radial strains numer-

ically and we show that the usually neglected shearing stresses are not always small.

As an example of a case where the standard approach is valid we present the mechanical analysis of a flux concentrator coil, which, to our knowledge, has not been published before. (§ 6). Although we have not been able to do an experimental test the results agree qualitatively with the evidence obtained by other investigators.

In § 7 we present a short discussion of some non-stationary phenomena occurring in pulsed magnets and of an experiment we did on these effects.

§ 8 contains the experimental data obtained by the testing of a number of pulsed magnet coils. The coil parameters and the details of some calculations are given in appendices.

In this chapter we generally express the magnetic induction in the rationalised unit W/m^2, which is the most convenient unit of magnetic induction in a discussion of technical problems. $1\ W/m^2 = 10^4$ Gauss which is equivalent to 10^4 Oersteds.

We call the attention to the fact that we take the length of the coil to be 1, in place of the usual 2l. In our opinion the factor 2 is rather artificial. It can be omitted without any change in the existing analyses.

Throughout the discussions the current distribution is supposed to be homogeneous with a rectangular cross section of the winding space.

§ 2. *Principles of the generation of pulsed magnetic fields by a capacitor bank.*

(Alternative treatments have been given by Cotti[2] and de Klerk[3,4]).

The generation of pulsed magnetic fields by means of a capacitor bank is done in principle by short circuiting the capacitor over a small magnet coil. In our installations we have a capacitor bank with a capacity C of 3×10^{-2} F and a maximum voltage V_o of 3.5 kV, giving a maximum energy content of 180 kJoule. Initially the magnet coil is at liquid nitrogen temperature. The magnet coil has a self-inductance

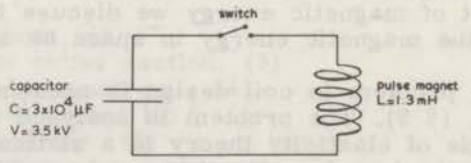

Fig. II. 1. Basic circuit.

L of 1.3 mH and a bore of about 12 mm. The magnetic induction which is generated per ampere of current through the windings of the coil ranges between 3×10^{-3} and 1.6×10^{-2} W/m^2A. The switch consists of a set of ignitrons. (fig. II. 1).

If we suppose that the circuit has an Ohmic resistance R, the current as a function of time can be described by the formula (II. 1),

$$\left.\begin{aligned} I &= \frac{V_o}{\omega L} \exp\left(-\frac{R}{2L}t\right) \sin \omega t \qquad 0<t<t_p \\ I &= 0 \qquad\qquad \text{at all other times.} \end{aligned}\right\} \tag{II.1}$$

because the ignitron does not permit the current to reverse its sign. Here $\omega = \pi/t_p$, t_p represents the pulse duration and t the time variable.

$$\omega = \sqrt{\frac{1}{LC} - \frac{R^2}{4L^2}} \tag{II.2}$$

In our case the factor $\exp(-\frac{R}{2L}t)$ at $t = t_p/2$ is 0.82, thus determining the resistive losses in a case with constant temperature. The shape of the current through the magnet coil and of the voltage over the magnet coil as functions of time are shown in fig. II. 2.

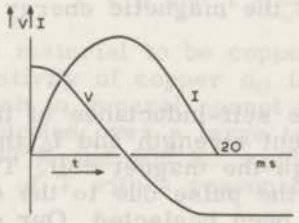

Fig. II. 2. Shape of coil current and voltage.

In a non-stationary case one has to calculate the temperature rise of the magnet coil. One can insert the result in equation (II. 1) to calculate the maximum current and from the current one can calculate the maximum field. We shall follow a slightly different procedure.

Starting with a certain amount of energy in the capacitors, the maximum attainable magnetic field is determined by the following quantities[2,3,4]:

a) The fraction of the capacitor energy which is converted into magnetic energy.

b) The temperature of the magnet coil at the end of the pulse.

The resistivity of the coil causes the dissipation of a certain fraction of energy as heat and this fraction rises with increasing coil currents. For a certain amount of dissipated energy the temperature of the coil will rise over the maximum permissible value for the insulator material in the coil. The araldite which is used in our coils to prevent the motion of the windings in consequence of the electromagnetic forces limits the temperature to 400°K.

c) The mechanical strength of the coil, which determines the field strength where the coil is damaged by the electromagnetic or Lorentz forces.

d) The stray coefficient of the coil, which determines the fraction of the magnetic energy which is contained in the experimental space.

These four points will be considered in the following sections.

§ 3. *Final temperature and efficiency.*

1. *Definition of efficiency.*

The final temperature and the efficiency of the system are connected closely with each other because the efficiency determines the amount of energy which is available for the heating of the coil.

To calculate the efficiency of the system we start from the following definition of efficiency:

The efficiency of the system is the fraction of the energy initially present in the capacitor bank which has been converted into magnetic energy at the maximum of the magnetic field.

For the maximum of the magnetic energy we put:

$$E_{\text{field}} = \frac{1}{2} L I_o^2 \qquad \text{(II. 3)}$$

where L represents the self-inductance of the magnet coil at low values of the current strength and I_o the maximum of the current strength through the magnet coil. The change of the self-inductance during the pulse due to the electromagnetic forces on the coil has been neglected. Our experiments indicate that this change of self-inductance is so small that it does not lead to corrections which are large in comparison to the overall accuracy which can be obtained in the experiments. The definition of efficiency is then given by:

$$\eta = \frac{\frac{1}{2} L I_o^2}{\frac{1}{2} C V_o^2} \qquad \text{(II. 4)}$$

The energy which is not converted into magnetic energy is converted into heat. This occurs mainly in the coil itself if we assume that the resistance of the coil is high in comparison to the resistance of the other parts of the circuit. In our

case this assumption is valid.

$$E_h = \int_0^{\frac{1}{2}t_p} I^2 R \, dt \qquad (II.5)$$

(II.4) and (II.5) give finally

$$\eta = \frac{\frac{1}{2} L I_0^2}{\frac{1}{2} L I_0^2 + \int_0^{\frac{1}{2}t_p} I^2 R \, dt} \qquad (II.6)$$

E_h depends on the shape of the current through the magnet coil as a function of time, on the geometry of the magnet coil, on the specific heat, and on the specific resistivity of the coil material.

2. Assumptions and numerical data.

We assume that the shape of the current as a function of time is:

$$\left.\begin{aligned} I &= I_o \sin \omega t \qquad 0 < t < \frac{\pi}{\omega} = t_p \\ I &= 0 \qquad\qquad t < 0 \text{ and } t > \frac{\pi}{\omega} \end{aligned}\right\} \qquad (II.7)$$

We assume the coil material to be copper.

The specific resistivity of copper ρ_{el} is a function of the temperature T, which in general cannot be described by a simple analytical function over a large temperature range. However, between 70° K and 600° K, $\rho_{el}(T)$ can be represented as a linear function of T with a reasonable accuracy (fig. II.3):

$$\rho_{el} = 5.2 \times 10^{-11} \; T \; \Omega m^{5)} \qquad (II.8)$$

The specific heat $c_p(T)$ of copper is a function of temperature which in general cannot be represented by a simple analytical function over a large temperature range. However, it turns out to be possible to make the following approximation:

$$\begin{aligned} 70 < T < 170^\circ K &: c_p = 131 + 1.27 \; T \text{ joule/kg } ^\circ K \\ 170 < T < 330^\circ K &: c_p = 284 + 0.42 \; T \text{ joule/kg } ^\circ K \\ 330 < T < 600^\circ K &: c_p = 386 + 0.11 \; T \text{ joule/kg } ^\circ K \end{aligned} \qquad (II.9)$$

(fig. II.4)

The numerical evaluation of the problem can be simplified by neglecting the third temperature interval and by extending the second interval to 400° K, which gives rise to an error of

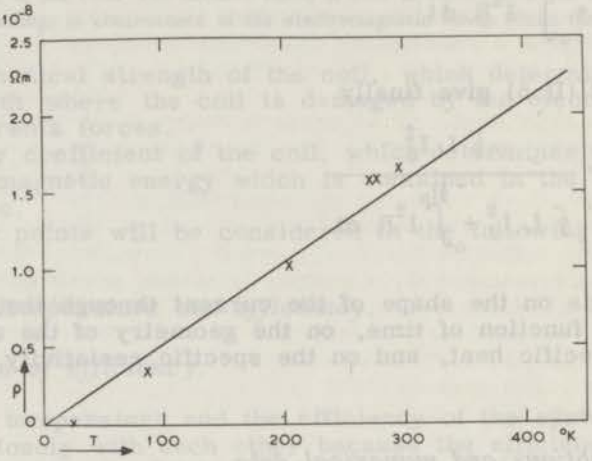

Fig. II. 3. Specific resistivity of copper as a function of temperature.
X some experimental values.
— approximation (II.8).

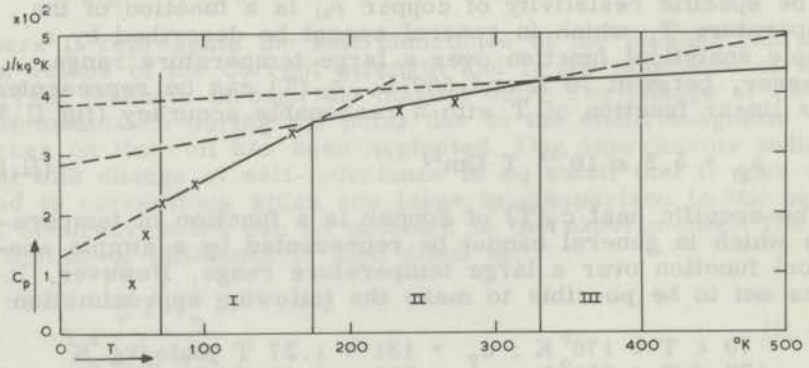

Fig. II. 4. Approximation to specific heat of copper.
X experimental points (> 330° K solid line).
— approximation.
-- extrapolation of approximation II into region III.

5% at 400° K.

The specific mass of copper is considered to be independent of temperature.

$$\rho_m = 8.9 \times 10^3 \text{ kg m}^{-3} \qquad \text{(II.10)}$$

The pulse time is assumed to be 2×10^{-2} sec. We assume that there is no heat transport from the coil to the nitrogen bath during the pulse.

3. Temperature of the magnet coil.

The energy dissipated in the magnet coil at a time t after the beginning of the field pulse is given by:

$$E = \int_0^t I^2 R \, dt \qquad \text{(II.11)}$$

$$\text{with} \quad R = \rho_{el}(T) \frac{\pi \bar{D} n}{f} \qquad \text{(II.12)}$$

Here $\bar{D}$ represents the average diameter of the turns of the magnet coil, n the number of turns, and f the cross section of the conductor.

The dissipated energy is related to the temperature rise by

$$E = M \, c_p(T) \, (T - T_o) \qquad \text{(II.13)}$$

with M the total mass of the magnet coil and T_o the initial temperature of the coil. From (II.13): $\frac{dE}{dt} = M \, c_p(T) \frac{dT}{dt}$. From (II.11), (II.12) and (II.13):

$$\int_{T_o}^{T} \frac{c_p}{\rho_{el}} \, dT = \frac{\pi \bar{D} n}{f M} \int_0^t I^2 \, dt' \qquad \text{(II.14)}$$

Integrating (II.14) from t' = 0 to t' = t and writing

$$\left.\begin{aligned} M = \rho_m \pi \bar{D} n f \; ; \; \tau = \frac{t}{t_p} \; ; \; c_p(T) = c_o + c_1 T \\ \rho_{el} = \rho_o T \; ; \; \Theta = \frac{T}{T_o} \; ; \; \delta = \frac{c_o}{c_1 T_o} \; ; \; \epsilon = \frac{\rho_o \pi}{2 \rho_m \omega c_1 T_o} \end{aligned}\right\} \qquad \text{(II.15)}$$

$$\text{gives} \quad (\Theta - 1) + \delta \ln \Theta = \epsilon \frac{I_0^2}{f^2} \left(\tau - \frac{\sin 2\pi\tau}{2\pi} \right) \qquad \text{(II.16)}$$

If one assigns the indices 1 and 2 to the symbols (II.15) for the two temperature ranges given above, we have:

$$(\Theta_1 - 1) + \delta_1 \ln \Theta_1 = \epsilon_1 \frac{I_0^2}{f^2}\left(\tau - \frac{\sin 2\pi\tau}{2\pi}\right) \qquad \text{(II.17)}$$

referring to $T_o = 77^\circ$ K, for $77 < T < 170^\circ$ K and

$$(\Theta_2 - 1) + \delta_2 \ln \Theta_2 = \epsilon_2 \frac{I_0^2}{f^2}\left[(\tau - \tau_1) - \frac{1}{2\pi}(\sin 2\pi\tau - \sin 2\pi\tau_1)\right] \qquad \text{(II.18)}$$

referring to $T_1 = 170^\circ$ K, for $170 < T < 400^\circ$ K, with τ_1 the reduced times when the temperature T_1 is reached.

The temperature of the coil at the reduced timed $\tau = \frac{1}{2}$ and $\tau = 1$ as a function of current density is shown in fig. II.5.

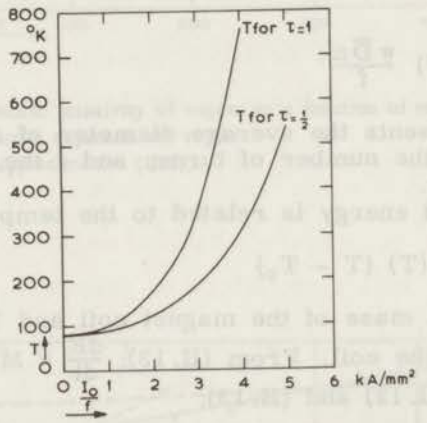

Fig. II.5. Coil temperature as a function of current density.

4. Energy converted into heat.

If the temperature of the coil rises an amount ΔT, the thermal energy of the coil rises an amount

$$\Delta E = M\, c_p(T)\, \Delta T \qquad \text{(II.19)}$$

This amount of energy has been produced by joule heating, thus giving the total amount of energy losses.

Integrating over the temperature, and referring to the temperature ranges given in (II.9) we have

$$E_1 = M\left[c_{01}(T - 77) + c_{11}(T^2 - 77^2)\right] \qquad \text{(II.20)}$$

for $77 < T < 170^\circ$ K, and

$$E_2 = M\left[\, c_{02}(T - 170) + c_{12}(T^2 - 170^2)\right] + E_1(170) \qquad \text{(II. 21)}$$

for $170 < T < 400^\circ$ K. If one inserts

$$M = \rho_m \, \pi \, D_i \, \frac{\alpha+1}{2} \, n \, f \qquad \text{(II. 22)}$$

with α the ratio of the outer diameter D_u to the inner diameter D_i of the magnet coil, one obtains finally

$$\frac{E_1}{(\alpha+1)\,n\,f} = \left[183(T - 77) + 0.89(T^2 - 77^2)\right] \times 10^{-5}\,\text{kJoule/mm}^2 \qquad \text{(II. 23)}$$

for $77 < T < 170^\circ$ K, and

$$\frac{E_2}{(\alpha+1)\,n\,f} = \frac{E_1(170)}{(\alpha+1)\,n\,f\,D_i} + \left[399(T - 170) + 0.29(T^2 - 170^2)\right] \times 10^{-5}\,\text{kJoule/mm}^2 \qquad \text{(II. 24)}$$

for $170 < T < 400^\circ$ K. $\frac{E}{(\alpha+1)nfD_i}$ as a function of the current density of the coil is shown in fig. II. 6. This quantity is an energy dissipation per cubic millimetre. The conversion of temperature to current density has been made by means of fig. II. 5.

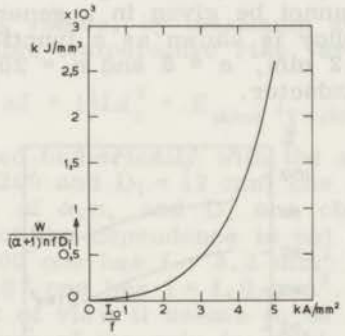

Fig. II. 6. Reduced heat dissipation in the magnet coil as a function of the current density.

The pictures II. 5 and II. 6 have a quite general meaning. Only the initial temperature of 77° K, the pulse duration of 20 msec and the conductor material copper have been presupposed. Moreover they can be adapted to other frequencies simply by multiplying the current density scale by $\left[2 \times 10^{-2}/t'_p\right]^{\frac{1}{2}}$ where t'_p represents the new pulse time. For other initial tem-

peratures and conductor materials the curves have to be recalculated.

5. Efficiency.

If we take into account that

$$E = \int_{T_o}^{T} M c_p(T)\, dT = \int_{o}^{t} I^2(t)\, R\, dt \qquad \text{(II. 25)}$$

this gives in combination with (II. 4)

$$\eta = \frac{\frac{1}{2} L I_0^2}{\frac{1}{2} L I_0^2 + (\alpha+1)\, D_i n f \left[183\ (T-77) + 0.89(T^2 - 77^2)\right] x10^{-5}} \qquad \text{(II. 26)}$$

for $77 < T < 170^\circ$ K, and

$$\eta = \frac{\frac{1}{2} L I_0^2}{\frac{1}{2} L I_0^2 + E_1(170) + (\alpha+1) D_i n f \left[399(T-170) + 0.29(T^2 - 170^2)\right] x10^{-5}} \qquad \text{(II. 27)}$$

for $170 < T < 400^\circ$ K.

The efficiency depends upon the geometrical properties of the magnet coil and cannot be given in a generalised picture. In fig. II. 7 the efficiency is shown as a function of the current density for D_i = 12 mm, α = 5 and n = 200 for some cross sections of the conductor.

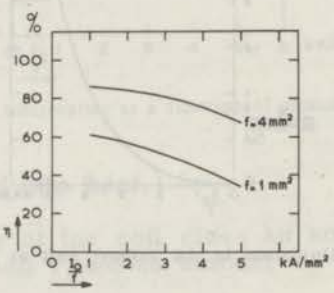

Fig. II. 7. Efficiency as a function of current density.

6. Limiting values.

In fig. II. 8 we have drawn the temperature and energy characteristics for two practical examples for α = 5, n = 200 and D_i = 12 mm.

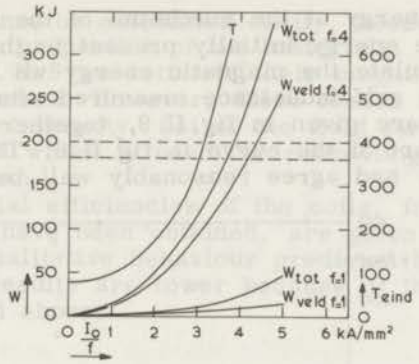

Fig. II. 8. Limiting values of the current density.
400°K = maximum admissible temperature of the magnet coil.
180 kJ = maximum available energy.

The total amount of energy at the maximum of the pulse determines the maximum current which can run through the magnet coil.

The temperature rise, which is not specific for the type of coil, limits the current density to 3.15 kA/mm^2.

If the maximum admissible temperature has been reached before the total amount of energy has been taken from the capacitor bank, as is the case for these two examples, it is not possible to use the full capacitor energy without damaging the coil thermally.

The two limiting values, by maximum available energy and maximum admissible temperature rise, are the same if

$$W_{tot} = 180 \text{ kJ} = \left(\tfrac{1}{2}LI_0^2 + E_{therm}\right)_{T=400^\circ K} \qquad (II.28)$$

If this is calculated numerically with the aid of fig. II. 6 and the values $\alpha = 5$, $n = 200$ and $D_i = 12$ mm one obtains $f = 4.7$ mm^2 For other values of α, n, and D_i one obtains slightly different results, but the dependence is not very strong. For $(\alpha + 1)\, n\, D_i = 2400$ one has $f = 5.2$ mm^2 and for $(\alpha + 1)\, n\, D_i = 3 \times 10^4$ one has $f = 4.0$ mm^2.

From this point of view it seems to be favourable to make f very large because of the gain in efficiency. However it turns out that large copper cross sections cause unfavourable stray factors, so that, in spite of the large amount of magnetic energy, the maximum field is relatively low. Therefore we feel that 4 to 5 mm^2 is a relatively favourable range of wire cross sections for the chosen coil geometry and pulse time.

7. *Loss measurement.*

Experimentally we have determined the losses by subtracting

the magnetic energy at the maximum of the magnetic field, $\frac{1}{2}LI_0^2$, from the energy initially present in the capacitor bank, $\frac{1}{2}CV_0^2$. To calculate the magnetic energy we have used the static value of the self-inductance measured after the pulse.

The results are given in fig. II. 9, together with the low current density part of the curve in fig. II. 6. The points are from different coils, and agree reasonably well between each other.

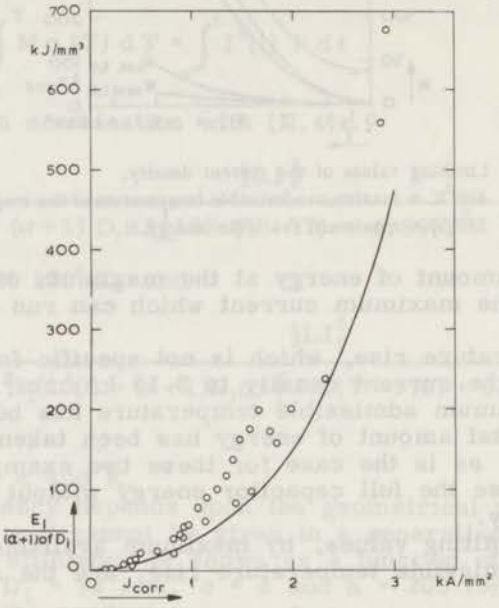

Fig. II. 9. Comparison of calculated and measured losses.

The current densities have been corrected for the experimental pulse duration. (See §3, section 4 last paragraph.)

The curve, calculated for thermal losses only, is too low, but reasonably good in the region below 0.8 kA/mm^2.

We describe the differences to the following two effects.

1. The static self-inductance may be smaller than the self-inductance at the maximum of the pulse. We have not been able to determine the dynamic self-inductance, so we have no good estimate of the order of magnitude of the effect. A crude estimate can be obtained by observing that in the high field region the change of self-inductance caused by a pulse can be as high as 1%, as we have shown by experiment. Because in the region of plastic flow of the material, the elastic deformation is not larger than the plastic deformation, an upper limit will be 1%, which only accounts for the difference below 0.8 kA/mm^2.
2. At high field strength other loss sources are present.

We mention the kinetic energy of the coil material, the deformation energy, both elastic and plastic, and friction. Most of these losses are converted into heat.

These losses cannot be calculated easily, because they depend upon the dynamic properties of the materials, which are not known. From fig. II. 9 we estimate their magnitude to 60 - 100% of the thermal losses. However, these losses are not a function of the current density, but of the field strength, and the generalised model which is used for estimating the thermal losses breaks down.

The experimental efficiencies of the coils, from which the data for fig. II. 9 have been obtained, are given in fig. II. 10. They show the qualitative behaviour predicted by fig. II. 7 but the quantitative results are lower because of the additional losses, discussed above.

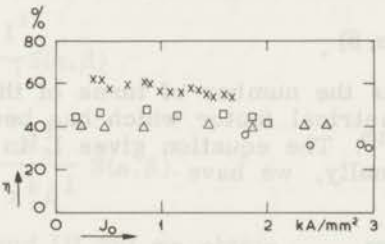

Fig. II. 10. Experimental efficiency for 4 magnet coils.

§ 4. *Magnetic field in the central area of the magnet coil.*

Given a certain amount of available magnetic energy, the maximum field strength which is actually available in the center of the magnet coil is determined by the geometry of the magnet coil. Usually this is taken into consideration by means of a stray factor in the formula for the calculation of the magnetic field[2,3,4,8].

In the following discussion we calculate the stray factor for the case that one fixes a priori the self-inductance of the coil, the inner diameter of the coil, and the maximum current available.

We start with the Fabry formula[8]:

$$H = G \sqrt{\frac{W.\lambda}{\rho_{el} \cdot r_i}} \qquad (II.29)$$

In this formula H represents the magnetic field, W the power of the power supply, λ the fraction of the winding space filled with conductor material, r_i the inner diameter of the magnet coil, ρ_{el} the resistivity of the conductor material, and G a geometrical factor

$$G = G(\alpha, \beta) = \frac{(2\pi)^{\frac{1}{2}}}{5} \left(\frac{\beta}{\alpha - 1} \right)^{\frac{1}{2}} \ln \frac{\alpha + (\beta^2 + \alpha^2)^{\frac{1}{2}}}{1 + (\beta^2 + 1)^{\frac{1}{2}}} \qquad \alpha = \frac{D_u}{D_i} \quad \beta = \frac{1}{D_i} \tag{II. 30}$$

which has been tabulated [9]. The numerical values, given in reference [9], have been chosen in such a way that insertion of W in watts, ρ_{el} in Ωcm, and r_i in cm gives H in oersteds. To change to a consistent system of units, e.g. the MKS units, one has to multiply by a factor, which in the case of MKS units amounts to 10^{-6} giving B in W/m^2, or to $10 \times (4\pi)^{-1}$ giving H in A/m. In the following we use B, the magnetic induction.

For the self-inductance of the coil we write [10]

$$L = n^2 r_i \, \Lambda(\alpha, \beta) , \tag{II. 31}$$

Here n represents the number of turns of the magnet coil and $\Lambda(\alpha,\beta)$ a geometrical factor which has been given graphically in reference [10]. The equation gives L in henries if r_i is given in cm. Finally, we have

$$n = \frac{2r_i^2}{f} (\alpha - 1) \beta l \tag{II. 32}$$

To calculate from (II. 29) the maximum field which can be obtained with a capacitor discharge device, one has to express the maximum power W which is available in terms of the maximum current. For a certain current I the power W is

$$W = I^2 R \tag{II. 33}$$

with R the resistance of the magnet coil.

From (II. 29), (II. 31), (II. 32), and (II. 33) we obtain

$$\frac{B}{I} = \frac{L^{\frac{1}{2}}}{r_i^{\frac{3}{2}}} K(\alpha, \beta) \tag{II. 34}$$

with

$$K(\alpha, \beta) = \frac{G(\alpha, \beta)}{\Lambda^{\frac{1}{2}}(\alpha, \beta)} \frac{\left[\frac{\pi}{2} \beta(\alpha^2 - 1) \right]^{\frac{1}{2}}}{\beta(\alpha - 1)} \mu_o \tag{II. 35}$$

In table II. 1 we give $K(\alpha, \beta)$ for some values of α and β. The numerical values in table II. 1 are consistent with MKS units and give the magnetic induction in W/m^2.

The formula (II. 34) is consistent with a straightforward way to calculate the magnetic induction [2,3,4]. The magnetic induction per unit volume in the magnet coil is equal to the energy

Table II.1.
$K(\alpha,\beta) \times 10^5$ for MKS units. To obtain oersteds, multiply by 10^4.

α \ β	1	2	4	8
1.5	30.48	26.07	---	---
2	25.14	21.89	16.30	12.02
4	14.02	12.34	10.52	7.68
8	7.11	6.59	5.58	4.40

of the magnetic field divided by the inner volume of the coil and multiplied by a stray factor which is smaller than 1.

$$\frac{B^2}{2\mu_o} = \frac{L I^2}{v} S(\alpha,\beta)$$

or
$$\frac{B}{I} = \frac{L^{\frac{1}{2}} \mu_o^{\frac{1}{2}}}{r_i^{\frac{3}{2}} \pi^{\frac{1}{2}} \beta^{\frac{1}{2}}} S(\alpha,\beta). \qquad \text{(II. 36)}$$

From (II. 34) and (II. 36) we obtain

$$S(\alpha,\beta) = \frac{\pi^{\frac{1}{2}} \beta^{\frac{1}{2}}}{\mu_o^{\frac{1}{2}}} K(\alpha,\beta) \qquad \text{(II. 37)}$$

However, the factor $K(\alpha,\beta)$ is simpler to use because the factor $\beta^{\frac{1}{2}}$ is already contained in it. Furthermore our derivation has the advantage that, firstly, the connection is made clear between the stray factor and the G factor about which an extensive literature exists, and, secondly, because the derivation gives directly the quantities important from a designers point of view, namely, n, L, and f.

Now if one choses a coil diameter and a coil self-inductance, a table of B/I as a function of α and β can be made. It is more practical, however, to give in a graph the lines of constant B/I as a function of α and β, as is shown in fig. II. 11.

From a fundamental point of view one should make graphs of $K(\alpha,\beta)$, but in our practice we worked with fixed self-inductance and semi-fixed inner diameter. In that case the B/I picture is the one which is used actually.

From fig. II. 11 one readily determines the geometry of a coil with a prescribed induction per ampere. If one has determined α and β one can calculate the wire cross section to be used from the equation:

$$f = \frac{2\lambda r_i^{\frac{5}{2}}}{L^{\frac{1}{2}}} \beta(\alpha-1)\, \Lambda^{\frac{1}{2}}(\alpha,\beta). \qquad \text{(II. 38)}$$

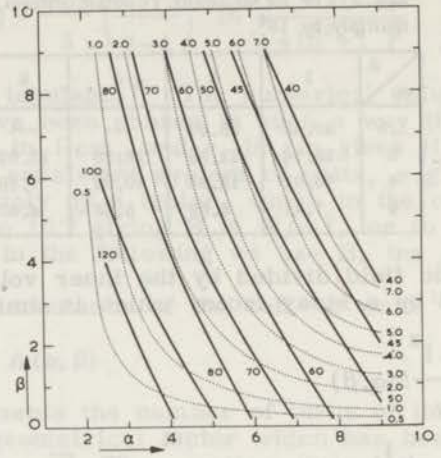

Fig. II. 11. Electrical coil design, for L = 1.3 mH and D_i = 12 mm.
----- curves of constant wire cross section in mm^2.
—— curves of constant induction per ampere in 10^{-4} W/m^2.
1 W/m^2 is equivalent to 10 k0e.

For a fixed self-inductance and inner diameter of the magnet coil the curves of constant f can be computed from (II. 38). The results are shown in fig. II. 11 too.

Now one has from fig. II. 11 a practical designing method for pulsed field coils. Once the maximum current available, the desired magnetic field, and the desired current density have been fixed, one has the field strength per ampere and the wire cross section. The points of intersection of the B/I lines and the f lines give the possible values for α and β.

At this point we recall our remark made in section 3, that from a point of view of thermal efficiency of the magnet coil it is favourable to choose large wire cross sections. From the results of the sections 3 and 4 together we conclude that one should not exceed the minimum wire cross section which is allowed by the thermal considerations, because this results in unfavourable low values for the induction per ampere of coil current.

§ 5. *Mechanical stress caused by electromagnetic forces in a time independent case.*

If a current flows through the conductor turns of a magnet coil, the magnetic field generated by the coil will exert a

force on the conductor. A current flowing tangentially and a homogeneous field directed axially give a resultant force which is purely radial and directed outwards. If a magnetic field has a radial component this results in an axial force component which is directed to the axial plane of symmetry of the coil.

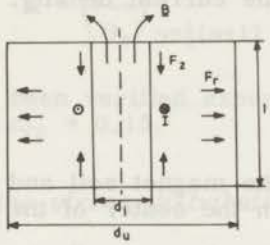

Fig. II. 12. Force distribution in a magnet coil.

In this section we calculate the electromagnetic forces and the stress distribution in the magnet coil and we give an estimate of the magnetic induction which causes the stresses to surpass the breaking stress of the coil material.

In this section we only study the time independent problem. In the next section some remarks are made on the consequences of the fact that the mechanical loading of the coil is a shock loading and thus strongly time dependent.

1. Electromagnetic forces.

The electromagnetic forces are essentially volume forces. However, the tangential stresses in the coil material can be approximated with fair accuracy by describing the electromagnetic forces as surface forces on the inner surface of the coil.

a. Surface forces.

The system is described by a thick-walled cylinder, which replaces the copper volume of the coil, and a mechanical pressure

$$P = \int H dB = \frac{B_o^2}{2\mu_o} \qquad \text{(II. 39)}$$

on the inner surface of the coil, which replaces the volume forces.

This is equivalent to the assumption that inside the coil a pressurised gas is present with an energy density equal to the energy density of the magnetic field.

b. Volume forces.[11]

If we have an infinitesimal conductor element with a length dl and a volume dv, carrying a current I, and placed in a

magnetic induction field B, the contribution to the total force from this element is

$$dF = BIdl = BJdv. \tag{II.40}$$

where J represents the current density.
We write

$$J = \frac{n\,I}{l(r_u - r_i)} \tag{II.41}$$

with l the length of the magnet coil and n the number of turns.
For the induction in the center of the magnet coil we write[11]

$$B_o = \mu_o \frac{n\,I}{l} \Phi \tag{II.42}$$

with Φ a geometrical factor,

$$\Phi = \frac{\beta}{\alpha-1} \ln \left[\frac{\alpha+(\alpha^2+\beta^2)^{\frac{1}{2}}}{1+(1+\beta^2)^{\frac{1}{2}}} \right] = G\left(\frac{5}{2\pi}\right)^{\frac{1}{2}}\left(\frac{\beta}{\alpha-1}\right)^{\frac{1}{2}} \tag{II.43}$$

From (II.40), (II.41), and (II.42) and the fact that the force is the vector product of B and I, we have for the force components per unit volume

$$F_r = \frac{B_z\,B_o}{\mu_o(r_u-r_i)\,\Phi}$$

$$F_z = \frac{B_r\,B_o}{\mu_o(r_u-r_i)\,\Phi} \tag{II.44}$$

with B_z representing the axial component and B_r the radial component of the magnetic induction at the place of the conductor element.

For the components of the magnetic induction we take from Hord[11]

$$B_z = B_{z\,(r=0)} \frac{\alpha-\gamma}{\alpha-1} \cong B_o \left\{1-\left(\frac{z}{2\,l}\right)^2\right\} \frac{\alpha-\gamma}{\alpha-1}$$

$$\gamma = r/r_i \quad 1 < \gamma < \alpha \tag{II.45}$$

$$B_r = B_o \frac{z}{l}\left[m_1 + m_2 \sin\left(\pi \frac{\gamma-1}{\alpha-1}\right)\right] \tag{II.46}$$

$$m_1 \frac{z}{l} = \frac{1}{2}\left\{\left(\frac{B_r}{B_o}\right)_{\gamma=1} + \left(\frac{B_r}{B_o}\right)_{\gamma=\alpha}\right\} = K_o$$

$$m_2 \frac{z}{l} = \hat{K} - K_o \qquad \hat{K} = \left(\frac{B_r}{B_o}\right)_{\gamma=\frac{1}{2}(\alpha+1)} \tag{II.47}$$

These expressions have been verified experimentally by Hord[11]. We take $m_1 = 0.213$ and $m_2 = 0.15$.

2. General problem of the stress distribution.

The stress distribution in the magnet coil is determined by the general equations of the theory of elasticity, which have to be solved under consideration of the appropriate forces and boundary conditions. This approach is rigourously valid up to those values of the stresses where a plastic deformation of the material begins to occur. We extrapolate the results to get an estimate of the breaking point of the magnet coil under assumption that the changes in the geometry and the mechanical properties of the coil material are small in comparison with the values in the elastic region.

An exact solution of the three dimensional problem is very complicated. Usually a simplifying assumption is made, reducing the problem to two separate problems, one of plane stress determining the radial and tangential stresses and one of linear stress determining the axial stress. In the two dimensional equations we impose the condition for plane stress.

a. Equilibrium conditions.

To preserve the stability of the volume element we require the resultant force on the volume element to be zero. Because of the symmetry of the problem we give the equations in cylinder coordinates. The derivations are standard and are not repeated here. The symbols σ_r, σ_z, and σ_t represent the normal stress components, τ_{rt}, τ_{rz}, and τ_{tz} the shearing stress components. F_r is the radial force component per unit volume, F_z the axial force component per unit volume, r the radial coordinate, z the axial coordinate, and θ the polar angle.

A. Two dimensions.

$$\frac{\partial \sigma_r}{\partial r} + \frac{1}{r}\frac{\partial \tau_{rt}}{\partial \theta} + \frac{\sigma_r - \sigma_t}{r} + F_r = 0$$

$$\frac{1}{r}\frac{\partial \sigma_r}{\partial \theta} + \frac{\partial \tau_{rt}}{\partial r} + \frac{2\tau_{rt}}{r} = 0 \tag{II.48}$$

In the case of complete axial symmetry the derivatives with respect to θ and the shearing stress τ_{rt} vanish:

$$\frac{\partial \sigma_r}{\partial r} + \frac{\sigma_r - \sigma_t}{r} + F_r = 0 \qquad \text{(II. 49)}$$

B. Three dimensions.

$$\text{radial} \quad \frac{\partial \sigma_r}{\partial r} + \frac{1}{r}\frac{\partial \tau_{rt}}{\partial \theta} + \frac{\partial \tau_{rz}}{\partial z} + \frac{\sigma_r - \sigma_t}{r} + F_r = 0$$

$$\text{axial} \quad \frac{\partial \tau_{rz}}{\partial r} + \frac{1}{r}\frac{\partial \tau_{tz}}{\partial \theta} + \frac{\partial \sigma_z}{\partial z} + \frac{\tau_{rz}}{r} + F_z = 0$$

$$\text{tangential} \quad \frac{\partial \tau_{rt}}{\partial r} + \frac{1}{r}\frac{\partial \sigma_t}{\partial \theta} + \frac{\partial \tau_{tz}}{\partial z} + \frac{2\tau_{rt}}{r} = 0 \qquad \text{(II. 50)}$$

In the case of axial symmetry these equations reduce to

$$\frac{\partial \sigma_r}{\partial r} + \frac{\partial \tau_{rz}}{\partial z} + \frac{\sigma_r - \sigma_t}{r} + F_r = 0$$

$$\frac{\partial \tau_{rz}}{\partial r} + \frac{\partial \sigma_z}{\partial z} + \frac{\tau_{rz}}{r} + F_z = 0 \qquad \text{(II. 51)}$$

b. Compatibility conditions.

A solution of the equilibrium equations with boundary conditions has to be connected with the strain distribution in the material by means of Hooke's law. Because the strain components are not mutually independent this condition gives rise to another set of equations, one equation in the two dimensional problem, six equations in the three dimensional one.

In the case of cylinder symmetry in three dimensions these six equations reduce to four.

A. Two dimensions (plane stress).

$$\sigma_r = \frac{1}{r}\frac{\partial \phi}{\partial r} + \frac{1}{r^2}\frac{\partial^2 \phi}{\partial \theta^2}$$

$$\sigma_t = \frac{\partial^2 \phi}{\partial r^2} + F_r r \qquad \text{(II. 52)}$$

$$\tau_{rt} = \frac{1}{r^2}\frac{\partial\phi}{\partial\theta} - \frac{1}{r}\frac{\partial^2\phi}{\partial r\partial\theta}$$

$$\nabla^2\nabla^2\phi = -(1+\nu)\left(\frac{\partial F_r}{\partial r} + \frac{Fr}{r}\right); \quad \nabla = \frac{\partial^2}{\partial r^2} + \frac{1}{r}\frac{\partial}{\partial r} + \frac{1}{r^2}\frac{\partial^2}{\partial\theta^2}$$

vervolg (II.52)

Here ν is Poisson's modulus, which for copper will be taken to be 0.34. The first three equations of the set (II.52) satisfy the equilibrium equations (II.48) identically.

In the case of cylinder symmetry the equations (II.52) reduce to

$$\sigma_r = \frac{1}{r}\frac{\partial\phi}{\partial r}$$

$$\sigma_t = \frac{\partial^2\phi}{\partial r^2} + F_r r$$

$$\frac{1}{r}\frac{\partial^2\phi}{\partial r^3} + \frac{1}{r^2}\frac{\partial^2\phi}{\partial r^2} - \frac{1}{r^3}\frac{\partial\phi}{\partial r} = -(1+\nu)\left(\frac{\partial F_r}{\partial r} + \frac{F_r}{r}\right) \qquad \text{(II.53)}$$

B. Three dimensions, cylinder symmetry.

$$\nabla^2\sigma_r - \frac{2}{r^2}(\sigma_r - \sigma_t) + \frac{1}{1+\nu}\frac{\partial^2\Theta_m}{\partial r^2} = -\frac{1}{1-\nu}\left[(2-\nu)\frac{\partial F_r}{\partial r} + \nu\frac{F_r}{r} + \nu\frac{\partial F_z}{\partial z}\right]$$

$$\nabla^2\sigma_t + \frac{2}{r^2}(\sigma_r - \sigma_t) + \frac{1}{1+\nu}\frac{1}{r}\frac{\partial\Theta_m}{\partial r} = -\frac{1}{1-\nu}\left[\nu\frac{\partial F_r}{\partial r} + (2-\nu)\frac{F_r}{r} + \nu\frac{\partial F_z}{\partial z}\right]$$

$$\nabla^2\sigma_z + \frac{1}{1+\nu}\frac{\partial^2\Theta_m}{\partial z^2} = -\frac{\nu}{1-\nu}\left(\frac{\partial F_r}{\partial r} + \frac{F_r}{r} + \frac{\partial F_z}{\partial z}\right) - 2\frac{\partial F_z}{\partial z} \qquad \text{(II.54)}$$

$$\nabla^2\tau_{rz} - \frac{\tau_{rz}}{r^2} + \frac{1}{1+\nu}\frac{\partial^2\Theta_m}{\partial r\partial z} = -\left(\frac{\partial F_r}{\partial z} + \frac{\partial F_z}{\partial r}\right)$$

$$\nabla^2 = \frac{\partial^2}{\partial r^2} + \frac{1}{r}\frac{\partial}{\partial r} + \frac{\partial^2}{\partial z^2}$$

$$\Theta_m = \sigma_r + \sigma_t + \sigma_z$$

c. General solution.

To find a general solution of a set of simultaneous inhomogeneous differential equations, we have to find the general so-

lution of the homogeneous set and add a particular solution of the inhomogeneous set. For the two dimensional equations this is readily performed and the results will be given in part 3. Firstly we shall discuss the specific difficulties of the three dimensional system in a qualitative way.

A. General solution of the homogeneous equations in three dimensions.

It can be shown[1] that a solution of the homogeneous set of equations has been found if we write the stresses in terms of a stress function ϕ which has to obey

$$\nabla^2\nabla^2\phi = 0 \qquad \text{(II. 55)}$$

with

$$\begin{aligned}
\sigma_r &= \frac{\partial}{\partial z}\left(\nu\nabla^2\phi - \frac{\partial^2\phi}{\partial r^2} \right) \\
\sigma_t &= \frac{\partial}{\partial z}\left(\nu\nabla^2\phi - \frac{1}{r}\frac{\partial\phi}{\partial r} \right) \\
\sigma_z &= \frac{\partial}{\partial z}\left([2-\nu]\,\nabla^2\phi - \frac{\partial^2\phi}{\partial z^2} \right) \\
\tau_{rz} &= \frac{\partial}{\partial r}\left([1-\nu]\,\nabla^2\phi - \frac{\partial^2\phi}{\partial z^2} \right)
\end{aligned} \qquad \text{(II. 56)}$$

Unfortunately there does not exist an exact solution of (II. 56) except in the form of an infinite set of polynomials. However, for some sets of boundary conditions most of the coefficients in the sum of polynomials cancel and an exact solution can be found. However, if one imposes practical boundary conditions, an approximation has to be made in most cases.

B. Particular solution.

There exists no general method to find a particular solution of the system consisting of (II. 51) and (II. 54). In some cases a solution can be found by trial and error.

d. Boundary conditions.

The correct boundary conditions which have to be imposed are that the normal stresses are zero everywhere on the outer surface of the coil. In formula:

$$\begin{aligned}
(\sigma_r)_{r=r_i} &= 0 \qquad (\sigma_z)_{z=\frac{1}{2}l} = 0 \\
(\sigma_r)_{r=r_u} &= 0 \qquad (\sigma_z)_{z=-\frac{1}{2}l} = 0
\end{aligned} \qquad \text{(II. 57)}$$

In case of presence of shearing stress at the boundary the

conditions have to include them. Further one expects the solutions to have the symmetry of the problem. Imposing symmetry with respect to the plane $z = 0$ we see that the last two boundary conditions are identical. However, one can show that with this number of boundary conditions one needs at least fifth and seventh order polynomials for ϕ. For each boundary condition of the type (II.57) and for a polynomial of the n^{th} degree one needs n adjustable constants to make each power of r and z zero on the boundary. The number of required constants rises faster than the number of available constants if one increases the number of polynomials. Only that type of boundary conditions which makes some of the powers coincide on the boundary can be satisfied.

To avoid this difficulty usually one uses Saint Venant's principle which states that if one replaces the boundary condition on a part ΔS of the boundary by another, statically equivalent, boundary condition, the stress distribution changes significantly only in distances from the boundary which are of the order of magnitude of the linear dimensions of ΔS or smaller[13].

Applying this principle one can replace the boundary condition of the type

$$(\sigma_r)_{r=r_i} = 0$$

by a boundary condition of the type

$$\left[\int_{-\frac{1}{2}l}^{\frac{1}{2}l} \sigma_r \, dz\right]_{r=r_i} = 0 \qquad \text{(II.58)}$$

The integration removes all powers of z and the number of adjustable parameters can be chosen to satisfy all boundary conditions.

However, the use of the principle of Saint Venant is justified only if the surface concerned is only a small part of the total surface of the body and in our case this is not so. The dimensions of the magnet coil are generally comparable with the dimensions of the surfaces where the boundary conditions have to be applied.

The only thing one can do is to slice the coil into discs normal to the cylinder axis and solve the radial problem under neglect of the axial forces. The same procedure can be followed for the axial stress problem. However, because axial and radial forces are of the same order of magnitude the justification of this procedure is by no means self-evident.

We calculate the plane stresses for three plane configurations: for the plane $z = 0$, for the cylinder plane $r = r_i$, and for a plane θ is a constant. We compare the numerical results to obtain the relative magnitude of the usually neglected force components. The numerical results are compared with our experiments on a number of magnet coils.

3. Approximate solution

a. Solution in the plane z = 0.

Starting from the equations (II.49) and (II.53) with the first two of the boundary conditions (II.57) we have as a solution

$$\sigma_r = K_o \left\{ \left(\frac{3+\nu}{8}(\alpha^2+1) - \frac{2+\nu}{3}\left[\frac{\alpha^2(\alpha^2-\alpha)}{\alpha^2-1} + \alpha \right] \right) + \right.$$
$$\left. + \frac{1}{\gamma^2}\left(-\frac{3+\nu}{8}\alpha^2 + \frac{2+\nu}{3}\frac{\alpha^2(\alpha^2-\alpha)}{\alpha^2-1} \right) + \frac{2+\nu}{3}\alpha\gamma - \frac{3+\nu}{8}\gamma^2 \right\}$$

$$\sigma_t = K_o \left\{ \left(\frac{3+\nu}{8}(\alpha^2+1) - \frac{2+\nu}{3}\left[\frac{\alpha^2(\alpha^2-\alpha)}{\alpha^2-1} + \alpha \right] \right) + \right. \qquad \text{(II.59)}$$
$$\left. + \frac{1}{\gamma^2}\left(\frac{3+\nu}{8}\alpha^2 - \frac{2+\nu}{3}\frac{\alpha^2(\alpha^2-\alpha)}{\alpha^2-1} \right) + \frac{1+2\nu}{3}\alpha\gamma - \frac{1+3\nu}{8}\gamma^2 \right\}$$

$$K_o = -\frac{B_o^2}{\mu_o(\alpha-1)^2\Phi}$$

with $\gamma = r/r_i$.

σ_r has a maximum value between $\gamma = 1$ and $\gamma = \alpha$ and this in the case $\alpha = 5$ for $\gamma = 1.7$. The maximum value for σ_t is always reached for $\gamma = 1$.

For a numerical example we insert $\mu_o = 4\pi \times 10^{-7}$, $B = 50\ W/m^2$, $\alpha = 5$ and $\beta = 5$ and we obtain $(\sigma_t)_{max} = 9.31 \times 10^8 N/m^2$ and $(\sigma_r)_{max} = 2.67 \times 10^8 N/m^2$. These values have to be compared with the breaking stress of hard-drawn copper which is $7.5 \times 10^8 N/m^2$.

b. Solution in the plane z = 0 for finite boundary condition.

In the case that one reinforces the magnet coil at the outer side by means of a wall of some strong material, one has to change the boundary condition on the outer surface of the coil and we set

$$(\sigma_r)_{\gamma=\alpha} = -P_w \qquad \text{(II.60)}$$

with P_w the pressure on the outer surface which is set as a boundary condition. Formally this boundary condition is not exact. One should add another set of simultaneous differential equations which describe the stresses in the reinforcing material and set again the stress at the outer side of the reinforcing wall equal to zero. We avoid this complication by assuming that the elasticity modulus of the wall material is much larger than that of the coil material and that the outer dimension of the magnet coil does not change. Moreover we calculate

the stresses only for the case that the stress in the reinforcing wall is equal to the breaking stress of the wall material. In that way we calculate the maximum stress which can occur in the coil material. Under the boundary conditions (II.60) the solution of the equations (II.49) and (II.53) is

$$\sigma_r = -\frac{\alpha^2}{\alpha^2-1} P_w \left(1-\frac{1}{\gamma^2}\right) + K_o \left\{\left(\frac{3+\nu}{8}(\alpha^2+1) - \frac{2+\nu}{3}\left[\frac{\alpha^2(\alpha^2-\alpha)}{\alpha^2-1}+\alpha\right]\right) + \right.$$

$$\left. + \frac{1}{\gamma^2}\left(-\frac{3+\nu}{8}\alpha^2 + \frac{2+\nu}{3}\frac{\alpha^2(\alpha^2-\alpha)}{\alpha^2-1}\right) + \frac{2+\nu}{3}\alpha\gamma - \frac{3+\nu}{8}\gamma^2\right\}$$

$$\sigma_t = -\frac{\alpha^2}{\alpha^2-1} P_w \left(1+\frac{1}{\gamma^2}\right) + K_o \left\{\left(\frac{3+\nu}{8}(\alpha^2+1) - \frac{2+\nu}{3}\left[\frac{\alpha^2(\alpha^2-\alpha)}{\alpha^2-1}+\alpha\right]\right) + \right.$$

$$\left. + \frac{1}{\gamma^2}\left(\frac{3+\nu}{8}\alpha^2 - \frac{2+\nu}{3}\frac{\alpha^2(\alpha^2-\alpha)}{\alpha^2-1}\right) + \frac{1+2\nu}{3}\alpha\gamma - \frac{1+3\nu}{8}\gamma^2\right\}$$

$$K_o = -\frac{B_o^2}{\mu_o(\alpha-1)^2\,\Phi} \qquad \text{(II.61)}$$

The stress in the wall depends on the pressure on the inner surface in the following way

$$\sigma_{tw} = P_w \frac{1}{\alpha_w - 1} \qquad \text{(II.62)}$$

with α_w the ratio of the outer to the inner diameter of the wall cylinder. For $\alpha_w = 1.25$ this gives $\sigma_{tw} = 4P_w$.

For a numerical example we take $\sigma_{w,break} = 8 \times 10^8 N/m^2$. (stainless steel), $\alpha = 5$, $\beta = 5$, $\gamma = 1$, and $\nu = 0.34$. Then $\sigma_r = 0$ and $\sigma_t = 5.2 \times 10^8 N/m^2$. The amount of reduction in comparison with the result under a is about 40%. For $\gamma = \alpha$ the reduction is about one half of that at $\gamma = 1$.

c. Solution in the cylinder plane $r = r_i$.

The problem is a problem in rectangular coordinates z and θ with only a force present in the z direction. The boundary conditions are

$$\sigma_z = 0 \text{ for } z = \pm \tfrac{1}{2} l$$

and we require that all solutions are independent of θ both to make the problem single valued and to preserve the axial symmetry in the initial problem. Because of the axial symmetry we put $\tau_{tz} = 0$. The force F_z is supposed to be linear in

z. (see equations (II.44) and (II.46).)

$$F_z = \frac{0.426\ B_o^2}{\mu_o \beta(\alpha-1)\ \Phi\ r_i^2}\, z = -\ K_1 z \qquad \text{(II.63)}$$

The force can be described by a potential function

$$V = \tfrac{1}{2}\ K_1 z^2 \qquad \text{(II.64)}$$

Under these conditions the set of differential equations is

$$\begin{aligned} &\frac{\partial \sigma_z}{\partial z} + \frac{\partial \tau_{zt}}{\partial \theta} = \frac{\partial V}{\partial z} \\ &\frac{\partial \sigma_t}{\partial \theta} + \frac{\partial \tau_{zt}}{\partial z} = \frac{\partial V}{\partial \theta} \\ &\left(\frac{\partial^2}{\partial z^2} + \frac{\partial^2}{\partial \theta^2}\right)(\sigma_z + \sigma_t) = -\ (1-\nu)\left(\frac{\partial^2 V}{\partial z^2} + \frac{\partial^2 V}{\partial \theta^2}\right) \end{aligned} \qquad \text{(II.65)}$$

These equations can be satisfied by solutions of the type

$$\begin{aligned} \sigma_z &= \frac{\partial^2 \phi}{\partial \theta^2} + V \\ \sigma_t &= \frac{\partial^2 \phi}{\partial z^2} + V \\ \tau_{tz} &= -\ \frac{\partial^2 \phi}{\partial z \partial \theta} \end{aligned} \qquad \text{(II.66)}$$

with ϕ satisfying

$$\frac{\partial^4 \phi}{\partial \theta^4} + 2\ \frac{\partial^4 \phi}{\partial \theta^2 \partial z^2} + \frac{\partial^4 \phi}{\partial z^4} = -\ (1-\nu)\left(\frac{\partial^2 V}{\partial \theta^2} + \frac{\partial^2 V}{\partial z^2}\right) \qquad \text{(II.67)}$$

With appropriate use of the boundary conditions one finds readily

$$\begin{aligned} \sigma_z &= -\ \frac{1}{8}\ K_1 (l^2 - 4z^2) \\ \sigma_t &= \frac{\nu}{2} K_1 z^2 \\ \tau_{tz} &= 0 \end{aligned} \qquad \text{(II.68)}$$

If we insert $B_o = 50\ W/m^2$, $\beta = 5$, $\alpha = 5$ we find $(\sigma_z)_{max} = 7.11 \times 10^8\ N/m^2$ for $z = 0$ and $(\sigma_t)_{max} = 2.42 \times 10^8\ N/m^2$ for $z = \pm \frac{1}{2} l$.

d. Solution for the plane $\theta = 0$.

Again we have a problem in rectangular coordinates, and the equations are

$$\frac{\partial \sigma_r}{\partial r} + \frac{\partial \tau_{rz}}{\partial z} + F_r = 0$$

$$\frac{\partial \sigma_z}{\partial z} + \frac{\partial \tau_{rz}}{\partial r} + F_z = 0 \qquad \text{(II. 69)}$$

$$\left(\frac{\partial^2}{\partial r^2} + \frac{\partial^2}{\partial z^2} \right) (\sigma_r + \sigma_z) = - (1+\nu) \left(\frac{\partial F_r}{\partial r} + \frac{\partial F_z}{\partial z} \right)$$

Because the system is rather complicated if one carries out the calculation for the exact forces, we take for the force in the radial direction the mean value in the radial direction and for the force in the axial direction the mean value in the axial direction, thus making F_r independent of r and F_z independent of z. The set of equations changes into

$$\frac{\partial \sigma_r}{\partial r} + \frac{\partial \tau_{rz}}{\partial z} = \tfrac{1}{2} K_o \left\{ 1 - \left(\frac{z}{21} \right)^2 \right\}$$

$$\frac{\partial \sigma_z}{\partial z} + \frac{\partial \tau_{rz}}{\partial r} = - \frac{1}{4} K_o \left\{ m_1 + m_2 \sin \pi \left(\frac{\gamma - 1}{\alpha - 1} \right) \right\} \qquad \text{(II. 70)}$$

$$\left(\frac{\partial^2}{\partial r^2} + \frac{\partial^2}{\partial z^2} \right) (\sigma_r + \sigma_z) = 0$$

with the use of the equations (II. 44), (II. 45), and (II. 46).

A particular solution can be found by using the stress function

$$\phi = \frac{K_o}{4} m_2 \frac{(\alpha - 1)^2}{\pi^2} r_i^2 z \sin \pi \frac{\gamma - 1}{\alpha - 1} + \frac{K_o r^5}{480\ l^2}$$

giving

$$\sigma_r = \frac{\partial^2 \phi}{\partial z^2} + F_r r = \tfrac{1}{2} K_o r \left\{ 1 - \left(\frac{z}{21} \right)^2 \right\} \qquad \text{(II. 71)}$$

$$\sigma_z = \frac{\partial^2 \phi}{\partial r^2} + F_z z = \frac{K_o r^3}{24 l^2} - \frac{1}{4} K_o z m_1$$

$$\tau_{rz} = -\frac{\partial^2 \phi}{\partial r \partial z} = \frac{K_o}{4} m_2 \frac{\alpha - 1}{\pi} r_i \cos \pi \left(\frac{\gamma - 1}{\alpha - 1} \right)$$

vervolg (II. 71)

A general solution can be found by adding a general solution of the homogeneous system. In this case we take the sum of a polynomial of the second degree, one of the third degree and one of the fifth degree. Using the principle of Saint Venant we take as boundary conditions

$$\int_{-\frac{1}{2}l}^{\frac{1}{2}l} \sigma_r dz = 0 \text{ for } r = r_i \text{ and } r = r_u$$

$$\int_{r_l}^{r_u} \sigma_z dr = 0 \text{ for } z = \pm \tfrac{1}{2} l \qquad \text{(II. 72)}$$

After some calculation we get the following result

$$\sigma_r = K_o r \left\{ \frac{1}{96} - \left(\frac{z}{2l} \right)^2 \right\}$$

$$\sigma_z = \frac{K_o r^3}{96 l^2} - \frac{K_o (r_u^4 - r_i^4)}{96 (r_u - r_i) l^2} \qquad \text{(II. 73)}$$

$$\tau_{rz} = \frac{K_o}{4} m_2 \frac{\alpha - 1}{\pi} r_i \cos \pi \left(\frac{\gamma - 1}{\alpha - 1} \right) - \frac{1}{4} K_o m_1 r + \frac{47}{96} K_o z$$

These solutions have a smaller degree of accuracy than (II. 59), (II. 61), and (II. 68) because of the approximations on the forces and the boundary conditions. The numerical results have been compiled in table II. 2 together with the results of 3a, b, and c.

4. Approximation with surface forces and volume force zero.

In this case the equilibrium conditions reduce to

$$\left| \frac{d\sigma_r}{dr} \right| + \frac{\sigma_r - \sigma_t}{r} = 0 \qquad \text{(II. 74)}$$

Table II.2.
Numerical results of stress calculations.

	z	γ	σ_r	σ_t	σ_z	τ_{rz}
Plane z = 0 and 0 at boundary (§ 3a).	0	1.0	0	9.31×10^8	--	--
	0	1.6	2.67×10^8	--	--	--
Plane z = 0 and finite at outer boundary (§ 3b).	0	1.0	0	5.20×10^8	--	--
Cylindrical plane r = r_i (§ 3c).	0	1.0	--	0	7.11×10^8	--
	$\pm\frac{1}{2}l$	1.0	--	2.42×10^8	0	--
Plane θ = constant (§ 3d).	0	1.0	5×10^6	--	-9.3×10^6	-2.9×10^6
	0	1.6	8×10^6	--	--	--
	0	3.0	--	--	--	-9.2×10^7
	0	5.0	3×10^7	--	-1.9×10^6	-5.8×10^7
	$\frac{1}{2}l$	1.0	--	--	--	1.4×10^9
	$\frac{1}{2}l$	3.0	--	--	--	1.3×10^9
	$\frac{1}{2}l$	5.0	--	--	--	1.4×10^9
	$-\frac{1}{2}l$	1.0	--	--	--	-1.4×10^9
	$-\frac{1}{2}l$	3.0	--	--	--	-1.5×10^9
	$-\frac{1}{2}l$	5.0	--	--	--	-1.5×10^9

and the compatibility conditions to

$$\frac{d^3g}{dr^3} + \frac{2}{r}\frac{d^2g}{dr^2} - \frac{1}{r^3}\frac{dg}{dr} + \frac{g}{r} = 0 \qquad \text{(II. 75)}$$

with $\sigma_r = \frac{g}{r}$ and $\sigma_t = \frac{dg}{dr}$

Now the boundary conditions are

$$\sigma_r = -P \quad \text{for} \quad r = r_i$$
$$\sigma_r = 0 \quad \text{for} \quad r = r_u \qquad \text{(II. 76)}$$

With substitution of (II. 39) the solution is

$$\sigma_r = \frac{1}{\alpha^2 - 1}\left(\frac{\alpha^2}{\gamma^2} - 1\right)\frac{B_o^2}{2\mu_o}$$
$$\sigma_t = \frac{1}{\alpha^2 - 1}\left(\frac{\alpha^2}{\gamma^2} + 1\right)\frac{B_o^2}{2\mu_o} \qquad \text{(II. 77)}$$

Both σ_r and σ_t have a maximum at $\gamma = 1$, the inner surface of the coil. With $B_o = 50$ W/m^2 and $\alpha = 5$ one obtains $\sigma_r = 10^9$N/m^2 and $\sigma_t = 1.08 \times 10^9$N/m^2. The result for σ_r does not agree with the solution by means of volume forces but the result for σ_t is in rather close agreement.

5. Average stress.

Although the results of the sections 3 and 4 for $(\sigma_t)_{max}$ are in rather close agreement with each other, the averages of the stresses over the radial coordinate are different.

The average of (II.59) over γ gives, with substitution of the same values for B_o, α, and β as in 3a and 4; $(\sigma_r)_{av} = 0.98 \times 10^8$N/m^2 and $(\sigma_t)_{av} = 6.47 \times 10^8$N/m^2.

The averages over the results in section 4 are

$$(\sigma_r)_{av} = \frac{B_o^2}{2\mu_o} \frac{1}{\alpha+1} = 2 \times 10^8 \text{N/m}^2$$

$$(\sigma_t)_{av} = \frac{B_o^2}{2\mu_o} \frac{1}{\alpha-1} = 3.3 \times 10^8 \text{N/m}^2 \qquad \text{(II. 78)}$$

The latter result can be obtained in a straightforward way without the use of the differential equations (II.74) and (II.75).

Because the average stress in the material can be connected with the total elastic energy content, both approximations lead to rather different results for the elastic energy of the strained magnet coil.

6. Buckling.

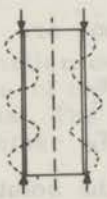

Fig. II.13. Buckling of an axially loaded cylindrical shell.

A cylindrical shell which is subjected to a uniformly distributed axial load will show buckling at a certain value of the load. (Fig. II.13). This buckling effect will show cylindrical symmetry [14] but this symmetry may be spoilt by small deviations of the cylindrical symmetry which are initially present in the undeformed shell. Usually this is the case in wire wound

magnet coils. It can be shown that the minimal load which causes buckling has been reached if the stress surpasses [14]

$$\sigma_{cr} = \frac{2\,E_e(\alpha - 1)}{(\alpha+1)\left[3(1-\nu^2)\right]^{\frac{1}{2}}} \qquad \text{(II. 79)}$$

if σ_{cr} is situated in the elastic region of the material and

$$\sigma_{cr} = \frac{2(\alpha-1)}{\alpha+1}\left[\frac{E_e E_t}{3(1-\nu^2)}\right]^{\frac{1}{2}} \qquad \text{(II. 80)}$$

if σ_{cr} is situated in the region of plastic deformation of the material. Here E_e represents the elasticity modulus of the material and E_t the slope of the stress strain curve at σ_{cr}.

For copper we use the formula (II. 80). $E_e = 12.5 \times 10^{10} N/m^2$ and with $\sigma_{cr} = 10^8 N/m^2$, $E_t = 1.5\ N/m^2$, and $\alpha = 1.15$ the equation is satisfied. For a coil with an inner diameter of 12 mm this gives a layer thickness of 1 mm if the buckling of the inner layer is studied. A thickness of 1 mm for the inner layer is a reasonable value in practice.

However, the windings in the layer are glued together with araldite, with a value for E_e of $4 \times 10^9 N/m^2$. E_t values of araldite do not appear to be available in the literature, but from breaking strain and elongation we estimate a mean value of $8 \times 10^7 N/m^2$. Calculating from this a mean slope of the stress strain curve, we obtain that σ_{cr} is situated in the elastic region of araldite. Using (II. 79) we obtain $\sigma_{cr} = 5.5 \times 10^7 N/m^2$. This value has to be compared with the flow stress of araldite which has values up to $8 \times 10^7 N/m^2$.

Comparison with the results of section 3c shows that buckling is a possible cause of damage in a magnet coil as soon as there is empty space in the coil which gives rise to unsupported layers. Empty space always tends to occur by plastic deformation caused by the forces in radial direction. The practical value of the field strength where buckling occurs will be determined both by the axial stress and by the radial strain.

In practice buckling-like damage is frequently found at the inner layer of our magnets. It is not possible, however, to attribute this to buckling unequivocally, because of non-stationary effects, which we shall show to be able to cause similar deformations. (§ 7).

§ 6. *Mechanical stress caused by electromagnetic forces in a flux concentrator coil.*

A flux concentrator coil is a device which is used to reduce the mechanical forces on the conductor windings of a pulsed magnet

coil. The main part is a massive cylinder with a slot. (Fig. II. 14). In the outer surface a spiral groove is made, in which the primary windings are mounted because it is a field free space. The field from the primary windings induces a current in the cylinder. If the skin depth is sufficiently small the current pattern is as sketched in fig. II. 14.

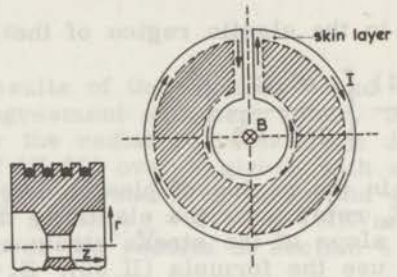

Fig. II. 14. Skin layer and current pattern in a flux concentrator coil. Inset: axial cross section.

The forces on the primary windings are removed and transmitted to the cylinder. The forces are largest at the slot, whose opposite sides repel each other.

For an analysis of the electrical behaviour of the system we refer to the paper by Hoffman and Scheuing[15].

The analysis of the mechanical stresses in a flux concentrator coil is much simpler than in a wire wound coil, because of the following reasons.

Firstly, in a flux concentrator coil the current is flowing in the skin layer at the surface of the material. In the case of an ideal conductor the skin layer is infinitesimally thin and the volume forces in the current carrying layer reduce to surface forces from the point of view of the bulk material.

Secondly the current density is able to establish a force free equilibrium with respect to axial forces. In this case the axial component of the Lorentz force is cancelled by an increased space charge density in the neighbourhood of the symmetry plane $z = 0$, and for that reason the slicing of the coil in thin plates as in § 5 is justified.

For the general formalism we refer to § 5 and we have as a set of differential equations:

$$\frac{\partial \sigma_r}{\partial r} + \frac{1}{r}\frac{\partial \tau_{r\theta}}{\partial \theta} + \frac{\sigma_r - \sigma_t}{r} = 0 \qquad \text{(a)}$$

$$\frac{1}{r}\frac{\partial \sigma_t}{\partial \theta} + \frac{\partial \tau_{r\theta}}{\partial r} + \frac{2\tau_{r\theta}}{r} = 0 \qquad \text{(b)} \qquad \text{(II. 81)}$$

$$\nabla^2\nabla^2\phi = 0 \qquad \text{(c)}$$

$$\sigma_r = \frac{1}{r}\frac{\partial \phi}{\partial r} + \frac{1}{r^2}\frac{\partial^2 \phi}{\partial \theta^2} \qquad (d)$$

$$\sigma_t = \frac{\partial^2 \phi}{\partial \theta^2} \qquad (e) \qquad (II.81)$$

$$\tau_{rt} = -\frac{\partial}{\partial r}\left(\frac{1}{r}\frac{\partial \phi}{\partial \theta}\right) \qquad (f)$$

Equations (a) and (b) are satisfied identically by equations (d), (e), and (f), and we have to solve (c) under appropriate boundary conditions. (fig. II. 15)

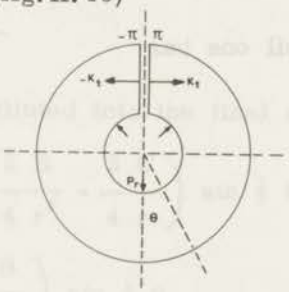

Fig. II. 15. Boundary conditions in a flux concentrator coil.

Both sides of the slot are pressed apart in tangential direction by a force K_t. In the case of the ideal conductor we put as the boundary condition for $r = r_i$: $\sigma_r = P_r$, and for $r = r_u$: $\sigma_r = 0$.

Applying Saint Venant's principle we have:

$$\left(\int_{-\pi}^{\pi} \sigma_r \, d\theta\right)_{r=r_i} = 2\pi P_r$$

$$\left(\int_{-\pi}^{\pi} \sigma_r \, d\theta\right)_{r=r_u} = 0 \qquad (II.82)$$

$$\left(\int_{r_i}^{r_u} \sigma_t \, dr\right)_{\theta=\pm\pi} = \pm \frac{K_t}{l}$$

with l the length of the coil.

To calculate the pressure on the boundary we write

$$dK_r = B_z J \, dv$$

$$J = \frac{I}{l\delta}$$

with δ the skin depth:

$$\delta = \left(\tfrac{1}{2}\ \omega\mu\sigma \right)^{-\frac{1}{2}}$$

For the skin layer:

$$v = \pi D_i l \delta$$

Giving:

$$F_r = BID_i \qquad \text{(II.83)}$$

$$P_r = \frac{BI}{l} \qquad \text{(II.84)}$$

For a single turn coil one has

$$B_o = \mu_o \frac{I}{D_i}$$

or

$$P_r = \frac{B_o^2}{\mu_o \beta} \qquad \text{(II.85)}$$

For the tangential force one has

$$K_t = -\mu_o \frac{2I^2}{D_s}(r_u - r_i) = -\frac{8}{\mu_o}\frac{B_o^2 \cdot r_i^3}{D_s}(\alpha - 1) \qquad \text{(II.86)}$$

with D_s the width of the slot.

Because of the third boundary condition we try a solution of the type

$$\phi = f(r) \sin \tfrac{1}{2}\theta \qquad \text{(II.87)}$$

which changes equation (II.81c) into a linear differential equation of the Cauchy-Euler type which has as a solution

$$f(r) = A r^3 + \frac{B}{r} + C r + D r \ln r \qquad \text{(II.88)}$$

or

$$\phi(r,\theta) = \left(A r^3 + \frac{B}{r} + C r + D r \ln r\right) \sin \tfrac{1}{2}\theta \qquad \text{(II.89)}$$

From the boundary conditions we obtain

$$A = -\frac{5}{29} K_t' - \frac{4}{29(\alpha^2-1)r_i} 2\pi P_r$$

$$B = \frac{11}{29} r_i^4 \alpha^2 K_t' + \frac{3\alpha^2 r_i^3}{29(\alpha^2-1)} 2\pi P_r$$

$$C = -\frac{55}{87} r_i^2 (\alpha^2+1) K_t' - \frac{r_i}{87(\alpha^2-1)} (44\alpha^2+15) 2\pi P_r \qquad \text{(II. 90)}$$

$$D = 0 \text{ (arbitrary choice)}$$

$$K_t' = \frac{K_t}{2\beta(\alpha^2-1)r_i^3}$$

which have to be substituted into the final solutions:

$$\sigma_r = \left(\frac{11}{4} A r - \frac{5}{4} \frac{B}{r^3} - \frac{3}{4} \frac{C}{r} \right) \sin \tfrac{1}{2}\theta$$

$$\sigma_t = \left(6 A r + \frac{2B}{r^3} \right) \sin \tfrac{1}{2}\theta \qquad \text{(II. 91)}$$

$$\tau_{rt} = \left(-A r + \frac{B}{r^3} \right) \cos \tfrac{1}{2}\theta$$

σ_r and σ_t have a minimum zero at a place directly opposite of the slot, where τ_{rt} has a maximum, tending to turn both halves of the ring on this point.

For a numerical example we take $\alpha = 5$, $\beta = 2$, $B_o = 50$ W/m^2, $D_i = 12$ mm, and $D_s = 1$ mm. The value 2 for β has been chosen because of the trapezoid shape of the flux-concentrator[15]. This choice gives

$P_r = 10^8$ N/m^2 $\qquad$ $A = 1.1 \times 10^{11}$ N/m^3

$K_t = 1.38 \times 10^7$ N $\qquad$ $B = -8.21 \times 10^3$ Nm

$C = 3.6 \times 10^8$ N/m

σ_t has an extremal value for $\gamma = 1.8$. In fig. II. 16 we have plotted the solutions given in equations (II. 91) as functions of γ for $\alpha = 5$, $\beta = 2$, $B_o = 50$ W/m^2, $D_i = 12$ mm, and $D_s = 1$ mm.

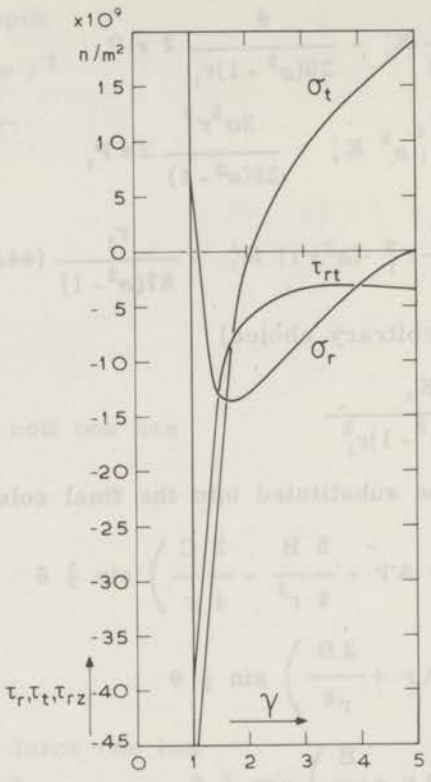

Fig. II. 16. Stress pattern in flux concentrator coil.
$\alpha = 5$, $\beta = 2$, $B_0 = 50$ W/m^2, $D_i = 12$ mm, and $D_s = 1$ mm.

σ_r and σ_t are plotted for $\theta = \pi$ and τ_{rt} for $\theta = 0$. The shape of σ_t shows that for $\theta \neq 0$ we have, apart from radial pressure and shearing stress, a bending process.

The influence of the factor $\sin \frac{1}{2}\theta$ on σ_r should not be considered as realistic, because it gives negative values of σ_r for $\theta < 0$. It is brought in by the application of Saint Venant's principle. In our opinion it is more realistic to take

$$(\sigma_r)_{\text{practical}} = \frac{1}{\pi} \int_0^{\pi} (\sigma_r)_{\text{calc.}} \, d\theta \qquad \text{(II. 92)}$$

resulting in averaging out of the factor $\sin \frac{1}{2}\theta$.

The numerical results suggest that the radial force is of little interest for the order of magnitude of the stresses. In fact, substitution of the numerical values in A, B, and C shows that the terms with P_r are rather small. They are needed to satisfy the boundary condition on the inner surface of the ring.

§ 7. *Dynamical effects.*
(For constructional details see chapter III.)

Although the behaviour of pulsed magnet coils can be described by stationary methods to some extent, one expects that the fact that the field is not constant in time will result in deviations from the statical behaviour, resulting in dynamical effects.

In some experiments we observed effects which we ascribe to dynamic causes. We shall describe our experiment and some experimental evidence obtained by other investigators, and we shall discuss the results from a dynamical point of view.

The magnet coils nos. 33, 35, 36, 37, and 38 (Appendix I) have been made according to about the same design. All were provided with a stainless steel jacket. From a static point of view one should not expect much difference in behaviour.

We have made the coils more rigid going up from 33 to 38, both by diminishing the amount of fiberglass and araldite and by shrinking the coils into the steel jackets. From a static point of view one would expect that the maximum attainable field strength should increase with increasing rigidity. However, the maximum field strength decreased with increasing rigidity. The coil 33, giving 41 W/m^2, has been destroyed by breaking of one of the connections. The coils 35, 36, 37, and 38, giving 36, 36, 34, and 27 W/m^2, have been destroyed by squeezing of the stainless steel inner tube. Apart from these coils, this type of damage only occurred in coils without inner reinforcing tube. The experimental evidence shows that in coils with stainless steel outer reinforcement the inwardly directed radial forces are much stronger than in fiber-glass reinforced coils, without stainless steel jacket.

Van Itterbeek, van Driessche, de Grave, and Myncke [16] have constructed pulsed magnets with an outer diameter considerably smaller than the inner diameter of the stainless steel jacket. The remaining space has been filled up with araldite and fiber glass. The coil, provided with araldite and fiber glass, has been shrunk into the steel jacket. This construction, although not very rigid, resulted in a reproducible 45 W/m^2 peak induction and an incidental 57 W/m^2 peak induction. The reported damage consisted of squeezing of the inner tube. The pulse duration has been 1 msec.

These results cannot be explained by a static theory, firstly, because a static theory predicts the best results from the most rigid construction, secondly, because the difference in damage at the inner side of the coil, which depends upon the type of the outer reinforcement, cannot be understood from a static point of view, and thirdly, because inwardly directed forces do not occur, apart from the buckling effects, which are equally strong in all types of coils at the same current and field strength.

We propose the following dynamic mechanism.

The copper windings are accelerated by the Lorentz force, resulting in a momentum which is directed outwards. If the outer surface is soft the momentum is absorbed and if sufficient damping is present the kinetic energy is converted into heat and deformation energy of the outer surface. If the momentum is sufficiently strong, the outer reinforcement tears. If the outer surface is completely rigid the momentum is reflected elastically and we are left with an inwardly directed momentum which tends to squeeze the inner tube. All mixed cases are possible, depending upon the damping coefficients of the construction materials.

It is known that metals have low damping coefficients, resulting in a reflection of the momentum and damage at the inner surface for a coil with copper and steel only as construction materials.

From the experimental evidence, we expect that araldite has a high damping coefficient in the temperature range between 80 and 270°K. No experimental data are available from literature in this region from damping measurements. However, the cooling down of araldite through this temperature range always results in cracks in the araldite. This possibly indicates a transition, which might be responsible for the high mechanical losses.

§ 8. *Comparison with experimental results.*

1. *Introduction.*

To compare the stress analysis given in the preceding paragraphs with experiment, we used the results obtained from tests on 38 pulse magnets (app. I). In the present paragraph we will give an outline of the way in which these results were obtained and a discussion of these results in view of the stress analysis. Details on the design and construction of the magnet coils will be given in chapter III.

2. *Measuring methods.*

The following data on the magnet coils are used: geometric dimensions of coil and reinforcing layer, elastic and plastic properties of materials, self-inductance, magnetic induction per ampere of coil current, and current and magnetic induction which cause breakdown of the coil.

The geometric dimensions have been obtained in a straightforward way. The inductance has been measured on an inductance bridge (brand-name Danbridge, type U 2 with a precision of 2%).

The elastic and plastic properties of the materials have been obtained from Landolt and Börnstein, ed. 1955, volumes IV a and b.

For the breaking stress of soft copper at 77°K we take $4 \times 10^8 N/m^2$, for the breaking stress of harddrawn copper at 77°K we take $7.5 \times 10^8 N/m^2$, and for the breaking stress of fibre-glass tissue impregnated with araldite (Atlas-Bindung) we take $3.5 \times 10^8 N/m^2$ at room temperature. The value at 77°K is not known to us, so we use the room temperature value, giving a lower limit of the breaking stress. The breaking stress of Sauereisen cement is not known to us but we estimate it to be $4 \times 10^8 N/m^2$.

The magnetic induction per ampere coil current has been measured in two ways:

1. Measurement of the induction voltage upon current reversal is made by means of a ballistic galvanometer, and comparison with a standard coil. This procedure has been used for the coils up to number 20.
2. Measurement is made by means of a Hall detector (brand-name Radio Frequency Laboratories, instrument type 1890, probe type HB-13470). This way of measurement has been used for the coils from number 21 upwards. For the coils 20 to 24 both methods have been compared and the results were found to be in agreement within experimental error, which has been estimated to be 3%.

The coil current has been determined by measuring the voltage over a resistor of $10^{-4}\ \Omega$, with an inductance less than 10^{-9} H, which has been connected in series with the magnet coil. A description of the resistor will be given in chapter III.

The signal is measured by displaying it on an oscilloscope (brand-name Tektronix, type 502, dual beam). The other beam is used to display the voltage over the magnet coil, but these data have not been used for quantitative evaluations.

The magnetic induction has been obtained by multiplying the coil current by the magnetic induction per ampere of coil current.

A priori it is not obvious that the magnetic induction per ampere of coil current should have the same value at low and at high values of the coil current because of coil deformation. Therefore in some cases the coil current has been compared with the integrator signal of a pick-up coil which is mounted in the center of the magnet coil. The difference between the two signals never exceeded 3%, but the integrated signal of the pick-up coil tended to be somewhat lower than a purely linear dependence on the coil current predicts, as was expected. Because the difference is small in comparison with other sources of error, it has been neglected in practice.

3. Comparison of predictions from plane stress theory.

The calculations of the theoretical expressions have been

given in § 5.3 and § 5.4.

The results are given in fig. II.17, II.18, and II.19 numerically. This has been done for soft copper ($\sigma_{break} = 4 \times 10^8 N/m^2$) and for hard drawn copper ($\sigma_{break} = 7.5 \times 10^8 N/m^2$). Along the horizontal axis either α or β are used as variables, along the vertical axis the magnetic induction which causes σ to exceed σ_{break}.

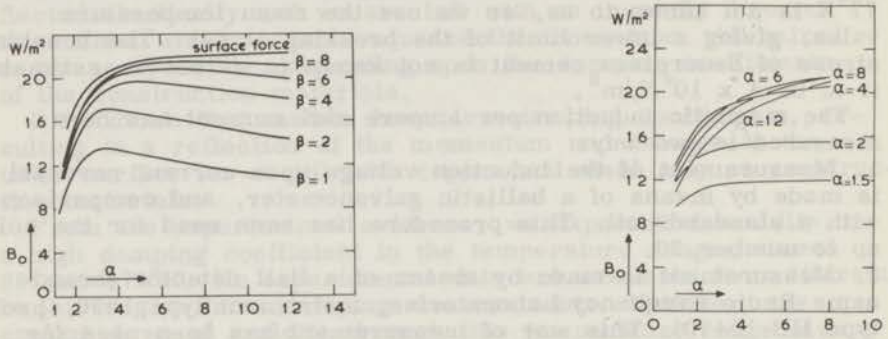

Fig. II.17. Predicted burst induction as a function of α and β for soft copper.

From fig. II.17 it can be seen that the addition of turns in axial direction always gives an increase in the central field, however small, whereas the radial force on the additional turns is relatively small, so that the mechanical stress on the central turns does not change appreciably.

However, if the thickness of the coil is small in comparison with the length, the additional field will be small and the curves tend to a constant value with increasing β.

An increase in α, however, will not always give an increase in maximum field. In general an increase in α gives a stronger winding package and a stronger central induction for a given current strength. However, for short coils the fraction of the magnetic energy in the central area decreases rapidly, so that one has to increase the current by a much larger amount than α has been increased. This is expressed mathematically by means of the geometrical factor Φ (app. III). From eq. (II.40) it may be seen that in this way the forces in the coil increase much faster than the induction in the central area and an optimum geometry is obtained [8].

In fig. II.18 the same curves as in fig. II.17 are plotted, together with the surface force prediction from eq. (II.77) for $\gamma = 1$.

In each of the figures II.18 a - e the experimental results are indicated by an asterisk.

Using eq. (II.61) one can calculate a correction for the burst induction in the case that the coil has been surrounded by a layer of reinforcing material. In the case of fiber glass this

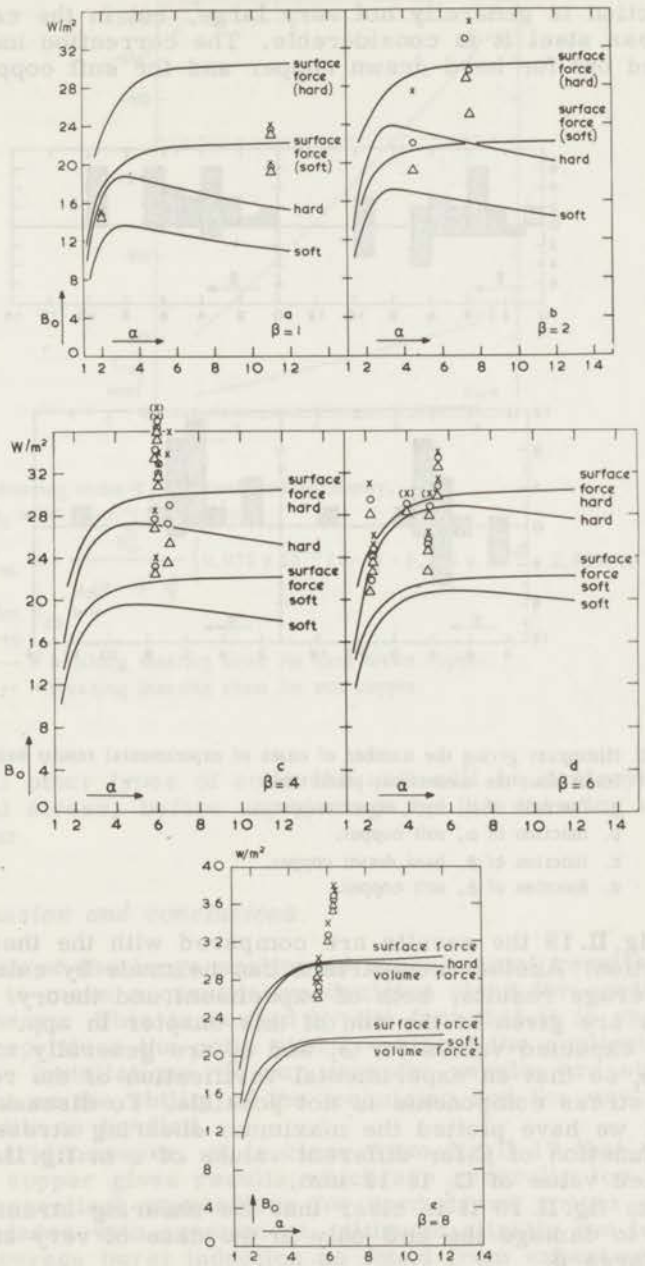

Fig. II. 18. Comparison of predicted burst induction and experimental data.
X = experimental points.
O = experimental points, corrected for reinforcement in the case of hard copper.
△ = experimental points corrected for reinforcement in the case of soft copper.

correction is generally not very large, but in the case of stainless steel it is considerable. The correction has been carried out for hard drawn copper and for soft copper.

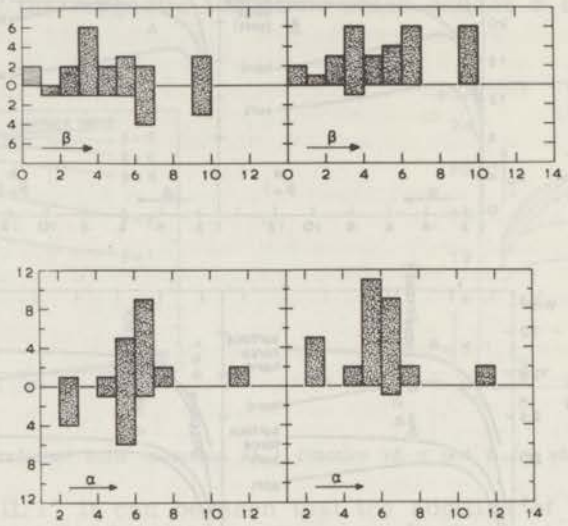

Fig. II. 19. Histogram giving the number of cases of experimental results being higher or lower than the theoretical prediction.
a. function of α, hard drawn copper.
b. function of α, soft copper.
c. function of β, hard drawn copper.
d. function of β, soft copper.

In fig. II. 19 the results are compared with the theoretical prediction. Another comparison can be made by calculating the average results, both of experiment and theory. The averages are given at the end of this chapter in app. III.

The expected values for σ_r and σ_z are generally much lower than σ_t so that an experimental verification of the results for these stress components is not possible. To discuss the shearing stress we have plotted the maximum shearing stress for $B = 50\ W/m^2$ as a function of β for different values of α in fig. II. 20. The assumed value of D_i is 12 mm.

From fig. II. 20 it is clear that the shearing stresses are bound to damage the coil only in the case of very small α and very large β.

For this type of magnet coil we have no experimental data available. Moreover, an experimental evaluation would be difficult, because the normal stresses are considerable in this

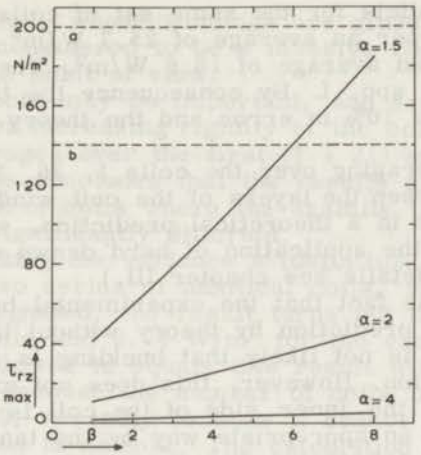

Fig. II. 20. Shearing stress τ_{rz} as predicted by theory.
$B_o = 50$ W/m^2; $D_i = 12$ mm.

$$\tau_{rz} = -\frac{B_o^2}{\mu_o(\alpha-1)^2\,\Phi}\left\{0.072 \times 10^{-3}(\alpha-1) - 0.318 \times 10^{-3} + 2.68 \times 10^{-3}\beta\right\}$$

$$\lim_{\beta \to o} \tau_{rz} = \infty$$

—— = breaking shearing stress for hard drawn copper.
--- = breaking shearing stress for soft copper.

case too.

For all other types of coils the coil will be destroyed by the tangential stress, before any damage by the shearing stress will occur.

4. *Discussion and conclusions.*

Because of the large scatter of experimental results it is difficult to make a quantitative decision about the applicability of the theory. This is caused by the fact that it is very difficult to reproduce the coils exactly without the application of expensive installations. In our case the results are strongly dependent on the ability of the technician and the way in which the araldite is handled.

In general however, it is clear from fig. II. 19 that the theory for soft copper gives results which are generally too low.

The theoretical expressions for hard drawn copper are more in accordance with experiment, although slightly too low.

The average burst induction as found from experiment, and corrected for reinforcement on the outer side, is 28.3 W/m^2 if the correction is carried out for hard drawn copper, and 26.2 W/m^2 if the correction is carried out for soft copper.

The theory predicts for the same set of coils in the case of hard drawn copper an average of 25.7 W/m^2 and in the case of soft copper an average of 18.6 W/m^2. The numerical values are gathered in app. I. By consequence the theory for hard drawn copper is 10% in error and the theory for soft copper 41%.

However, averaging over the coils 1, 36, 37, 38, where no fibre-glass between the layers of the coil windings has been applied, results in a theoretical prediction, which is 2.5% too low, assuming the application of hard drawn copper. (For constructional details see chapter III.)

Because of the fact that the experimental burst induction is higher than the prediction by theory without the assumption of instabilities, it is not likely that buckling is a primary cause of coil destruction. However, this does not exclude the possibility that once the inner side of the coil is critically loaded or deformed in an appropriate way by the tangential forces, the damage which is seen after destruction has a bucklinglike character, because of the simultaneous influence of tangential and buckling forces. In experiment, a bucklinglike damage is seen in cases where the reinforcement on the inner side of the coil is weak or absent.

Summarizing our results we assert:

1. The important quantity for a stress analysis of a pulse magnet is the tangential stress σ_t. This is in agreement with the results by Kuznetsov[17] and Hord[11]. However, some of the experimental results have to be explained by assuming buckling of the inner surface under the influence of the axial stress σ_z.

   From theory it follows that the shearing stress τ_{rz} is important only in solenoid shaped coils. Our experiment was not suitable to test the validity of this assertion.

   The quantities σ_r, σ_t, σ_z, and τ_{rz} can be calculated with a plane stress analysis. Although the theoretical validity of this approximation has not been proved, the agreement with experiment suggest its validity for the calculation of σ_t and σ_z. This remark has to be taken with the reserve of the possibility of dynamic effects.

2. For a calculation of the strength of a pulse magnet under the conditions as used in our experiment, the plane stress analysis tends to give results of the right order of magnitude, if one uses the mechanical constants of hard drawn copper. The results tend to be too low.

3. The reinforcement of a coil with a cylinder of strong material at the outer side is useful. The result is described in a quantitative way by plane stress analysis.

4. The insertion of fibre-glass between the layers of the coil seems to improve the resulting induction with, on the average, about 6%. However, the number of coils without fibre-glass is rather too small to give a sound basis for a quantitative conclusion.

5. A multi-turn coil, whose windings are glued together with araldite, can be considered to be a massive copper cylinder from a mechanical point of view.
6. Dynamical effects may be important, and are likely to be more dangerous for increasing rigidity of the coil construction.
7. By taking averages over the first (1 - 21) and the later (22 - 38) coils one concludes that the results of vacuum impregnated coils and of coils where the araldite is brought in by painting are not significantly different.

However, by taking the variance s (definition in app. III) of burst fields for two series of identical coils, one painted and one vacuum impregnated, the result turns out to be 6.30 W/m^2 for the painted coils and 2.74 W/m^2 for the vacuum impregnated coils. It is not allowed to equate this result with the standard deviation, firstly because the number of coils in this sample is smaller than 30, secondly because it cannot be expected that the distribution is normal. The calculation has been made for the coils 17, 18, 19, 20, and 23, 24, 25, 26.
8. The fact that the results of a stress analysis for coils made from hard drawn copper gives reasonable results for experimental coils which are made from rather soft copper wire can be explained by assuming that the coil material is stress hardened by the forces generated by successive pulses far below the breaking limit. From our experience it is reasonable to assume that in the cases that a magnet coil is tested with a testing program which starts with inductions in the vicinity of the breaking limit, the breakdown occurs at induction values which are lower than in the case of more gradual testing (coils numbers 10 to 14 and 23 to 26).

References.

1. S.Timoshenko and J.N.Goodier, Theory of elasticity, New York 1951.
2. P.Cotti, Z. ang. Math. Phys. 11 (1960), 17.
3. D.de Klerk, Ned. T. Natuurk. 27 (1961), 353.
4. D.de Klerk, The construction of electromagnets, Newport Pagnell, 1965.
5. H.J.Wallbaum, Landolt und Börnstein, 6 ed. 1964, pt IV 2b, p.687.
6. H.J.Wallbaum, Landolt und Börnstein, 6 ed. 1964, pt IV 2b, p.671.
7. H.J.Wallbaum, Landolt und Börnstein, 6 ed. 1964, pt IV 2b, p.671.
8. J.C.A.van der Sluijs, H.R.de Beun, B.A.Zweers, and D.de Klerk, Bull. Belg. Phys. Soc. V, 2 - 3 (1966), p.165.
9. D.B.Montgomery and J.Terrell, Nat. Magn. Lab. report No AFOSR 1561 (1960).
10. K.S.W.Champion, Proc. Phys. Soc. London, A 115 (1927), 658.
11. J.N.Hord, J.Res. Nat. Bur. Stand. 69 C (1965), 287.
12. F.Bitter, High magnetic fields, New York 1961, p.85.
13. Saint Venant, Mémoires des Savants Étrangers, 14 (1855), 233 - 560.
14. S.Timoshenko, Theory of elastic stability, New York 1936.
15. L.Hoffmann and V.Scheuing, CERN 63 - 36, 1963.
16. A.A.van Itterbeek, W.van Driessche, I.de Grave, and H.Myncke, Bull. Belg. Phys. Soc., V, 2-3, (1966), 188.
17. A.A.Kuznetsov, Zh. Tekhn. Fiz. 30 (1960), 589 and 592.
18. J.C.A.van der Sluijs, High magnetic fields, New York 1961, p.290.

APPENDIX I.

(the numbers between brackets refer to footnotes)

Mechanical and electrical data of experimental magnet coils.

Coil no.(11)	D_i mm	f mm^2	α	β	α_w	$\sigma_w \times 10^{-8}$ N/m^2	L mH	$B/I \times 10^3$ W/m^2A
1	6	0.9 ø	5.0	6.0	1.33	4.0	3.60	14.8
2	12	1.0 ø	4.0	5.0	1.07	3.5	2.92	11.6
4	6	1.4 x 0.4	6.7	9.0	1.07	3.5	1.31	15.6
5	6	1.2 x 0.6	6.7	9.0	1.07	3.5	1.60	15.2
10	12	1.2 x 0.6	2.5	6.0	1.10	3.5	0.53	6.80
11	12	1.2 x 0.6	2.5	6.0	1.10	3.5	0.60	5.60
12	12	1.2 x 0.6	2.8	6.0	1.10	3.5	1.10	9.00
13	12	1.2 x 0.6	2.8	6.0	1.10	3.5	1.10	8.90
14	12	2.2 x 1.5	5.5	5.5	1.07	3.5	0.68	5.50
15	12	2.2 x 1.5	6.0	3.0	1.07	3.5	0.55	5.80
16	12	2.2 x 1.5	6.0	3.0	1.07	3.5	0.84	6.40
17	12	2.2 x 1.5	5.8	4.0	1.07	3.5	0.83	6.00
18	12	2.2 x 1.5	5.8	4.0	1.07	3.5	1.39	7.50
19	12	2.2 x 1.5	5.8	4.0	1.07	3.5	1.27	6.20
20	12	2.2 x 1.5	6.0	3.8	1.07	3.5	0.66	3.50
21	12	3.6 x 1.4	5.5	6.0	1.08	3.5	1.89	6.50
22	80	8.0 x 3.0	2.0	1.0	1.03	3.5	0.96	1.25
23	12	3.6 x 1.4	6.0	9.0	1.07	3.5	1.67	5.40
24	12	3.6 x 1.4	5.5	9.0	1.08	3.5	1.19	5.50
25	12	3.6 x 1.4	5.5	9.0	1.08	3.5	1.18	4.80
26	12	3.6 x 1.4	5.5	9.0	1.08	3.5	1.64	5.98
27	12	3.4 x 1.2	5.2	5.0	1.08	3.5	1.19	6.00
28	12	5.0 x 0.8	11.0	0.9	1.05	3.5	0.63	3.17
29	12	3.4 x 1.2	6.2	3.5	1.07	3.5	0.92	5.50
30	12	5.0 x 0.8	11.0	0.9	1.05	3.5	0.61	3.29
31	12	3.4 x 1.2	6.2	3.5	1.07	3.5	1.13	5.90
33	12	3.4 x 1.2	7.3	2.5	1.25	8.0	0.84	5.65
34	16	3.4 x 1.2	5.0	5.5	1.08	3.5	3.41	7.13
35	12	3.6 x 1.4	7.5	3.0	1.25	8.0	0.76	4.80
36	12	3.4 x 1.2	6.6	3.3	1.25	8.0	1.06	5.80
37	16	3.4 x 1.2	6.5	3.2	1.25	8.0	1.54	6.50
38	20	3.4 x 1.2	4.5	2.0	1.25	8.0	1.00	4.80

I_{br} kA	B_{br} W/m^2	B_{br} in W/m^2 corrected for		B_{br} in W/m^2 calculated for		max. current density I_{br}/f kA/mm^2	type of reinforcement	
		hard drawn copper	soft copper	hard drawn copper	soft copper			
2.00	29.6	25.3	22.8	28.5	20.6	2.22	cement	(1)
2.60	30.0	29.1	28.3	27.4	19.8	2.60	FAP[6]	(1)
2.43	38.0	36.9	35.8	29.4	21.5	4.33[10]	FAP	(1)
2.47	37.5	36.4	35.4	29.4	21.5	3.43[10]	FAP	
4.56	31.0	29.5	28.1	24.6	17.7	6.33[10]	FAP	
4.10	23.0	21.9	20.9	24.6	17.7	5.69[10]	FAP	(2)
2.80	25.2	24.0	22.9	25.6	18.2	3.88[10]	FAP	(2)
2.92	26.0	24.8	23.6	25.6	18.2	4.16[10]	FAP	(2)
5.70	31.4	30.8	29.9	28.5	20.6	1.73	FAP	
6.30	38.2	37.1	36.0	23.5	17.2	1.91	FAP	
5.50	37.4	36.3	35.3	23.5	17.2	1.67	FAP	
4.10	24.0	23.3	22.6	27.2	19.6	1.25	FAP	
4.70	35.3	34.3	33.4	27.2	19.6	1.43	FAP	
4.60	28.5	27.7	26.9	27.2	19.6	1.39	FAP	
5.80	20.3	19.7	19.2	27.2	19.6	1.76	FAP	
5.20	33.8	32.5	31.6	28.7	20.8	1.05	FAP	
12.0	15.0	14.7	14.6	16.4	11.8	0.50	FAV[7]	(3)
6.30	34.0	32.7	32.1	29.6	21.6	1.26	FAV	
5.50	30.3	29.1	28.3	29.6	21.6	1.10	FAV	
5.80	27.8	26.7	26.0	29.6	21.6	1.16	FAV	
4.70	28.2	27.1	26.4	29.6	21.6	0.94	FAV	
5.00	30.0	28.8	28.0	28.1	20.2	1.00	FAV	
6.30	20.0	19.6	19.2	15.5	11.1	1.27	FAV	(4)
6.10	34.0	33.0	31.7	26.2	18.8	1.34	FAV	
7.30	24.0	23.6	23.1	15.5	11.1	1.83	FAV	(4)
5.70	33.0	32.0	30.8	26.2	18.8	1.40	FAV	
7.20	40.7	32.9	28.7	23.6	17.0	1.76	FAVS[8]	
3.70	26.4	25.5	24.7	28.5	20.6	0.90	FAV	(5)
7.40	35.6	28.7	25.1	24.8	17.9	1.48	FAVS	
6.20	36.0	29.0	25.4	24.6	17.5	1.51	AVSS[9]	
5.20	33.8	27.3	23.8	24.6	17.5	1.27	AVSS	
5.70	27.4	22.1	19.3	23.4	16.9	1.39	AVSS	

Appendix I, second part.

Recent coils without strength calculations.

Coil n.	D_i mm	f mm^2	α	β	α_w	L mH	B/I $W/m^2A .10^{-3}$	B_{br} W/m^2	I_{br} kA	J_{br} kA/mm^2	type reinf.	D_w[16] mm	remarks
39	18.0	3.6x1.4	4.5	2.8	1.25	0.91	4.75	31.8	6.70	1.34	FAVSS[13]	0.5	(5)
40	12.8	1.2x0.6	4.4	1.0	1.07	1.59	11.0	23.1	2.10	3.00	FAV	0.5	(12)
41	18.0	3.6x1.4	4.5	2.8	1.25	1.01	5.00	32.0	6.40	1.28	FAVSS	0.5	
44	18.0	3.2x1.7	4.1	4.5	1.25	1.33	5.67	36.3	6.60	1.21	FAVSS	1.0	(5)
45	18.0	3.2x1.7	4.1	4.6	1.25	1.34	5.60	41.7	7.45	1.37	FAVSS	1.0	(14)
46	30.0	1.2x0.6	1.4	1.0	1.07	0.78	5.00	14.0	2.75	3.89	FAV	12.0	(12,15)

1) Tested with preliminary installation[18].
2) Tested without stress hardening.
3) Tested at room temperature.
4) Disk-wound.
5) Not destroyed. Maximum induction value for safe use of the coil.
6) FAP = fibre-glass tissue + araldite, painted.
7) FAV = fibre-glass tissue + araldite, vacuum impregnated.
8) FAVS = fibre-glass tissue + araldite, vacuum impregnated + stainless steel jacket.
9) AVSS = araldite, vacuum impregnated + stainless steel jacket, shrunk around the coil.[16].
10) The failure of these coils occurred at an experiment with an effective frequency a factor 2 higher than assumed in chapter II, § 3, giving a maximum current density of 4.4 kA/mm^2. In coils 4 and 5 thermal damage to the araldite could be seen, so that thermal destruction may not be excluded. Coils 10 to 13 blew up in an explosion which made traces of the cause of the damage unclear.
11) The coil numbers which are omitted refer to coils which have not been tested because of constructional errors.
12) Thermal efficiency experiment.
13) FAVSS = fibre-glass + araldite, vacuum impregnated and shrunk in stainless steel jacket.
14) Coil damaged by sqeezing of inner tube with wall thickness of 1 mm. The results from this coil suggest that there is a possible systematic error by which all field values in this thesis are not more than 6% too low.
15) Nylon inner tube.
16) D_w = wall thickness inner tube.

APPENDIX II.

Tables of Φ and B_{br}

a. Φ as a function of α and β.

$$\Phi = \frac{\beta}{\alpha - 1} \ln \left[\frac{\alpha + (\alpha^2 + \beta^2)^{\frac{1}{2}}}{1 + (1 + \beta^2)^{\frac{1}{2}}} \right] \qquad \text{(II. 33)}$$

α \ β	1	2	4	6	8
1.5	0.6268	0.8448	0.9560	0.9784	0.9912
2	0.5649	0.7992	0.9368	0.9726	0.9784
4	0.4045	0.6509	0.8458	0.9202	0.9557
5	0.3580	0.5823	0.8012	0.8820	0.9314
6	0.3224	0.5344	0.7587	0.8592	0.9101
8	0.2713	0.4611	0.6841	0.8009	0.8658
12	0.2096	0.3658	0.5722	0.6921	0.7795

b. B_{br} as a function of α and β as calculated from eq. (II. 59) (plane stress) in W/m^2, based on $\sigma_B = 4.10^8 N/m^2$.

α \ β	1	2	4	6	8
1.5	9.58	11.11	11.82	11.96	12.04
2	11.81	14.05	15.22	15.51	15.55
4	13.41	17.01	19.39	20.23	20.61
5	13.11	16.73	19.62	20.59	21.16
6	12.74	16.41	19.55	20.80	21.41
8	11.97	15.62	19.02	20.58	21.40
12	10.92	14.43	18.05	19.86	21.07

To calculate B_{br} for another material strength σ_B' one should multiply the numbers above with $\left(\frac{\sigma_B'}{4.10^8} \right)^{\frac{1}{2}}$

APPENDIX III.

Statistical calculations on coils mentioned in Appendix I.

a. *Average.*

$$B_{br\,AV} = \frac{1}{N} \sum_{i=1}^{N} B_{br\,i} \qquad \text{(II. 92)}$$

1. Average B_{br}, corrected for hard copper, taken over all coils: 28.3 W/m^2.
2. Average B_{br}, corrected for soft copper, taken over all coils: 26.2 W/m^2.
3. Average B_{br}, calculated for hard copper, taken over all coils: 25.7 W/m^2.
4. Average B_{br}, calculated for soft copper, taken over all coils: 18.6 W/m^2.
5. Average B_{br}, corrected for hard copper, taken over all painted coils: 29.4 W/m^2.
6. Average B_{br}, calculated for hard copper, taken over all painted coils: 26.8 W/m^2.

$$\frac{B_{br\,AV\,corr.}}{B_{br\,AV\,calc.}} = 1.097 \text{ for painted coils.}$$

7. Average B_{br}, corrected for hard copper, taken over all impregnated coils: 27.1 W/m^2.
8. Average B_{br}, calculated for hard copper, taken over all impregnated coils: 23.3 W/m^2.

$$\frac{B_{br\,AV\,corr.}}{B_{br\,AV\,calc.}} = 1.092 \text{ for impregnated oils.}$$

We conclude that there is no evidence for a difference in quality.

b. *Variance.*

We calculate the variance s for two series of coils. The series were composed in such a way that the coils in a series were built according to the same mechanical design.

$$s = \left(\frac{\sum_{i=1}^{N} (x_i - x_{AV})^2}{N - 1} \right) \qquad \text{(II. 93)}$$

Series A: coils 17, 18, 19, 20; painted.

coil no	$B_{br\ corr.}$
17	23.3
18	34.3
19	27.7
20	19.7

$\rightarrow B_{br\ AV} = 26.6;\ s = 6.30.$

Series B: coils 23, 24, 25, 26; vacuum impregnated.

coil no	$B_{br\ corr.}$
23	32.7
24	29.1
25	26.7
26	27.1

$\rightarrow B_{br\ AV} = 28.9;\ s = 2.74.$

We conclude that there is a significant difference in s.
Units of B and s: W/m^2.

III. PRACTICAL DESIGN AND CONSTRUCTION OF PULSED MAGNETS.

§ 1. *Introduction.*

The design of a pulsed magnet is determined firstly by the requirements which have to be made on the magnetic field and secondly by the mechanical and electrical properties of the materials available for construction of the magnet.

The requirements on the magnetic field concern the duration of the pulse, the shape of the pulse as a function of time, the maximum magnetic induction to be generated, and the homogeneity of the magnetic field. These requirements have to be fixed by the experiment which one wants to do.

Generally a short pulse simplifies the mechanical problem. Apart from the simplification arising from the dynamical behaviour at pulse times of the order of 50 μsec. and less, a short pulse means a low inductance of the magnet coil. One needs a small number of turns and the conductor wire can be chosen quite solid.

In our case we have t_p = 20 msec. In some respects the problem can be handled quasi-statically (chapter II, § 5), though dynamic effects, which in this case work unfavourably, may occur too (chapter II, § 7).

The pulse shape is determined completely by the energy source and will not be discussed here. The maximum magnetic induction is the main requirement determining the coil design. The theoretical considerations on this subject are given in chapter II, and the practical consequences will be discussed in the following sections.

We did not consider any requirements on the homogeneity in a practical design. However, we made a preliminary design for a split coil system. The mechanical problem is not much different from that in single coils, apart from the forces which the two coils exert on each other. The reduction of field strength can be calculated in a straightforward way[1].

The requirements on the materials are generally a good mechanical strength, and a good commercial availability. The resistivity of the conductor material should be as low as possible, the resistivity of the reinforcing material should be high enough to reduce the field distortion arising from eddy currents to an acceptable level. As a conductor material we use copper and for reinforcement araldite, fibre glass, and stainless steel 18/8.

Finally we draw the attention to the fact that many of the considerations which are discussed in this chapter were not quite realized, until recently. In the list of magnet coils (chapter II, app.I) many coils can be found which are designed in a not quite ideal way.

§ 2. *Electrical design.*

The electrical design is discussed in chapter II. We give a short summary and some practical points here.

The design is determined by the choice of the current density, the maximum current, the magnetic induction per ampere of coil current, and the self-inductance.

In general we fix the self-inductance at 1.3 mH. In the construction of the coil we do not stick very closely to this number. In practice the inductance varies between 0.8 and 1.3 mH, giving a variation of 25 % in the pulse duration, which is not very serious from the point of view of the experiments. In designing the coil one has to recognise that the inductance decreases a certain amount in cooling down the coil to 77° K.

The maximum current is determined by the energy source. In this case it amounts to 15 kA. To generate 50 W/m^2 one needs an induction per ampere of 3.4×10^{-3} W/m^2A.

Together with a limit of 3.15 kA/mm^2 arising from thermal considerations the wire cross section should not be less than 4.7 mm^2.

These data together with fig. II. 11 give an area of possible values of α and β to make a practical choice. In general we take the combination which results in a B/I which is as high as possible.

If the inner diameter of the coil is different from 12 mm, the resulting B/I should be multiplied by a correction factor (eq. II. 34).

§ 3. *Mechanical design.*

The main features of the mechanical design are shown in fig. III. 1 and fig. III. 2.

The theoretical considerations connected with the mechanical design have been discussed in chapter II. The dimensions depend on the requirements which the experiments put on the geometry of the inner volume.

The requirement that the tail of a glass cryostat should be insertable in the inner volume of the magnet coil and the (excellent) abilities of the glass blowers fix the minimum inner diameter to 12 mm. To improve the rigidity of the cryostat we sometimes use 16 mm for the inner diameter of the magnet coil. The thickness of the inner tube of the magnet coil has to be added to this number to get the actual inner diameter.

From the considerations of chapter II it is clear that it is not favourable to use small values of either α or β (see also chapter II. app. I, coils 28 and 30).

During the winding process the winding tension which has to be exerted on the conductor wire to achieve a tight filling of

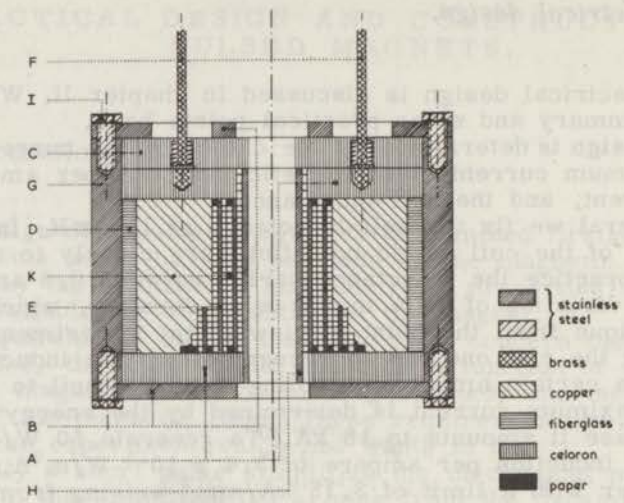

Fig. III. 1. Cross section of magnet coil.

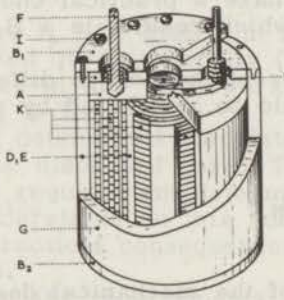

Fig. III. 2. Expanded view of magnet coil.

Legenda fig. III. 1 and III. 2.:

A = celoron coil flanges.
B = stainless steel flanges.
C = insulation flange.
D = outer reinforcement glass.
E = inter layer reinforcement glass.
F = brass connector
G = outer reinforcement stainless steel
H = stainless steel inner tube.
I = stainless steel bolts.
K = copper windings.

the winding volume causes the windings to slip away in axial direction. To prevent this, we use *celoron flanges* (A) at the ends of the coil. These flanges serve also to balance the

bouncing of the windings caused by the inwardly directed axial force pulse F_z (see chapter II, § 5). In the more recent designs without stainless steel reinforcement these celoron flanges were connected mutually by 12 brass bolts at the outer side of the coil (coils 21 to 31, 34). These bolts are not shown in fig. III.1.

If a stainless steel outer reinforcement is used, the celoron flanges are fixed to the coil by bolting *stainless steel flanges* (B) to the stainless steel *outer cylinder* (G). To insulate the conductor wire between the *connectors* (F) and the coil proper from the steel flanges an *additional celoron flange* (C) is mounted at the connector side of the coil.

In most coils a *reinforcement of fibre glass* tissue is used. It consists of an outer layer (D) with a thickness varying between 2 and 5 mm and interlayer reinforcements which have a thickness of some tenths of a millimeter (E). The interlayer reinforcement is mounted mainly in the inner part of the winding space.

All coils are filled up with *araldite*.

Initially the araldite was painted on the layers during the winding process. The disadvantage of this procedure is that the gas which is dissolved in the araldite is taken into the coil and causes occasional weak spots, resulting in less favourable properties of the magnet coil. The maximum field values of painted coils tend to scatter strongly.

At present the araldite is brought into the coil by vacuum-impregnation (§ 7), giving better results.

According to a static theory the inner side of the magnet coil does not need any reinforcement against electromagnetic forces. A number of coils (nrs. 9-20) have been wound on a segmented winding core, which could be removed after the hardening of the araldite. However, it turned out that without significant lowering of the maximum field the tendency to buckling of the inner layer increased. Because of the danger this presents to the cryostat we abandoned this way of construction. Because of the mechanical properties of stainless steel we use this material for the inner tube. An estimation shows that the decrease in magnetic induction caused by eddy currents in the inner tube can be neglected. This has been confirmed by experiment[1].

If B' represents the loss in induction and B_o the induction enclosed by the inner tube one can put:

$$\frac{B'}{B_o} = \mu_o \omega \frac{1 d_w}{4 \rho_{steel}} \qquad \text{(III.1)}$$

with d_w the thickness of the steel tube and ρ_{steel} the resistivity of the tube material.

However, the actual correction is much less because B' is proportional to $\frac{dB}{dt}$ and is 0 for maximum B apart from a phase.

correction. The amount which the phase differs from $\pi/2$ is about $\omega L/R$, if $\omega L/R \ll \pi/2$, giving an additional factor of about:

$$\mu_o \omega \frac{l\, d_w}{4\, \rho_{steel}}$$

resulting in a correction of the maximum value of B:

$$\Delta_{i.t.} = \frac{B'_{for\ t = t_{B_{max}}}}{B_{max}} \cong \left(\mu_o \omega \frac{l\, d_w}{4\, \rho_{steel}} \right)^2 \qquad \text{(III. 2)}$$

For $d_w = 1$ mm; $\omega = 2\pi \times 25$ rad/sec; $l = 10$ cm; $\rho_{steel} = 8 \times 10^{-7}$ Ωm one has $\Delta_{i.t.} = 9 \times 10^{-6}$; for $d_w = 2$ mm, $\Delta_{i.t.} = 3.6 \times 10^{-5}$.

Initially the outer reinforcement has been made from fibre glass tissue, which tended to tear up at high field strengths. With moderate inner tube thickness no damage at the inner side of the coil occurred.

After replacement of the outer reinforcement by stainless steel the maximum field did not increase, and the coils broke down by damage at the inner side.

We decided to keep the glass reinforcement at the outer side and to mount an additional reinforcement of steel. This combination made the best performance up to now, which is in accordance with the results of van Itterbeek, van Driessche, de Grave, and Myncke[2].

To calculate the decrease in maximum induction caused by the stainless steel outer tube, one has to integrate B over the whole coil volume. Together with the phase correction one has:

$$\Delta_{o.t.} = \frac{B'_{for\ t = t_{B_{max}}}}{B_{max}} \cong \mu_o^2 \omega^2 \frac{l^2 d_w^2}{16 \rho_{steel}^2 \alpha^2} \left(1 + \frac{\alpha^2 - 3\alpha + 2}{3(\alpha - 1)} \right) \qquad \text{(III. 3)}$$

For the shape of B in the winding space we used eq. (II.35) for $z = 0$. With $l = 10$ cm; $\alpha = 5$; $\rho_{steel} = 8 \times 10^{-7}$ Ω m; $d_w = 1$ cm; $\omega = 2\pi \times 25$ rad/sec one finds $\Delta_{o.t.} = 5.6 \times 10^{-4}$, which can be neglected.

The current leads to the capacitor bank are soldered to connectors (F). The lower ends of the 6 mm connectors are threaded and fitted into holes in the upper celoron coil flange (A). The connectors pass through holes in the insulation flange (C) and the upper steel flange (B). The holes in the steel are chosen so wide, that no danger of sparking is present.

In our earlier designs the conductor wire was passed to the connector through little holes in the upper coil flange (A). At high fields the inner connection made in this way turned out to be a weak point, and so we decided to spiral the inner con-

nection outwards between the inner tube and the coil flange (fig. III. 3).

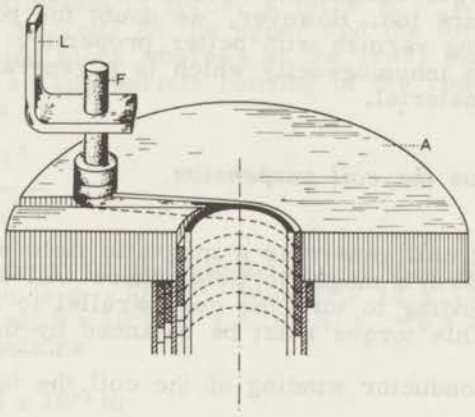

Fig. III. 3. Construction of inner electrode.
A = upper coil flange.
F = connector.
L = current lead.

§ 4. *Materials.*

A discussion of the choice of the materials has been presented in § 1 of this chapter. Here only a technical specification of the materials actually used is presented.

Conductor material: Electrolytic pure copper, slightly hardened by the manufacturing process. The insulation material is a polyvinylacetate varnish, commercial name duroflex, patented by Schweizerische Isola Werke, Basel, Switzerland, manufactured in licence by W. Smit Transformatorenfabriek, Nijmegen, Netherlands.

Steel: Stainless steel, 18 % Cr, 8 % Ni, remainder iron.

Celoron: Constructional insulator material, consisting of linen tissue impregnated with a phenol-type varnish.

Fibre glass tissue: Commercially available in several thicknesses. The tissue which we use has generally a fibre thickness between 10 and 13 μm. We use two tissue thicknesses: 0.3 and 1 mm. The former is preferred for use as interlayer reinforcement whereas both can be used at the outer side.

Araldite: A two component varnish. We use a product of CIBA, Basel, Switzerland, named Araldite D and Lancast A. This combination has been advised to us by the manufacturer for vacuum impregnation at moderate temperature and for reasonable strength of the hardened product. We do not claim

that this is the best choice that can be made although it works rather satisfactorily. A disappointing property is the tendency to crack at lower temperatures under pressure and sometimes without pressure too. However, we doubt the possibility fo find an impregnating varnish with better properties in this respect, because of the inhomogeneity which is a general property of this kind of material.

§ 5. *Forces on the coil suspension.*

If a magnet coil generates a magnetic field which is not parallel to the earth's magnetic field, there will be a torque acting on the coil tending to turn the coil parallel to the earth's magnetic field. This torque must be balanced by the suspension of the coil.

For each conductor winding of the coil the torque is

$$M_1 = IBS \sin \psi \qquad \text{(III. 4)}$$

with I the current, B the earth's induction, S the surface of the winding, and ψ the angle between the induction of the coil and the induction of the earth. If the coil is mounted vertically, ψ is the inclination of the earth's magnetic field.

Integrating over the coil one has

$$M_{tot.} = \frac{1}{3} n I B \sin \psi \, \pi \, r_i^2 (\alpha^2 + \alpha + 1) \qquad \text{(III. 5)}$$

with n the number of turns and $\alpha = D_u / D_i$.

Now we suppose that the coil is suspended on a copper rod of rectangular cross section, l meters long, h meters thick, and b meters wide.

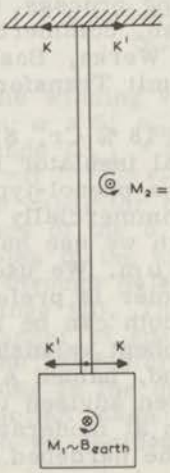

Fig. III. 4. Forces on the suspension of a coil in the earth's magnetic field.

For static equilibrium of torque against $M_1 = IBS \sin \psi$ a second torque M_2 is required, which we imagine to be made up from forces K acting on the ends of the rod (fig. III.4). To preserve equilibrium of force, a force $K' = K$ is required on both ends of the rod. At the upper end the force K' is delivered by the mounting block whereas at the lower end it has to be delivered by an appropriate bending of the rod, the deviation δ being given by

$$\delta = \frac{K l^3}{E h^3 b} \qquad \text{(III. 6)}$$

The earth's magnetic field in Leiden is 0.47×10^{-4} W/m^2 and the inclination is $\psi = 66°57'$. With $E = 12 \times 10^{10}$ N/m^2; $l = 1$ m; $h = 10^{-3}$ m; $b = 10^{-2}$ m; $I = 10^3$ A; $r_i = 6 \times 10^{-3}$ m; $\alpha = 5$; $n = 200$ one obtains

$$\delta = 7.8 \times 10^{-2} \text{ m}$$

In practice the amplitude is reduced by the gravitational force on the magnet coil. If one wants to solve the dynamical problem one has

$$m l^2 \ddot{\phi} + \phi \frac{E h^3 b}{l} = M_1 \sin \omega t \qquad \text{(III. 7)}$$

for a coil of mass m and a moment harmonic in time. The solution is:

$$\phi = \frac{M_1}{m l^2} \frac{1}{\mu^2 - \omega^2} \left[\frac{\omega}{\mu} \sin \mu t + \sin \omega t \right] \qquad \text{(III. 8)}$$

where $\mu = \left(\frac{E h^3 b}{m l^3} \right)^{\frac{1}{2}}$ (III. 9)

is the mechanical frequency of the suspended system. For $\omega \gg \mu$:

$$\phi = - \frac{M_1}{m l^2} \left(\frac{1}{\omega \mu} \sin \mu t + \frac{1}{\omega^2} \sin \omega t \right) \qquad \text{(III. 10)}$$

With $E = 12 \times 10^{10}$ N/m^2; $h = 10^{-3}$ m; $b = 10^{-2}$m; $m = 1$ kg; $l = 1$ m, we have $\mu = 1.2$. Hence the last term can be omitted and we have a considerable reduction in amplitude.

The occurrence of these forces can be prevented by mounting the coil either parallel to the earth's magnetic field or in a

pair of Helmholtz coils which cancel the earth's magnetic field. Both solutions turned out to be impossible in practice because of the extreme inhomogeneity of the local magnetic field, caused by iron in the vicinity.

§ 6. *Construction.*

After the manufacturing of the separate parts the winding is done on a lathe with a simple device to provide the required wire tension.

Initially the coil was turned by hand, but to improve the wire tension we made a device to turn the coil with a velocity of about two turns per minute.

It is of rather great importance that the turns be put as regularly and as closely to each other as possible because the coil performance depends critically on this aspect of the construction process. At the ends of the coil the occurrence of some open space cannot be prevented. To prevent difficulties with the next layer we fill up these spaces with paper. Paper is chosen because it is easy at hand and impregnable with araldite.

The winding of the fibre glass tissue is done by hand.

If no stainless steel reinforcement is provided, the holes for the brass bolts are made after completion of the winding process. To mount the stainless steel outer cylinder we used some different methods, which up to now did not lead to significantly different results:

1). We mount the unimpregnated coil at room temperature in the stainless steel cylinder and impregnate the whole afterwards.
2). We shrink the unimpregnated coil in the steel cylinder with the coil at 77°K and the cylinder at 373°K, to get a tighter packed coil by thermal shrink, and impregnate the whole afterwards.
3). We shrink the impregnated coil in the steel cylinder.

Method 3 is essentially the method used by van Itterbeek, van Driessche, de Grave, and Myncke[2] who use a conical stainless steel jacket, but it is simpler from a constructional point of view to use a cylindrical jacket. Furthermore, the support of the lower celoron coil flange is better, which is of some importance because we often found broken celoron flanges in non-supported coils. Apparently celoron is brittle at low temperatures.

§ 7. *Impregnation.*

After the mounting of the parts of the coil, sometimes with the exception of the stainless steel reinforcement, the coil is

either impregnated under vacuum with araldite or completely cast in araldite. The impregnation apparatus is shown in fig. III. 5.

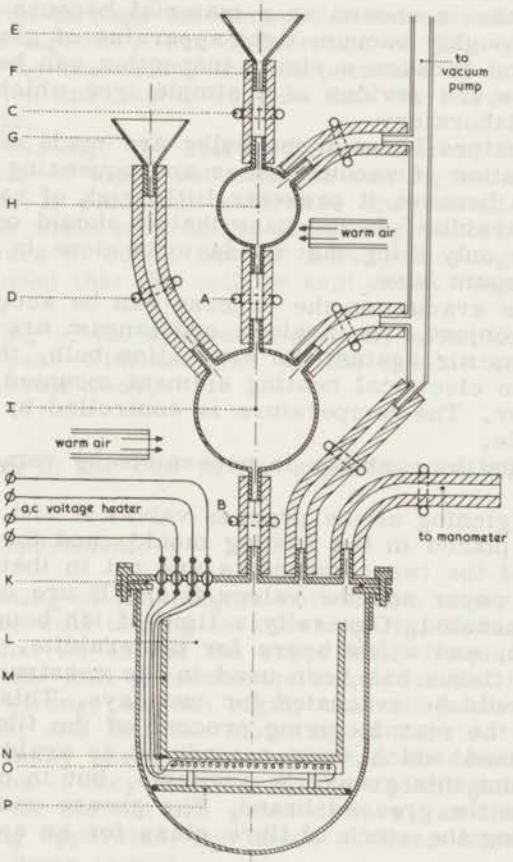

Fig. III. 5. Apparatus for vacuum impregnation of magnet coils.
A, B, C, D = squeezing valves.
E = filling funnel Lancast A.
F = vacuum hose.
G = filling funnel araldite.
H = evacuation bulb Lancast A.
I = evacuation bulb araldite.
K = o-ring.
L = evacuation chamber coil.
M = casting mould.
N = thermocouple.
O = heater.
P = mounting plate.

The apparatus is quite simple, and is based on the way in which vacuum casting is achieved in large industrial processes.

The apparatus consists of two glass evacuation bulbs and a glass chamber in which the coil is evacuated and the casting is done. Glass is chosen as a material because it is easy to make a thoroughly vacuum tight apparatus of glass, because it is cheap, and because a visual inspection can be made.

The valves are devices of a simple type which are in general use in our laboratory.

The connectors between the bulbs are made of vacuum hoses. The combination of vacuum hoses and squeezing valves has been chosen because it presents little risk of valves becoming stuck with araldite. In the case that it should occur nevertheless, the only thing that needs to be done is to replace the piece of vacuum hose.

During the evacuation the process can be accelerated by heating the object. The araldite and lancast are heated by a flow of warm air against the evacuation bulb, the coil is heated by an electrical heating element mounted in the evacuation chamber. The temperature is controlled by means of a thermocouple.

The evacuation chamber is accessible by removal of the brass cover.

At the beginning of the process valves A and B are closed, the coil is placed in the casting mould, and the calculated quantities of the two components are put in their respective bulbs. The cover and the valves C and D are closed and everything is evacuated. Generally a time of ten hours is sufficient for the coil, and a few hours for the araldite. However, if fibre glass tissue has been used in the construction of the coil, the coil should be evacuated for two days. This is necessary because in the manufacturing process of the fibre glass silicone grease is used which does not adhere to araldite. Fibre glass tissue without this grease is available, but in our case less readily than the greased brand. The grease can also be removed by evacuating the stock of fibre glass for an appropriate length of time.

The casting mould is made from glass or brass, depending on whether impregnation or casting is the intended process. In the case that casting is required the inner volume of the coil is filled up with a brass bar. All brass parts which should be removed after the hardening process are covered with a layer of silicone grease.

After sufficient evacuation, valve A is opened and the lancast flows into the araldite. For good results a thorough mixing is required, which is achieved by shaking the mixing bulb. The connection hoses to the mixing bulb should be taken long enough to make easy motion possible.

After sufficient mixing, valve B is opened and the mixture flows into the casting mould. After the araldite level has risen over the top of the coil, the valves to the vacuum pump and

the manometer are closed and air is admitted by opening valve C or D.

The casting should be completed within five minutes after the beginning of the mixing, because otherwise the mixture is too viscous to run through the connection hoses and everything becomes glued together. The occurrence of this type of accident is promoted by increasing the temperature of the mixture. In this connection one has to realize that the hardening reaction is exothermic.

After the casting, the coil is removed from the araldite bath (impregnation) or taken out with the casting mould (casting) and the whole is placed in a furnace and heated for 24 hours at 90°C. The main part of the hardening process is completed after two hours at 90°C, but for a very thorough hardening it is recommended that the coil be kept much longer at an elevated temperature.

The cleaning of the apparatus directly after completion of the process is done with acetone. If this is omitted the apparatus has to be thrown away.

§ 8. *Mounting of the coil in the experimental apparatus.*

a. *Testing experiment.*

The mounting of the magnet coil in the experimental arrangement for coil testing is shown in fig. III. 6a.

The fact that we extend the experiment frequently to the explosion of the coil presents the requirements that the mounting is strong, but not rigid, that all parts are cheap and easy to make, and that the mounting is carried out in such a way that as many parts as possible can be detached easily from the ruins if they turn out to be undamaged.

Therefore we did not use glass dewars, as they are used in the measuring apparatus, but made a cheap dewar of styrofoam and a brass inner vessel.

The coil is supported from the bottom of the vessel. The current leads are attached to each other by means of celoron blocks, to withstand the repulsive forces during normal use. However, the leads are so slack that an explosion of the coil usually leaves the top connections undamaged.

The top connections are brass bars imbedded in perspex creep shields and mounted in p.v.c. sheet. Although p.v.c. is a sufficiently good insulation material under normal conditions, the vertical planes of the creep shields are required to prevent the formation of a continuous ice layer between the connectors. The connections to the capacitor bank are flexible.

In most cases after a coil explosion, the brass liquid nitrogen vessel and the styrofoam insulation vessel are damaged at the lower end by the expanding nitrogen vapour. If the ex-

plosion is caused by a short circuit, the current leads are detached from the celoron blocks and swept outwards, damaging the nitrogen vessel at the upper end. In that case, the p.v.c. mounting plate and the creep shields are destroyed too. In case of explosion by rupture of the conductor, the upper part of the installation is not damaged.

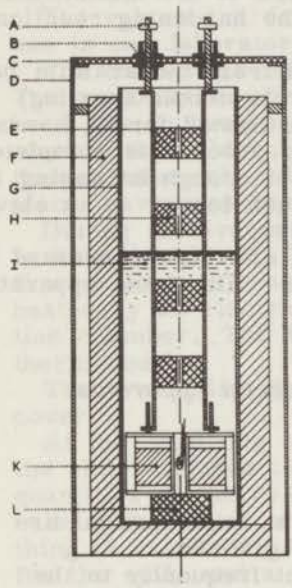

Fig. III. 6a.

Coil mounting in test cryostat.
A = brass connectors to capacitor bank.
B = insulation for creep currents.
C = p.v.c. mounting plate.
D = mounting frame.
E = copper currents leads.
F = styrofoam vessel.
G = brass nitrogen vessel.
H = celoron reinforcement.
I = liquid nitrogen.
K = coil.
L = coil support.

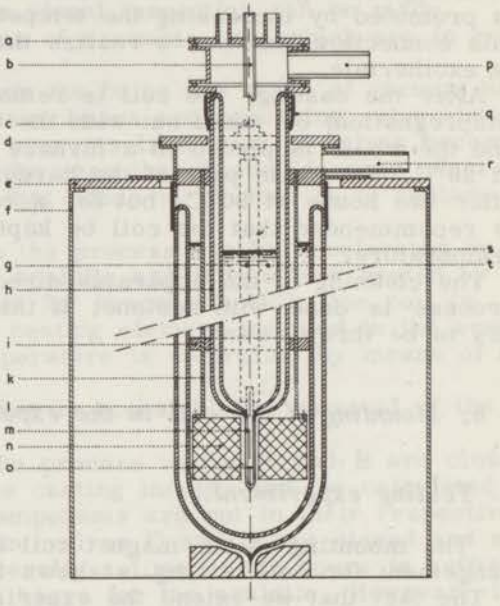

Fig. III. 6b.

Coil mounting in measuring cryostat.
a = cover of the liquid helium dewar.
b = coaxial leads measuring system.
c = connector to capacitor bank (dotted).
d = p.v.c. mounting cover of the nitrogen dewar.
e = mounting plate.
f = mounting frame.
g = current lead (dotted).
h = liquid helium dewar.
i = celoron suppor of the helium dewar.
k = stainless steel support.
l = nitrogen dewar.
m = tail helium dewar.
n = magnet coil.
o = experimental space.
p = to helium vapour line.
q = vacuum hose.
r = nitrogen vapour out.
s = liquid nitrogen.
t = liquid helium.

b. *Measuring cryostat.*

The measuring cryostat with the coil mounted in it is shown in fig. III. 6b. The magnet coil is mounted in a large glass liquid nitrogen dewar and the thin tail of a liquid helium dewar is inserted in the coil.

In this case every stress exerted by the coil on the dewar vessels will result in damage of the dewar vessels.

As to motion in the earth's magnetic field we solved this problem by suspending the coil from a tubular steel support in which the inner dewar vessel is mounted rather loosely. Any motion of the coil is transferred to the dewar vessel by the support and there are no forces on the tail of the dewar vessel.

The upper end of the support is the only part of the whole which is rigidly attached to the mounting frame. The liquid nitrogen dewar is mounted loosely by means of a cork support and a rubber hose, which can take up violent shocks easily.

The currents leads are attached to the steel support by means of tubular perspex insulators. These can be quite thin walled because of the high specific breakdown voltage of perspex, but their surface is chosen so large as to prevent surface creep currents.

In practice this construction is sufficient for the prevention both of shocks caused by motion in the earth's magnetic field and of shocks caused by the forces which the current leads exert on each other.

No protection is present against coil explosion, because this would make necessary a so heavy construction as to reduce either the experimental space or the available magnetic induction considerably. In practice the protection is ensured by a careful inspection of the coil properties after each pulse.

§ 9. *Coil testing.*

a. *Introduction.*

After the completion of a coil either to investigate the coil construction or for use in a measuring device the coil properties are inspected.

A coil which is made to investigate a specific constructional problem is tested until the coil is destroyed, whereas a coil for use in a measuring device is tested until a certain change in properties has occurred. This change should be so large as to ensure a certain amount of strain hardening. We assume that in that case the coil properties are improved by strain hardening and that fields up to the in this way experimentally fixed maximum field can be generated a large number of times without damage to the coil. This assumption is confirmed in practice.

During the actual experiments the coil properties are checked very carefully and we stop the experiment, if the coil tends to become unstable.

b. *Testing method.*

The test is carried out by exposing the magnet coil to a large number of pulses, with a gradual increase of the peak current. After each pulse we wait until temperature equilibrium has been reached again. Then we measure the self-inductance and the resistance of the magnet coil.

c. *Measuring method.*

1. *Self-inductance.* Measurement with a Danbridge U 2 inductance bridge (Maxwell bridge); precision 3 %.
2. *Resistance.* (fig. III. 7).

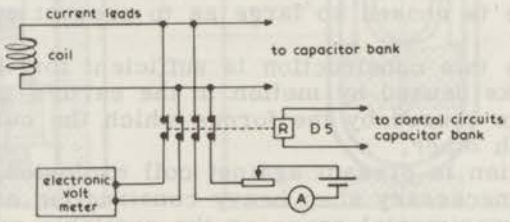

Fig. III. 7. Arrangement for resistance measurement of the magnet coil.

In principle one has to use a four point method because of the low resistance of the coil, typically 20 m Ω.

During the generation of a pulse the measuring device has to be disconnected from the coil. This is achieved by means of a relay which is automatically opened by the control system of the pulse current generator.

The measuring leads are connected to the current leads on the top of the cryostat. This introduces an error because of the resistance of the current leads in the cryostat. This error is of the order of several tenths of a milliohm.

The precision is estimated to be 3 %.

3. *Temperature equilibrium.* Temperature equilibrium is assumed to be reached if the coil resistance remains constant.
4. *Current through the magnet coil.* In series with the magnet coil we have connected a low-inductance resistor of 10^{-4} Ω ± 2 %.

The device is of a common type, which contains a sheet of resistor materials (see fig. III. 8).

The voltage over the resistor is fed into one of the beams of a Tektronix type 502 dual beam oscilloscope. The other beam

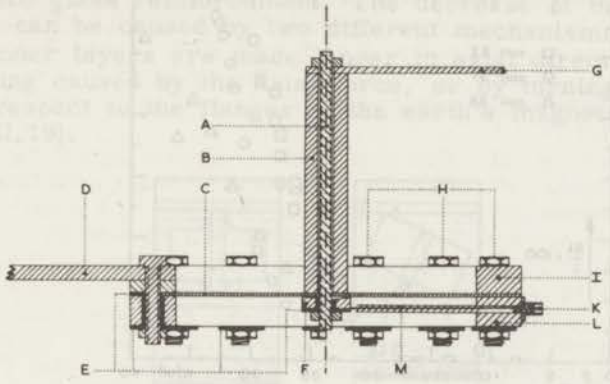

Fig. III. 8. Low-inductance resistor for the measurement of the coil current.
N.B. Left figure half has been turned over 15° around central axis.
A = central mounting bolt.
B = central current electrode.
C = resistance sheet.
D = current connection to capacitors (earth).
E = insulation of voltage electrodes.
F = central voltage electrode.
G = current connection to magnet coil.
H = circumferential mounting bolts.
I = circumferential current electrode.
K = coaxial connector to oscilloscope.
M = coaxial lead to central voltage electrode.

displays the voltage over the magnet coil, but the voltage diagram is not used for quantitative evaluations.
5. *Magnetic induction* (see also chapter II, § 8 and chapter V, § 2). In most cases the induction is calculated from the coil current. Some checks by means of a pick-up coil confirmed the validity of this approach.

d. *Results and discussion.*

Some typical results of the control measurements of self-inductance and resistance of the magnet coil are shown in fig. III. 9.

If the generated induction approaches 20 W/m^2 the resistance and self-inductance start to change. In general the behaviour of the self-inductance is more consistent between different coils than the behaviour of the resistance. It occurs that a coil explodes without any variation in resistance before.

The change of self-inductance which leads to damage of the coil is different for each type of magnet coil. A change of over 10 % is usually dangerous, but does not necessarily indicate

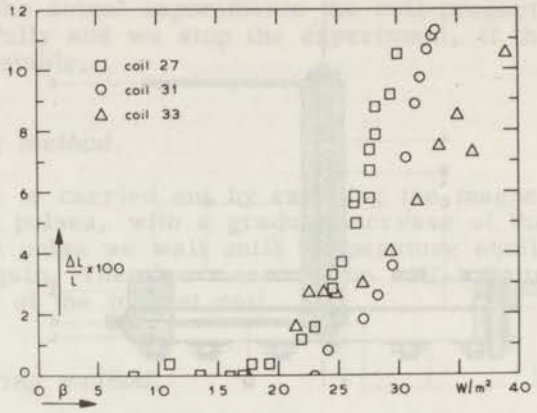

Fig. III. 9. a. Change of coil self-inductance in test experiment.

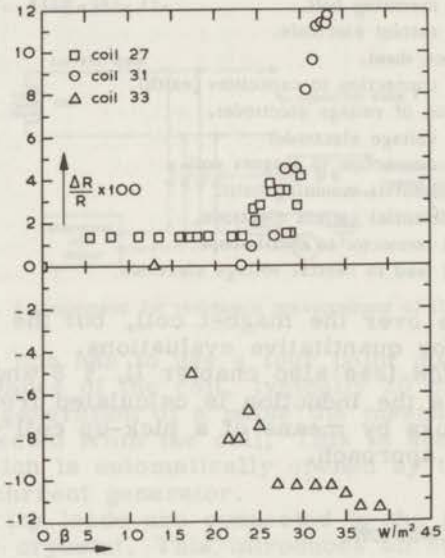

Fig. III. 9. b. Change of coil resistance in test experiment.

that the coil is already damaged. A change of resistance of that order of magnitude always indicates that heavy damage has been done.

If the self-inductance falls again after a rise of a few percent, this indicates almost surely heavy damage.

We interpret the rise of the self-inductance as caused by the increase of the average diameter of the windings by strain caused by the radial component of the force. A typical coil failure caused by this type of straining is tearing up of the

outer fibre glass reinforcement. The decrease of the self-inductance can be caused by two different mechanisms:

1) The inner layers are made longer in axial direction by bouncing caused by the axial force, or by turning of the coil with respect to the flanges in the earth's magnetic field (fig. III. 10).

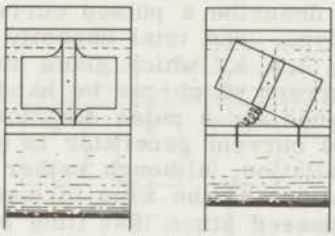

Fig. III. 10. Coil damage by lengthening of the inner layers.

2) Buckling-like compression of the inner layers in the radial direction, caused by either bouncing of the radial force or by actual buckling caused by the axial force.

The first type of damage can be excluded by a rigid axial construction, the second type by a strong inner tube. A strong inner tube, however, increases the danger of short circuit of the inner layer against the inner tube by flow of the insulator material.

The numerical results are given in chapter II, appendix I. The numbers of pulses which have been generated are not given, because they are strongly dependent on the way of testing and the end which one pursues.

Apart from coils 10 to 13 which were blown up without strain hardening, the numbers of pulses vary from several tens to several hundreds for measuring coils.

As a conclusion one can assert that the discussed construction results in magnet coils which can be used in a range up to 35 W/m^2 with occasional coils up to 40 W/m^2. Because of the scatter of the results, measuring coils up to 35 W/m^2 are rather scarce, but an upper limit of 30 W/m^2 is a quite reasonable goal.

The testing method yields a maximum magnetic induction which can be generated a quite large number of times without serious decrease of the lifetime of the coil.

References.

1) D.B.Montgomery and J.Terell, AFOSR 1561, (1960)..

2) A.van Itterbeek, W.van Driessche, I.de Grave, and H.Myncke, Bull. Belg. Phys. Soc., 2-3, (1966), 188.

IV. A PULSED CURRENT GENERATOR.

§ 1. *Introduction and basic design.*

In this chapter we describe a pulsed current generator of the capacitor discharge type. The total capacity is 3×10^{-2} F and the maximum voltage 3.5 kV which gives an energy content of 180 kJ. The peak current which can be handled by the switches is 18 kA. It is designed for a pulse duration of 20 msec.

This type of pulsed current generator is a very common one and the present installation, although rather large in comparison with existing installations at the time of construction (1961 - 1964), has been surpassed since that time by other ones of a comparable design[6].

Generally the older capacitor discharge devices have an energy content of less than 20 kJ. These energies can be released by a single switch, and connection of all capacitor cells directly in parallel presents no danger of explosion in case of a short circuit in a capacitor cell (fig. IV. 1)[1,2,3,4,5]

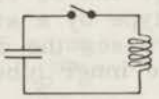

Fig. IV. 1. Single unit capacitor bank.

With rising energy content, the switches increase in complication and price. Moreover, if the energy content is of the order of 100 kJ or more, quite heavy explosions may occur in case of a short circuit in one of the capacitors.

We conclude that the capacitor bank should be divided into small parts, each part being handled by its own switch (fig. IV. 2).

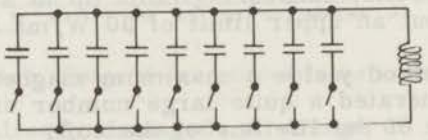

Fig. IV. 2. Multi-unit capacitor bank.

The problem to be solved is the synchronisation of the switches.

A similar design is presented by the capacitor bank described by Braunersreuther, Combe, Hoffmann, and Morpurgo[6].

The basic design of the present installation is shown in

fig.IV.3. The numbers of the connections refer to the detailed drawings, fig.IV.4 - 10. The total capacity has been divided into 9 equal parts. The switches are ignitrons, which present the additional advantage of their rectifier properties, reducing the possibility of one section discharging rapidly into another one.

In the following sections the apparatus will be considered in some detail.

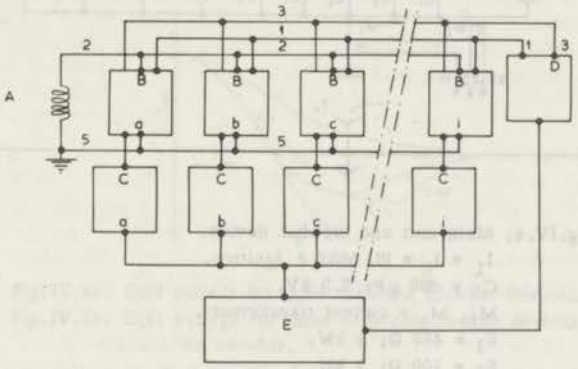

Fig.IV.3. Basic design present installation.
A = magnet coil.
B = main unit.
C = ignition.
D = charging rectifier.
E = control line.

In the apparatus only one earth connection is present, which is repeated in some of the detailed drawings.

§ 2. *Main unit and crowbar device.*

The main unit is shown in fig.IV.4.

The main unit contains 5 capacitors, each with 650 μF, 3.5 kV. The capacitors have been made by Haefely, Basel, Switzerland. They are oil-filled paper capacitors, with one pole connected to the container.

Each capacitor-unit is charged by the charging rectifier (§ 4) over a resistor of 450 Ω, 1 kW (R_1).

The resistors R_2 (100 Ω) provide the voltage to the comparing device in the charging rectifier (§ 5). Resistance has to be inserted to prevent oscillations between the main units. R_1 and R_2 together ensure the vanishing of possible voltage differences between the capacitor bank sections after charging.

Each section can be switched off by hand with S_1. The switch

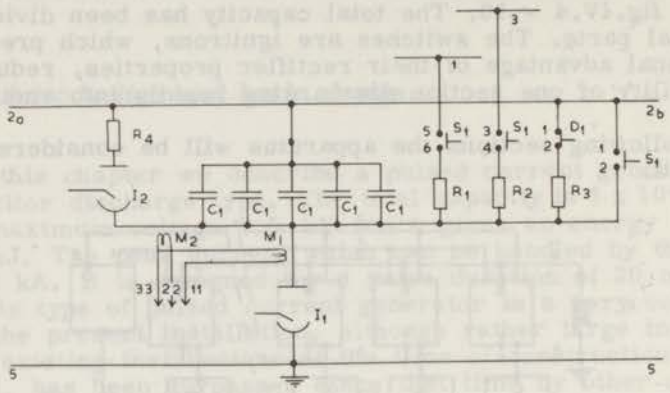

Fig.IV.4. Main unit and crowbar device.
I_1 = I_2 = PL 5552 A ignitron.
C_1 = 650 μF; 3.5 kV.
M_1, M_2 = current transformers.
R_1 = 450 Ω; 1 kW.
R_2 = 100 Ω; 1 kW.
R_3 = 20 Ω; 1 kW.
R_4 = 1.5 Ω; 2 kW.
S_1 = section switch
D_1 = safety relay.
1, 2_b, 3 = to charging rectifier and other sections.
2_a, 5 = to magnet coil.
11, 22, 33 = to ignition indication.

S_1 has auxiliary contacts in the ignition circuits (§ 3). The design is made in a way to permit use of any number of sections between one and nine that one desires.

In case of interruption of the mains voltage for the control line, and in emergency cases, relay D_1 is closed and the capacitors discharge over the resistor R_3 of 20Ω and 1 kW. During normal operation D_1 is opened.

The unit is fired by ignitron I_1, type PL 5552 A, made by Philips. The arc voltage is about 10 volts and the minimum anode voltage is about 50 V. The maximum current which can be carried is 2 kA and the maximum voltage which can be handled is 2 kV.

This voltage limit is determined by the voltage which can be switched off and it depends on the de-ionization time. The stationary voltages which can be put between the anode and the cathode are much higher.

The minimum time during which the arc remains stable is 25 msec, at least for high currents.

To prevent back firing of the ignitrons when operated at 3.5 kV, one can use several methods (fig.IV.5).

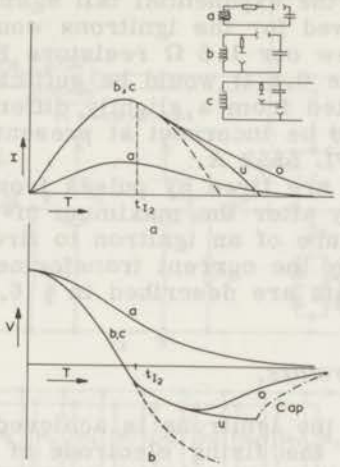

Fig.IV.5a. Coil current for three different crowbar devices.
Fig.IV.5b. Coil voltage for three different crowbar devices.
\- - - no crowbar.
u = undercritical
o = overcritical
cap = capacitor voltage.
t_{I_2} = ignition time I_2.

a. One prevents the capacitors from recharging with reversed sign of the voltage after the pulse by making the circuit overcritically damped by a sufficient coil resistance. This reduces the maximum coil current by a factor e and causes a long tail in the current characteristic, making it exceed the maximum current duration of the ignitrons in the case of a circuit with $\pi\sqrt{LC} \geqslant 2 \times 10^{-2}$ sec.
b. The coil is short-circuited by an ignitron with a resistor in series after the maximum of the pulse. The current through the ignitron is approximately equal to the coil current.
c. The capacitors are short-circuited by an ignitron with a resistor in series after the maximum of the pulse. The current through the crowbar ignitron is approximately equal to the current through the primary ignitron. This is an advantage in an apparatus which has been divided in sections, because in this case the crowbar switch can be kept as small as the primary switch.

After the closing of the crowbar switch the behaviour of the circuits b and c is determined by the quality factor of the damped circuit. In fig.IV.5 the behaviour is shown. The fraction of the inverse voltage on the primary ignitrons (without crowbar) which is retained with crowbar is determined by the damping resistor. It is best to make the resistor as small as possible, without running into an overcritically damped circuit, because

this would give the exponential tail again and the maximum pulse time allowed for the ignitrons would be exceeded. From this point of view our 1.5 Ω resistors R_4 are somewhat too large. The value 0.6 Ω would be sufficient. The 1.5 Ω resistors have resulted from a slightly different way of reasoning, which we feel to be incorrect at present. The crowbar ignitrons I_2 are of type PL 5552 A.

The ignitrons are fired by pulses from the ignition circuits (§ 3), I_2 slightly after the maximum of the current pulse.

To detect failure of an ignitron to fire, the anode currents are measured by the current transformers M_1 and M_2. The indication circuits are described in § 6.

§ 3. *Ignition circuits.*

The firing of the ignitrons is achieved by feeding a 10 μsec., 1 kV pulse into the firing electrode of the ignitron. All 18 circuit sections immediately connected to the two sets of nine firing electrodes are identical. They are separated from the operating devices by isolation transformers (fig.IV.6).

The relay D_2 is opened by the mains switch of the charging rectifiers, prohibiting ignition during the charging of the capacitors.

The ignition is started by closing relay D_3, which is operated by the control circuits (§ 6). After closing D_3 a current flows through R_{17} and R_{18} from capacitor C_5, raising the voltage of the plus pole of U_1 by 200 V. This makes the grid of thyratron T_1 positive and capacitor C_5 discharges further over T_1 and the ignitor circuit of I_3. The network with the inductance L_2, the resistors R_6, R_7, and the diodes N_2 extends the duration of the tail of the discharge to ensure ignition of I_3.

The firing of I_3 makes the capacitors C_2 discharge and the current flows through the primaries of the isolation transformers M_3 (fig.IV.6b). The induction current in the secondaries of M_3 fires the ignitrons I_1, which makes the main capacitors discharge.

The current pulse through T_1 induces a voltage in the current transformer M_4. This transformer is connected to a delay circuit with an adjustable delay time, which can be varied between 1 and 20 msec. The delay circuit gives a delayed pulse of 200 V, which makes the grid of T_2 140 V positive, and C_6 discharges. The further procedure is equal to that in the primary circuit described above, making I_2 fire a preset time after I_1.

The damping resistors R_{8a} to R_{8i} are necessary because without them the main ignitrons I_1 fire irregularly, probably because of oscillations in the current leads to the magnet coil. The values of the resistors have been determined empirically. We suppose the difficulty to be connected with the geometrical arrangement of the capacitor sections side by side in a linear

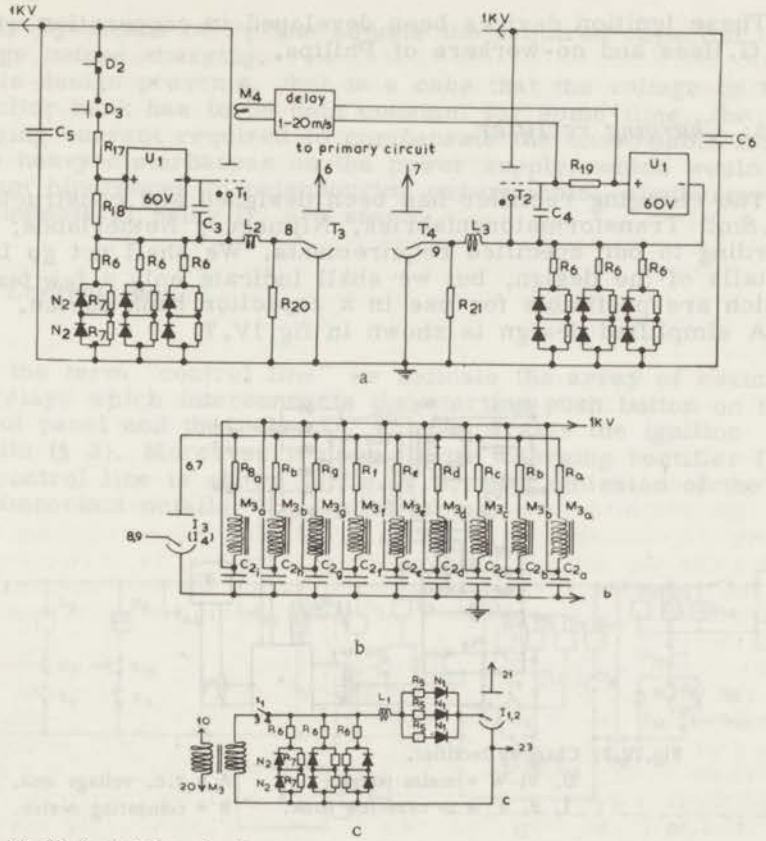

Fig. IV.6. Ignition circuits.

a. Operating circuit.
b. Primary circuit (2x).
c. Secondary circuit (18x).

$I_1 = I_2$ = PL 5552 A.
$I_3 = I_4$ = PL 5551 A.
$T_1 = T_2$ = PL 5684.
U_1 = Philips type 1289 voltage unit.
$N_1 = N_2$ = BY 100.
M_3 = transformer 1:1; 3.5 kV.
$L_1 = L_2 = L_3$ = 25 μH.
$C_2 = C_5 = C_6$ = 1 μF; 1 kV.
$C_3 = C_4$ = 100 pF.
$R_5 = R_6$ = 0.5 Ω.
R_7 = 110 kΩ.
$R_8 = R_9$ = 21 Ω.
$R_{10} = R_{11}$ = 16.5 Ω.
$R_{12} = R_{13}$ = 15 Ω.
R_{14} = 11 Ω.
$R_{15} = R_{16}$ = 10 Ω.
R_{17} = 40 kΩ.
R_{19} = 50 kΩ.
$R_{18} = R_{20} = R_{21}$ = 10 kΩ.
21, 23 = to main circuit.
10, 20 = to primary circuit.
8, 9 = to operating circuit.

row, making the distances from the sections to the coil rather different from each other. This feeling is confirmed by the fact that the nearer the sections are to the coil, the higher the damping must be.

These ignition devices been developed in cooperation with ir G.Hess and co-workers of Philips.

§ 4. *Charging rectifier.*

The charging rectifier has been designed and constructed by W.Smit Transformatorenfabriek, Nijmegen, Netherlands, according to our specified requirements. We shall not go into details of the design, but we shall indicate only a few features which are profitable for use in a capacitor bank device.
A simplified design is shown in fig.IV.7.

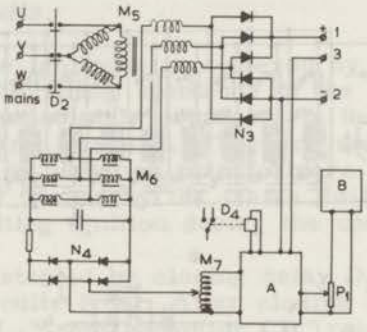

Fig.IV.7. Charging rectifier.
U, V, W = mains power. A = d.c. voltage unit.
1, 2, 3 = to capacitor bank. B = comparing device.

The city power is switched on by the relay D_2. Transformer M_5 transforms the 3 x 380 V a.c. up to 3 x 3 kV a.c., which is rectified by N_3, giving a 4 kV d.c. voltage, which is supplied to the capacitors.
In series with the secondary coils of the transformer M_5 the chokes M_6 are connected. The iron cores of these chokes can be presaturated by a direct current, supplied by the transformer M_7 via the rectifiers N_4. The variable transformer M_7 is mounted on the control panel. A high voltage delivered by M_7 gives a high d.c. current in M_6, increasing the charging current to the capacitor bank. The device enables charging with a constant current, adjusted by M_7, between 0 and 9 amperes.
The voltage for M_7 is supplied by an apparatus which compares the capacitor voltage in an indirect way with the voltage preset by potentiometer P_1. If the capacitor voltage approaches the preset value, the voltage at the primary of M_7 decreases, and the impedance of M_6 increases, which reduces the charging current to the capacitor bank. When the capacitor voltage has reached its preset value, relay D_4 is operated, and D_2 is opened by the control line (§ 5). P_1 is mounted on the control

panel. By means of P_1 one adjusts the required capacitor voltage before charging.

This design prevents, that in a case that the voltage on the capacitor bank has to be held constant for some time, the charging current required to compensate the unavoidable losses, gives heavy disturbances on the power supply, which would present hindrances to neighbouring experiments. Furthermore the contacts of relay D_2 are saved.

§ 5. *Control line.*

By the term "control line" we indicate the array of switches and relays which interconnects the starting push button on the control panel and the relay D_3 which operates the ignition circuits (§ 3). Moreover it controls the charging rectifier (§ 4). The control line is shown in fig.IV.8, with omission of the less important details, e.g. pilot lamps.

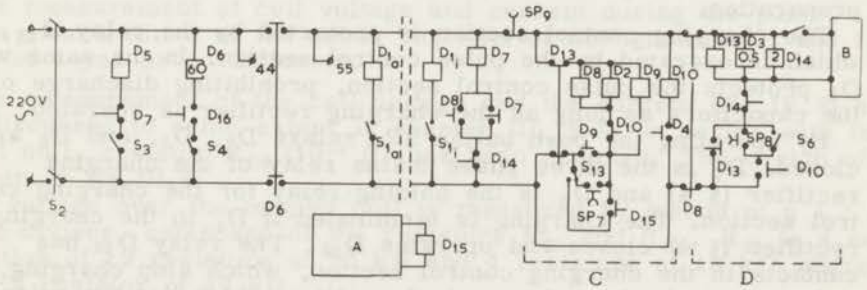

Fig.IV.8. Control line.

A = electronic timing device. S = switch.
B = camera. SP = push button switch.
C = charging control section. D_{10} = coil of relay D_{10}.
D = pulsing control section. D_{10} = contacts of relay D_{10}.
D_{10} [20] = coil of time relay D_{10} with 20 seconds retardation.

The following description is in chronological order of circuit operation, and generally from left to right in fig.IV.8.

The power for the control line is supplied by the 220 V a.c. mains, and switched on by the mains switch S_2.

If S_2 is closed, the relay D_5 is energized, which controls the circuits for measuring the self-inductance and the resistance of the magnet coil (§ 6). D_5 can be switched off by the switch S_3, and it is protected by the relay D_7, which is energized if the capacitor bank is, or has been, charged or is pulsed.

The relay D_6 switches on after 60 seconds, provided D_{16} and and S_4 have been closed. D_{16} and S_4 replace safety devices on

the flow of cooling water for the ignitrons, the closing of the entrance door of the high voltage room, and an emergency switch on the control panel. The 60 seconds have been introduced to permit the cathodes of the thyratrons T_1 and T_2 (fig.IV.6a) to reach their proper operating temperature before the anode voltage is switched on. The cathode heaters and the auxiliary equipment are connected to the contact 44.

If D_6 is closed, the connection 55 provides the 1 kV d.c. supply of the ignition circuits (§ 3). The nine parallel relays D_1 are operated, provided that the switches S_1 have been closed. We recall that D_1 is the safety relay and S_1 the main switch of the main unit (§ 2). This device ensures that the capacitor sections are discharged automatically if the mains voltage vanishes.

D_7 is the protecting relay of the measuring circuits (§ 6). It is only operated if D_8 in the charging control section is closed. Then it holds itself independently of D_8, until D_{14} in the pulse control section is opened.

The remaining control circuits can be blocked by the push button switch SP_9, permitting one to interrupt charging or pulse-preparation.

The charging control section is protected by the relay D_{13}, which is operated by the pulse control section. In the same way D_8 protects the pulse control section, prohibiting discharge of the capacitors as long as the charging rectifier is operated.

By operating the push button SP_7 relays D_2, D_8, and D_9 are closed. D_2 is the three phase mains relay of the charging rectifier (§ 4) and D_9 is the holding relay for the charging control section. The charging is terminated if D_4 in the charging rectifier (§ 4) closes and operates D_{10}. The relay D_{10} has contacts in the charging control section, which stop charging, and contacts in the pulse control section, which set the pulse control section free for operation.

The pulse control section can be put into operation in two ways:

a. If S_6 has been closed, the pulse control section is put into operation automatically by D_{10}.

b. If S_6 has been opened, the pulse control section is put into operation by pressing the push button SP_8.

If the pulse control section is operated, D_3, D_{13}, and D_{14} are energized and the shutter of the oscilloscope camera is opened, provided S_5 has been closed. D_{13} is the holding relay of the pulse control section, which protects the charging control section too. D_3 is the pulse relay which starts the ignition pulse (§ 3). It closes 0.5 sec. after the switching on of the power to circumvent the mechanical slowness of the camera shutter.

Two seconds after the switching on of the power, D_{14} opens all contacts, restoring the initial situation and closing the camera shutter. The two seconds permit one to take advantage of the persistance of the trace on the oscilloscope screen for

a brighter photograph without an undue trace intensity on the oscilloscope.
Not all functions of the relays have been shown in this picture. This accounts for the apparent duplication of some of the relays, e.g. D_7 and D_5, D_4, and D_{10}.
In this way a completely automatic control line is achieved if S_6 has been closed. The control line is protected against failure of the central supplies. The automatic process can be interrupted if necessary. The device is completed by D_{15}, which is controlled by an electronic timing device. This is not discussed here. The timing device closes D_{15} at regular time intervals between 30 sec. and 45 minutes, depending on the time required to cool the magnet coil down to its initial temperature after the pulse.

§ 6. *Devices for the measurement of circuit characteristics.*

To obtain some information on the behaviour of the coil and the apparatus, some devices have been constructed in addition to the ordinary voltage and current meters on the charging rectifier.
a. The measurement of coil voltage and current during the pulse.
b. The measurement of the anode currents of the ignitrons I_1 and I_2 by means of a yes or no indicator.

a. The measurement of the coil voltage and the current (fig. IV. 9) has been discussed to some extent in chapter III, § 9. In series with the magnet coil, resistor R_{24} ($10^{-4}\ \Omega$) has been mounted. The design of R_{24} is shown in fig. III. 8.
The voltage over the magnet coil is measured by means of a 1 : 100 voltage divider, composed of the resistors R_{22} and R_{23}. R_{22} is a series connection of 19 resistors of 50 kΩ and 4 resistors of 10 kΩ whereas R_{23} is a resistor of 10 kΩ.
In fig. IV. 9 the circuits for the measurement of the resistance and the self-inductance of the magnet coil after the pulse are shown too. The drawing is self-explanatory. The ampere meter is of a common 2 % panel-mount type, the voltmeter is a Philips GM 2010 electronic voltmeter and the inductance bridge a Danbridge UB 2. The circuits are protected by the 3.5 kV isolated contacts of D_5 (§ 5).

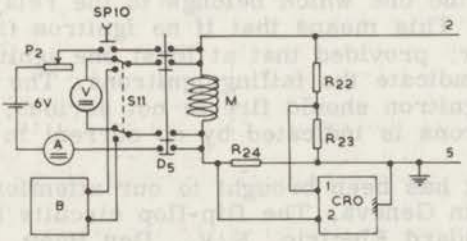

Fig. IV. 9. Device for the measurement of the coil characteristics.
B = inductance bridge. M = magnet coil.

b. The yes or no indicator to detect the anode current of the ignitrons I_1 and I_2 is shown in fig.IV.10.

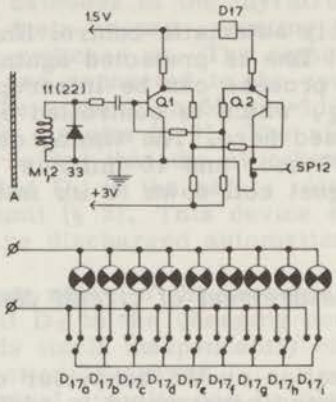

Fig.IV.10. Yes or no indicator for anode current ignitrons I_1 and I_2.
a. Flip-flop and reset.
b. Relay contacts and pilot lamps.
A = cathode lead ignitron.
Q = transistor.
SP = push button switch.
= pilot lamp.

The signal from the current transformers M_1 and M_2 (§ 2) is fed into a flip-flop circuit (fig.IV.10a), which is biased to make Q_1 conductive if SP_{12} is pressed.

If a positive signal is applied to the basis of Q_1, with SP_{12} closed, Q_2 becomes conductive. In the collector lead of Q_2, the relay coil of D_{17} has been mounted, so that D_{17} is operated. By pushing SP_{12}, Q_1 becomes conductive again and D_{17} switches back (reset).

The connection of the contacts of the 9 relays D_{17} for the I_1 ignitrons is shown in fig.IV.10b. The set for the I_2 ignitrons is identical.

In the position shown, which is not activated, none of the lamps is lighted. If one of the relays is operated, all lamps are lighted except the one which belongs to the relay which has been operated. This means that if no ignitron fires no lamp is lighted. However, provided that at least one ignitron fires, the lighted lamps indicate the failing ignitrons. The condition that at least one ignitron should fire is not serious, because failure of all ignitrons is indicated by no current in the magnet coil.

The relay circuit has been brought to our attention by dr N.Doble of CERN in Geneva. The flip-flop circuits have been constructed by Standard Electric, N.V., Den Haag.

§ 7. *Conclusions.*

The apparatus which has been described in this chapter provides a fully automatically operated capacitor bank pulse generator.

The crowbar device is, in contrast to common practice, slightly undercritically damped to prevent the exceding of the maximum duration of current flow which is permitted by the ignitrons. The crowbar device has been split over the capacitor bank sections.

Up to now we did not test the apparatus as a whole at its full energy.

We tested the current capacity of not more than three sections simultaneously on an existing 4 mH coil with a field of 22 Oe/A in a bore of 8 cm. The maximum current has been 2.1 kA per section, at 3.5 kV capacitor voltage, indicating sufficient current carrying capacity.

We have constructed a test coil of 1.3 mH (coil 22 in chapter II) which has been damaged at 12 kA with the capacitor voltage at 2.7 kV. This gives an energy content of the capacitor bank of 110 kJ and a current per section of 1.33 kA.

References.

1. P.Kapitza, Proc. Roy. Soc. A 105 (1924), 691.
2. H.P.Furth and R.W.Waniek, Rev. Sc. Instr. 27 (1956), 195.
3. S.Foner and H.H.Kolm, Rev. Sc. Instr. 28 (1957), 799.
4. I.S.Jacobs and P.E.Lawrence, Rev. Sc. Instr. 29 (1958), 712.
5. P.Cotti, Z. angew. Math. Phys. 11 (1960), 17.
6. E.Braunersreuther, J.C.Combe, L.Hoffmann, and M.Morpurgo, CERN report 62-7.

B. SOME EXPERIMENTS IN PULSED MAGNETIC FIELDS

V. MEASUREMENTS IN PULSED MAGNETIC FIELDS

§ 1. *Introduction.*

In the second part of this thesis we describe two investigations in pulsed magnetic fields and the experimental methods used for them. The methods are not entirely new, but we hope that we present a useful analysis of these methods. Special emphasis is laid on the removal of the heavy disturbances which are introduced in the measuring apparatus by the pulsed field itself.

To give an idea of the research that has already been done in pulsed magnetic fields we present in the next section a short survey of this work with a list of references, in which only the most important research is included.

The remainder of this chapter is devoted to the analysis and description of our measuring apparatus.

In the chapters VI and VII we give our measuring results, together with a discussion in the light of theoretical considerations, if these are available.

§ 2. *Historical survey, containing a short bibliography.*

(The reference numbers in this section correspond to appendix V.1).

The starting point of the research in pulsed magnetic fields is marked by Kapitza, who started the development of coils and current generators as well. From the review it will appear that he commenced research on an amazingly large number of subjects and some of his results, especially his ideas on measuring methods, are still of interest.

We now give the most important investigations, arranged by subject.

a. *Measurements of resistivity.*

In this part we summarize measurements of resistivity and Hall effect on metals and semiconductors. The measuring method is generally a fourpoint measurement, with or without a compensation scheme.

1. *Metals.*

Since Shoenberg's work[1,2] demonstrated the possibilities of using pulsed fields for the detection of the geometry of the Fermi surface, many measurements on the Shubnikov-de Haas effect in metals have been done in pulsed fields. For a review of data on Fermi surfaces see ref.[5] and the review article by Fawcett[6].

The first measurements on resistance in pulsed fields have been made by Kapitza[9,10]. These measurements have been done on single crystals of Bi and polycrystalline samples of Bi and a large series of other metals.

The measurements on polycrystalline samples have been repeated and extended by Olsen, Lüthi, and Cotti[11,12,13,14,15]. One of their main contributions is on the special difficulties of eddy currents and geometrical effects which are encountered in the study of metals in pulsed magnetic fields.

Recently Grassie[16] made some measurements on Sn and Pb.

2. *Semiconductors.*

The measurement of resistance of semiconductors in pulsed magnetic fields is basically more simple than in the case of metals, because of the high specific resistance of the materials. However, the interpretation is difficult, because of the complications which are introduced by the bandstructure.

We mention the work on n-Ge by Zavadskii and Fakidov[17,18], by Love, Wei, and Diesel[19,20], and by Hendrikx[21]; the work on InSb by Champness[22], on InSb, InAs, and $In(As_{0.8}\ Pb_{0.2})$ by Braunersreuther, Kuhrt, and Lippmann[23], and on p-Bi_2Te_3 by Auch and Landwehr[24].

3. *Superconductors.*

A number of investigations has been performed on the resistive transition of hard superconductors, as Nb 25 % Zr and Nb_3Sn. The measurement is simple, on one hand, because the effect is large, and because the specific resistance in the normal state is not very small. On the other hand, if one measures the transition field as a function of the transport current, large Lorentz forces act upon the sample, introducing noise.

The transition field of Nb_3Sn has been measured by Hart, Jacobs, Kolbe, and Lawrence[25] and by Cline, Kropschot, Arp, and Wilson[26]. For measurements on other materials we refer to the paper by Berlincourt and Hake[27].

However, the measurements by Dietrich and Weyl[28] and by Flippen[29] on Nb 25 % Zr wires and by van der Sluijs, de Beun, Zweers, and de Klerk[30] on Nb_3Sn ribbon showed that the behaviour of hard superconductors in pulsed magnetic fields can differ significantly from the behaviour in static fields. The work described in reference[30] is given in chapter VII of this thesis.

b. *Magnetisation.*

The first magnetisation measurements in pulsed magnetic fields have been made by Kapitza[31,32,33] by means of a spring balance, based on the force which a magnetic sample experiences in an inhomogeneous magnetic field.

A modern version of this method has been developed by Stevenson [34,35], who used a transducer. Kapitza studied several metals and gadolinium sulphate, while Stevenson studied some manganese compounds.

1. *Metals by the induction method.*

At present the most frequently used method for the measurement of magnetisation in pulsed magnetic fields is the method with compensated coils, developed by Shoenberg[1,3].

Shoenberg studied the de Haas-van Alphen effect in metals and made the first measurements on the Fermi surface of Cu, Ag, and Au. For a review article on the de Haas-van Alphen effect we refer to the papers by Shoenberg[2], Kahn and Frederikse[4], and to reference[7].

The many measurements of the de Haas-van Alphen effect which have been done since Shoenberg's pioneer work we arrange by material : Be[36], Na[40], Mg[37], Al[37], K[40], Cr[44], Fe[42], Cu[3], Rb[39,40], Ag[3], Cd[43], Sn[1], Cs[40,41], Gd[38], Au[3], Pb[1,45].

2. *Compounds by the induction method.*

Another field in which the pulsed field technique has proved to be successful is the study of the magnetic behaviour of compounds. Although some of the metal studies concern the magnetic order too[38,44], the compounds have been studied more extensively.

The pioneer work has been done by Jacobs, Rodbell, Lawrence, Kouvel, and Silverstein[46,47,48,49,50,51,52] on MnF_2, MnAs, $CoCl_2$, EuTe, if we forget for the moment about the older work done by Foner (see section c).

Special reference should be made to the work done by de Blois[53,54] on MnAs with a miniature coil technique. Finally we mention the work by Allain, Varret, and Miédan-Gros[55] on $ZnCr_2Se_4$, by Asti, Colombo, Giudici, and Levialdi[56] on $Ba0.6Fe_20_3$, and by Zweers, de Klerk, and the present author on $CuCl_2.2H_20$[57]. The measurements described in reference[57] are discussed in more detail in chapter VI of this thesis.

c. *Microwave experiments.*

In pulsed magnetic fields the measurements in the microwave or optical range are essentially simpler than the measurements sub a and b, because the noise spectrum, inherent to pulsed magnetic

fields, does not extend into the measuring frequency range.

The microwave measurements have been pioneered by Foner[6], who has done the greater part of the research in this field. His main object was antiferromagnetic resonance and he was able to make an estimate of exchange constants, which are too large to be attainable by d.c. methods. We mention his measurements on MnF_2[49] or Cr_2O_3[50], and compounds containing these materials[58,59,60,61].

A special branch in this field is the excitation of masers by pulsed fields[62,63,64,65].

d. *Optical experiments.*

Optical experiments were first made by Kapitza, who studied the Zeeman effect in pulsed fields[66,67].

The more recent optical studies concern the Faraday-effect[68,69,70,71], but these experiments are limited to field measurements only. To our knowledge there are no successful measurements of the magnetic properties of compounds by means of the Faraday effect up to now.

e. *Field measurement.*

A final remark should be made on the measurement of the field strength of the pulsed magnetic field. No references will be given, because an excellent bibliography has been published recently[8].

1. *Current through the magnet coil.*

$$H = \text{constant} \times I_{coil}.$$

The constant is determined by a conventional method at low field strength. This method is simple, but it has the draw-back of being sensitive to mechanical deformation of the magnet coil during the field pulse and to eddy current distortion of the magnetic field. However, our experiments indicate that this error is not more than a few percent up to 400 k0e.

2. *Pick-up coil.*

The induction voltage in a pick-up coil is integrated and displayed on an oscilloscope. The pick-up coil is calibrated at low fields against a field standard. The instrumental error is a few percent larger than in case 1, but the errors of case 1 are not present. However, the method is sensitive to motion of the pick-up coil in the magnetic field. Our experiments indicate that the method is equivalent to the former one.

3. *Physical effects.*

Of the physical effects, commonly used to measure d.c. magnetic fields, only these which are linear with the magnetic field are suitable. The Hall effect and magneto-resistance are unsuitable as long as their linearity in the high field region has not been established by independent methods. Proton resonance is excluded too because of the requirements which the method imposes on the homogeneity in space and time of the magnetic field. In principle the second objection can be removed by using electron spin resonance.

The only method which is successful is the Faraday effect in quartz, which has been used in a number of cases (e.g. reference [68, 69, 70, 71]).

§ 3. *Noise in pulsed magnetic fields.*

Measurements in pulsed magnetic fields are complicated by noise, as are all measurements. However, apart from the common sources of noise such as sources of statistical noise, vibrations of the building, other measuring devices, and traffic, one is also bothered with sources of nonstatistical noise which are inherent to the pulsed magnetic field. The most evident ones are:

1. Noise generated by the switches.
2. Noise which is caused by the short duration of the pulsed magnetic field.

The noise which is caused by the switches is generated in the beginning, and after the closing of the crowbar. The cause is the jitter of the ignitrons. In general this jitter consists of large numbers of very sharp pulses. Because the ignition time of the ignitrons is of the order of 10 μsec., we estimate the basic frequency of the jitter to be larger than 1 MHz. These frequencies are far outside the frequency range of the measuring apparatus which has been used in our investigations. In general the jitter is seen in the very beginning of the measuring period, perhaps via a capacitive coupling of the mains. The jitter noise can be reduced by careful decoupling of the measuring apparatus from the mains, e.g. via an isolation transformer. For an analysis of this high frequency noise we refer to a paper by Medley, Curzon, and Daugheney[1].

The short duration of the magnetic field itself causes noise too. This becomes clear if one expands the field, which can be written as a function of time as:

$$\begin{cases} H(t) = H_o \sin \omega t & \text{for } 0 \leqslant t < t_p \\ H(t) = 0 & \text{for all other } t \end{cases} \qquad (V.1)$$

$$\text{with } \omega = \pi / t_p .$$

in a Fourier series, assuming that the field signal is continued periodically in time with a period $2t_p$. One obtains readily:

$$H(t) = H_o \left[\frac{1}{2\pi} + \tfrac{1}{2} \sin \omega t - \frac{1}{\pi} \sum_{n=1}^{\infty} \frac{\cos 2n\omega t}{(2n)^2 - 1} \right] \qquad (V.2)$$

This field is introduced as disturbances in the circuit:

$$E_{ind.} = - \frac{d\phi}{dt} \qquad (V.3)$$

and the effective contribution of each series coefficient will be $\frac{2n\omega}{(2n)^2-1}$ making the high frequency terms more important than in (V.2).

We shall not proceed with the field derivative, but we suppose that we have a measuring circuit which is coupled to the magnet coil by means of a mutual inductance M_1. In practice one reduces the inductive signals by connecting a second inductance M_2 in series with M_1 (fig. V.1). As far as we know this analysis has not been published before.

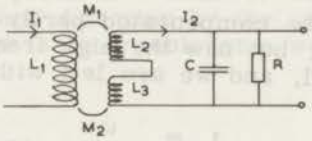

Fig. V.1. Model of a measuring circuit with inductive noise.

We assume that the measuring circuit is loaded by the input resistance of the measuring instrument, with the combined capacity of the cables and the measuring instrument connected in parallel.

The equation for the complex current in the measuring circuit I_2 is:

$$I_2 (j\omega L + z) = j\omega (M_2 - M_1) I_1 \qquad (V.4)$$

with $L = L_2 + L_3$ and $\frac{1}{z} = \frac{1}{R} + j\omega C$.

In practical cases the inductance $j\omega L$ is much smaller than z and the voltage on the input of the measuring instrument can be written:

$$U = j\omega (M_2 - M_1) I_1 \qquad (V.5)$$

For I_1 we substitute an expression of the form (V.2) with the d.c. term omitted:

$$U \equiv \mathrm{Re}\,(U) = \Delta M\, I_o \left[\frac{\omega}{2} \cos \omega t + \frac{1}{\pi} \sum_{n=1}^{\infty} \frac{2n\omega}{(2n)^2-1} \sin 2n\omega t \right] \quad (V.6)$$

This noise signal can be removed by subtraction of a signal of the form (V.4) with the proper amplitude, which we differentiate before subtraction. If this subtraction is successful the noise signal is reduced by a factor a:

$$U_{res.1} = a.\, \Delta M\, I_o \left[\frac{\omega}{2} \cos \omega t + \frac{1}{\pi} \sum_{n=1}^{\infty} \frac{2n\omega}{(2n)^2-1} \sin 2n\omega t \right] \quad (V.7)$$

However, practical inductances will never be purely imaginary and so ΔM will contain a real part. It cannot be expected that the real and the imaginary part can both be compensated, so that if the proportion of the real to the imaginary part is b, the resulting noise will be:

$$U_2 = b.\, \Delta M\, I_o \left[\frac{\omega}{2} \sin \omega t + \frac{1}{\pi} \sum_{n=1}^{\infty} \frac{2n\omega}{(2n)^2-1} \cos 2n\omega t \right] \quad (V.8)$$

This noise can be compensated partly by subtracting a signal of the form (V.2), but now the high frequency terms cannot be compensated at all, and we are left with:

$$U_{res.2} = b.\, \Delta M\, I_o \frac{1}{\pi} \sum_{n=1}^{\infty} \frac{\omega}{2n-1} \cos 2n\omega t \quad (V.9)$$

Finally the compensating signals will have a certain phase difference, say tg δ, which results in :

$$U_{res.3} = \mathrm{tg}\,\delta\, \Delta M\, I_o \left[\frac{\omega}{2} (\cos \omega t + b \sin \omega t) + \frac{1}{\pi} \sum_{n=1}^{\infty} \frac{2n\omega}{(2n)^2-1} \sin 2n\omega t \right] \quad (V.10)$$

and a similar term for (V.9). This term, however, is a second order contribution, which we omit.

Adding (V.7), (V.9) and (V.10) the residual noise is:

$$U_{res.} = \Delta M\, I_o \left[\frac{\omega(\mathrm{tg}\,\delta + a)}{2} \cos \omega t + \frac{\omega b\, \mathrm{tg}\,\delta}{2} \sin \omega t + \frac{b}{\pi} \sum_{n=1}^{\infty} \frac{\omega}{2n-1} \cos 2n\omega t + \frac{a + \mathrm{tg}\,\delta}{\pi} \sum_{n=1}^{\infty} \frac{2n\omega}{(2n)^2-1} \sin 2n\omega t \right] \quad (V.11)$$

To make a numerical estimate we take $I_0 = 5 \times 10^3$ A; $L_1 = 10^{-2}$ H; $L_2 = 10^{-3}$ H; $k = 0.1 \longrightarrow M_1 = -M_2 = 10^{-3}$ H and we assume ΔM to be 10^{-5} H. Further we assume the compensations to be made accurate to 1 %, so $a = b = \text{tg}\,\delta = 10^{-2}$. $\omega = 150$ rad/sec. The resulting noise is (in mV):

$$U_{res.} = 75 \cos \omega t + 0.75 \sin \omega t + 25 \cos 2 \omega t + 8.5 \cos 4 \omega t + \\ + 5 \cos 6 \omega t + \text{-----} + 50 \sin 2 \omega t + 12 \sin 4 \omega t + \\ + 9 \sin 6 \omega t + \text{-----} \qquad (V.12)$$

For a resistance measuring circuit L_2 is generally a factor 10^3 smaller, so M_1, M_2 and ΔM can be supposed to be lowered by a factor 30, and the noise is lowered by the same factor. In practice, however, it is more difficult to achieve good equality of the inductances in this type of devices.

In the case that the noise level is unacceptable, one can gain a factor 2n in each noise term by integrating the signal. The basic noise signal is in phase with the measuring signal and gives no serious distortion. In practical cases we had measuring signals of the order of some millivolts, a low frequency noise of the order of some parts of a millivolt and the high frequency noise suppressed beyond detection by the oscilloscope. The only terms which remained to be troublesome were the n = 1 and 2 terms.

§ 4. *Measuring apparatus.*

a. *Resistance measurement.*[3)]

We measured the change in resistance of a ribbon of superconductive material. The main signal was the appearance of the voltage caused by a current of at least 250 mA over the resistance in the normal state of 30 mΩ, though it was desirable to detect changes of a few percent of the normal resistance as well.

If the ribbon is mounted parallel to the axis of the magnetic field, no noise signal is present. It is not always possible to use this configuration and therefore we mounted a not adjustable dummy sample tightly against the measuring sample and the voltage leads (fig. V.2). In some cases this proved to be sufficient to reduce the noise to an acceptable level, but in other cases an extra compensation has to be added.

At the time we had no good electronic integrators, so we obtained the differentiated field signal by a pick-up coil placed in the field of the magnet coil. The use of phase shift devices proved to be unsatisfactory, because the phase equality which was attainable with these devices turned out to be inferior to

the phase equality which could be obtained by careful mounting of the sample and the voltage connections.

The measuring apparatus is shown schematically in fig. V.2.

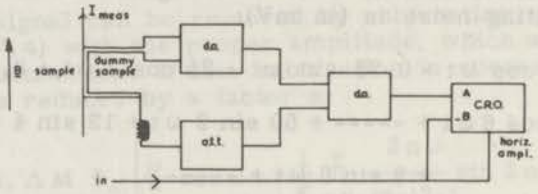

Fig. V.2. An apparatus for measuring resistance in pulsed magnetic fields.
d.a. = differential amplifier Tektronix 511.
att. = variable attenuator.
CRO = Tektronix RM565 with 3A72 plug in.
in = signal proportional to coil current.

b. *Magnetisation measurements*[4].

We wanted to make a measurement oi the transitions in magnetically ordered materials, by measuring the susceptibility. The experiments have been made on MnF_2, MnO_2, and $CuCl_2.2H_2O$. The respective susceptibilities below the Néel temperature T_N are:

MnF_2: $\chi_\perp = 1.08 \times 10^{-3}$ (Bizette[5]).
MnO_2: $\chi_\perp = 7.0 \times 10^{-5}$ (Bizette[5]).
$CuCl_2.2H_2O$: $\chi_\perp = 1.48 \times 10^{-4}$ (van den Handel c.s.[6]).

The experimental results on $CuCl_2.2H_2O$ have been described in chapter VI. The experiments on MnF_2 and MnO_2 did not yield positive results. In § 5 they will be summarized.

The measuring method is analogous to that developed by Jacobs and Lawrence[7].

Two coils with each n turns are connected in such a way that $M_1 = -M_2$. One of the coils contains the sample (fig. V.3).

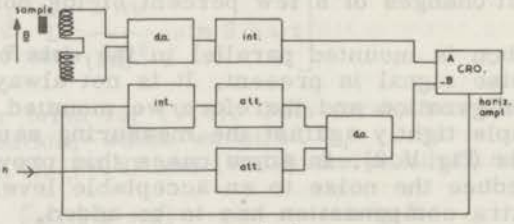

Fig. V.3. Circuit for magnetisation measurements.
d.a. = differential amplifier Tektronix 511.
att. = variable attenuator.
int. = electronic integrator Tektronix 3A8.
CRO = Tektronix RM565 with 3A72 plug in.
in = signal proportional to coil current.

The measuring signal is:

$$E_{ind.} = - n \varkappa S \frac{dB}{dt} \qquad (V.13)$$

Because of the dimensions of the cryostat, $S = \pi (1.5 \times 10^{-3})^2$ m^2 and $\frac{dB}{dt} \leqslant 4.5 \times 10^3$ W/m^{2}sec. The best coils we made have $n = 3 \times 10^3$, but most measurements have been made with $n = 1.6 \times 10^3$ the wire thickness being 30 μm. The self-inductance of the measuring coils is about 10 mH. The measuring signal then is $50 \varkappa$ V, so for MnF_2 50 mV, for MnO_2 0.35 mV, and for $CuCl_2.2H_2O$ 8.5 mV.

The signal to noise ratio is not very favourable, and in practice it turned out, that the signals were heavily disturbed by high frequency noise. Therefore we integrated the signal.

The sample can be removed from the measuring coil when immersed in the liquid helium, thus making it possible to make the initial adjustments after cooling down the coil system. This is necessary because temperature changes influence ΔM. Sometimes readjustments between measuring points have to be made.

The adjustment of ΔM can be made by moving the coil system up and down in the pulse magnet. After finding the optimum place, the coil system is fixed, and the remaining signal without sample is minimized by adjusting the attenuators (fig. V.3).

In this way the measurements on MnF_2 and $CuCl_2.2H_2O$ could be made easily. The measurements on MnO_2 required some more attention, but proved to be possible.

§ 5. *Summary of the measurements on MnF_2 and MnO_2.*

For the definitions of H_{a-b} and H_{b-p} we refer to chapter VI, § 2.

1. MnF_2. In experiments at liquid helium temperature we observed the H_{a-b} transition at 93 kOe, as measured previously by Jacobs[8]. A search for the H_{b-p} transition at 4° K did not yield any result below 300 kOe, as had to be expected from theory ($H_{b-p}(0)$ as predicted by molecular field theory = 600 kOe).
2. MnO_2. The magnetisation has been measured both at liquid helium temperature and in the neighbourhood of $T_N = 84°$K. In neither case any transition has been detected. The negative result in the neighbourhood of T_N suggests, that the curve of $H_{b-p}(T)$ rises sharply as in the case of $CuCl_2.2H_2O$ (see chapter VI), thus making a measurement without a very careful temperature control difficult. At T = 0 the transition field prediction by molecular field theory is of the order of 1 MOe.

References.

1. S.S.Medley, F.L.Curzon, and C.C.Daugheney, Can. J. Phys. 43 (1965), 1882.
2. J.C.A.van der Sluijs, H.R.de Beun, B.A.Zweers, and D.de Klerk, Bull.Belg.Phys.Soc. V, 2 - 3, (1966), 165.
3. J.C.A.van der Sluijs, H.R.de Beun, B.A.Zweers, and D.de Klerk, to be published (1967).
4. J.C.A.van der Sluijs, B.A.Zweers, and D.de Klerk, Phys. Lett. 24A (1967), 637.
5. H.Bizette, J. Phys. Rad. 12 (1951), 161.
6. J.van den Handel, H.M.Gijsman, and N.J.Poulis, Physica 18 (1952), 852.
7. I.S.Jacobs and P.E.Lawrence, Rev. Sci. Instr. 29 (1958), 713.
8. I.S.Jacobs, J. appl. Phys. 32 (1961), 61 S.

APPENDIX V.1. BIBLIOGRAPHY ON MEASUREMENTS IN PULSED MAGNETIC FIELDS.

A. *General orientation and review articles on related subjects.*

1) D. Shoenberg, Physica 19 (1953), 795, on the de Haas van Alphen effect in pulsed fields.
2) D. Shoenberg, Progress in low temperature physics, ed. C. J. Gorter, 2 (1957), 226, on the de Haas van Alphen effect.
3) D. Shoenberg, Phil. Trans. Roy. Soc. 255 (1962), 85, on the de Haas van Alphen effect in copper, silver and gold.
4) A. H. Kahn and H. P. R. Frederikse, Solid state phys. 9 (1959), 257, on the de Haas van Alphen effect in high magnetic fields.
5) The Fermi Surface, New York 1960, a symposium report.
6) E. Fawcett, Adv. Phys. 13 (1964), 139, on the galvanomagnetic phenomena.
7) S. Foner, High magnetic fields, Boston 1961, p. 489, on microwave measurements in pulsed magnetic fields.
8) C. Germain, Nucl. Instr. Meth. 21 (1963), 17, a bibliography on measuring methods of the magnetic field strength.

B. *Resistance.*

metals.

9) P. Kapitza, Proc. Roy. Soc. A 119 (1928), 358; 387; 401.
10) P. Kapitza, Proc. Roy. Soc. A 123 (1929), 292; 348.
11) B. Lüthi and J. L. Olsen, Nuovo Cimento X, 3 (1956), 840.
12) B. Lüthi, Helv. Phys. Acta 33 (1960), 161.
13) P. Cotti, Helv. Phys. Acta 33 (1960), 517.
14) P. Cotti, B. Lüthi and J. L. Olsen, High magnetic fields, Boston, 1961, p. 523.
15) P. Cotti, High magnetic fields, Boston, 1961, p. 517.
16) D. Grassie, Conf. High magnetic fields, Oxford, 1963, unpubl.

semiconductors.

17) I. G. Fakidov and E. A. Zavadskii, Fiz. Metal. Metallov. 7 (1959), 637.
18) E. A. Zavadskii and I. G. Fakidov, Fiz. Metal. Metallov. 11 (1961), 145, 147.
19) W. F. Love and W. F. Wei, Phys. Rev. 123 (1961), 67.
20) T. J. Diesel and W. F. Love, Phys. Rev. 124 (1961), 666.
21) H. Hendrikx, Thesis, Leuven. (1963).
22) R. Champness, High magnetic fields, Boston, 1961, p. 528.
23) E. Braunersreuther, F. Kuhrt, and H. J. Lippmann, Z. Naturf. 15a, (1960), 795.
24) K. Auch and G. Landwehr, Z. Naturf. 18a, (1963), 424.

superconductors.

25) H. R. Hart, I. S. Jacobs, C. L. Kolbe, and P. E. Lawrence, High magnetic fields, Boston 1961, p. 589.
26) D. Cline, R. H. Kropschot, V. Arp, and J. H. Wilson, High magnetic fields, Boston, 1961, p. 580.
27) T. G. Berlincourt and R. R. Hake, Phys. Rev. 131 (1963), 140.
28) I. Dietrich and R. Weyl, Phys. Lett. 13 (1964), 274.
29) R. B. Flippen, Phys. Rev. 137 (1965), A1822.
30) J. C. A. van der Sluijs, H. R. de Beun, B. A. Zweers, and D. de Klerk, Proc. Conf. High magnetic fields, Grenoble 1966, p. 429. (this thesis, chapter VII).

C. *Magnetisation.*

metals and compounds by the balance method.

31) P. Kapitza, Proc. Roy. Soc. A 131 (1931), 224; 243.
32) P. Kapitza and P. L. Webster, Proc. Roy. Soc. A 132 (1931), 442.
33) P. Kapitza, Proc. Roy. Soc. A 135 (1932), 537; 556; 568.
34) R. Stevenson, High magnetic fields, Boston, 1961, p. 544.
35) R. Stevenson, Rev. Sc. Instr. 32 (1961), 28.

metals by the induction method. (see also ref. 1, 2 and 3)

36) B. R. Watts, Proc. Roy. Soc. 282 (1959), 521.
37) M. G. Priestly, High magnetic fields, Boston, 1961, p. 499.
38) C. S. Gaskell and H. Motz, High magnetic fields, Boston, 1961, p. 561.
39) K. Okumura and I. M. Templeton, Phil. Mag. 7 (1962), 1239.
40) K. Okumura and I. M. Templeton, Oxf. Conf. High magnetic fields, 1963, unpubl.
41) K. Okumura and I. M. Templeton, Phil. Mag. 8 (1963), 889.
42) J. R. Anderson and A. V. Gold, Phys. Rev. Lett. 10 (1963), 227.
43) D. C. Grassie, Oxf. Conf. High magnetic fields, 1963, unpubl.
44) B. R. Watts, Phys. Lett. 10 (1964), 275.
45) J. R. Anderson and A. V. Gold, Phys. Rev. 139 (1965), A1459.

compounds by the induction method.

46) I. S. Jacobs and P. E. Lawrence, Rev. Sc. Instr. 29 (1958), 713.
47) P. E. Rodbell and P. E. Lawrence, J. appl. Phys. 31 (1960), 275S.
48) I. S. Jacobs, J. appl. Phys. 32 (1961), 61S.
49) I. S. Jacobs, High magnetic fields, Boston, 1961, p. 549.
50) I. S. Jacobs and J. S. Kouvel, Phys. Rev. 122 (1961), 412.
51) I. S. Jacobs, Oxford Conf. High magnetic fields, 1963, unpubl.
52) I. S. Jacobs and I. Silverstein, Phys. Rev. Lett. 13 (1964), 272.
53) R. W. de Blois, Rev. Sc. Instr. 32 (1961), 816; GE-rep. 61-RL-2897M.

54) R. W. de Blois, High magnetic fields, Boston 1961, p. 568.
55) Y. Allain, F. Varret, and A. Miédan-Gros, Cte Rend. Paris, 260 (1965), 4677.
56) G. Asti, M. Colombo, M. Giudici, and A. Levialdi, J. appl. Phys. 36 (1965), 3581.
57) J. C. A. van der Sluijs, B. A. Zweers, and D. de Klerk, Phys. Lett. 24A (1967), 637. (this thesis, chapter VI).

D. *Microwaves*. (see also ref. 7)

58) S. Foner, Phys. Rev. 107 (1957), 683.
59) S. Foner, J. Phys. Rad. 20 (1959), 336.
60) S. Foner, Proc. Int. Conf. Magnetism, Kyoto, 1961, dl I, p. 424.
61) S. Foner, J. appl. Phys. 32 (1961), 63S.
62) S. Foner, L. R. Momo, and A. Mayer, Phys. Rev. Lett. 3 (1959), 56.
63) L. R. Momo, R. A. Myers, and S. Foner, J. appl. Phys. 31 (1960), 443.
64) S. Foner, L. R. Momo, A. Mayer, and R. A. Myers, Quantum Electronics, N. York, 1960, p. 487.
65) E. Neckenbürger, Z. angew. Phys. 17 (1964), 464.

E. *Optics*.

66) P. Kapitza and R. Skinner, Proc. Roy. Soc. A 109 (1925), 224.
67) P. Kapitza, P. G. Strelkov, and E. Laurman, Proc. Roy. Soc. A 167 (1938), 1.
68) H. Hendrikx, A. van Itterbeek, H. Myncke, and G. Pitsi, Proc. Kon. Vlaamse Ac. Wetensch. 26 (1964), no. 6.
69) A. van Itterbeek, W. van Driessche, I. de Grave, and H. Myncke, Bull. Belg. Phys. Soc. V, no 2-3, (1966), 188.
70) F. Herlach, H. Knoepfel, R. Luppi, and J. van Montfoort, Bull. Belg. Phys. Soc. V, no 2-3 (1966), 179; Proc. Megagaus Conf., Frascati 1965, p. 471.
71) R. Wetzel, Exper. Techn. Phys. 12 (1964), 259.

VI. ON THE TRANSITION IN A MAGNETIC FIELD FROM THE ANTIFERROMAGNETIC TO THE PARAMAGNETIC STATE OF $CuCl_2.2H_2O$.

§ 1. *Introduction.*

In the present chapter we describe and discuss observations of the transition of $CuCl_2.2H_2O$ from the antiferromagnetic b-state to the paramagnetic state in an external magnetic field.

By antiferromagnetic b-state we indicate the state in which the still antiferromagnetically ordered spins are directed perpendicularly to the direction of the magnetic field, this in contrast with the antiferromagnetic a-state in which the spin direction is parallel to the axis of easy magnetisation of the crystal.

The magnetic field that induces the second order transition from the b-state to the paramagnetic p-state is called H_{b-p} from now on. The magnetic field that induces the first order transition from the a-state to the b-state is called H_{a-b}.

The observations have been obtained by measuring the magnetisation of a $CuCl_2.2H_2O$ powder sample in a pulsed magnetic field at constant temperature. The measuring temperature ranged from $1^\circ K$ to $4.3^\circ K$.

A short survey will be given of the development of the physics of antiferromagnetism and some information is presented on the crystallographic properties of $CuCl_2.2H_2O$. The data have been found in the review articles by Nagamiya, Yosida, and Kubo[1], Poulis and Gorter[2], Anderson[3,4] and in the work by Ubbink[5] and by Gijsman[6]. These papers contain detailed literature references.

§ 2. *Historical survey.*

Antiferromagnetism is the ordered state of a solid in which the microscopic magnetisation vectors of the magnetic ions, the spins, are supposed to be directed antiparallel to each other. The antiferromagnetic ordered state demonstrates its presence e.g. by anomalies in the susceptibility and the specific heat of the material though without the occurrence of a large macroscopic magnetisation.

The main starting points of the development are the proposition of the Heisenberg-Dirac hamiltonian, at first only for ferromagnetism[7,8] and the explanation of the behaviour of the susceptibility of certain metals and alloys by means of a negative internal field in the Weiss theory of the molecular field by Néel[9].

In fact, though not in historical development, the molecular field theory is a certain approximation of the Heisenberg theory.

By its simplicity Néel's theory is very suitable for a qualitative description of complicated cases. To the further development Bitter[10] and Van Vleck[11] contributed the microscopic and the statistical interpretations of the molecular field model. Among the later developments we mention the work on $CuCl_2.2H_2O$ by Gorter and Haantjes[12] and by Gorter and van Peski Tinbergen[13] because of the importance they have for the present research.

For a survey of the analysis of the Heisenberg model we refer to the review article by Walker[14]. In the Heisenberg model the behaviour of the spin system is characterised by its excitations. In the long wavelength case the interaction between the excitations can be shown to be small and the problem can be handled in terms of a one particle model. The excitations in the one particle approximation can be considered as quasi particles called spin waves[14].

The method has been applied to antiferromagnets by Fu-Cho-Pu[15] and Tyablikov[16] for $s = \frac{1}{2}$. The analysis for higher spin values has been given by Anderson and Callen[17], by Tahir-Kheli and ter Haar[18], by Hewson and ter Haar[19], and by Lines[20] by means of Green function techniques. Recently Hewson, ter Haar and Lines[21] adapted the method to $CuCl_2.2H_2O$ to obtain the exchange constants and the Néel temperature. For a review on the application of the Green function method to magnetic problems see the paper by Zubarev[22].

We do not discuss the Ising model, because we feel that the amount of anisotropy present in $CuCl_2.2H_2O$ is too small to justify the use of the Ising model.

§ 3. *Survey of the crystallographic properties of $CuCl_2.2H_2O$.*

$CuCl_2.2H_2O$ crystallizes in the orthorhombic system with a primitive unit cell. The Shoenfliess symbol is D_{2h}^7, the international symbol Pmna. The length of the a, b, and c axes are 7.39 Å, 8.05 Å, and 3.73 Å respectively.[23]

The chlorine ions are situated outside the a-b plane symmetrically to the copper ions, the oxygen ions of the water molecules being situated in the a-b plane. The position of the protons has been determined by Poulis and Hardeman[24] to be outside the a-b plane.

In fig. VI.1 that has been copied from Marshall[25] the $CuCl_2.2H_2O$ unit cell is shown.

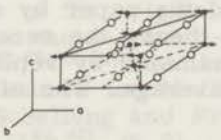

Fig. VI.1. The $CuCl_2.2H_2O$ unit cell.[25] • Cu o O

The susceptibility[26] and the specific heat[27] of $CuCl_2.2H_2O$ show an anomaly at $4.33^\circ K$ whereas measurements of nuclear magnetic resonance give evidence for antiferromagnetic order below $4.33^\circ K$[28,29].

The generally accepted picture is one of antiferromagnetic exchange ($s = \frac{1}{2}$) with an exchange integral of the order of $10\ k_B$ between nearest neighbours, along the c-axis, coordination number $z_1 = 2$, and a ferromagnetic exchange with an exchange integral of the order of k_B between next nearest neighbours, in the a-b plane, coordination number $z_2 = 4$. In this way one has a layered structure with parallel spins inside the layer and antiparallel layers. This picture has to be extended by a small canting of the spins in the c-direction in such a way that the net magnetisation along the c-axis remains zero[31].

The origin of the exchange between the magnetic Cu^{2+} ions has to be discussed in terms of the wave functions of the electrons of the Cu^{2+} ions, $3d^9$ state, and of the Cl^- ions, $3p^6$ state, by means of a superexchange model. We omit the details of this analysis which belongs to the domain of Ligand field theory.

§ 4. *The molecular field theory applied to $CuCl_2.2H_2O$.*

The generally used basis for the treatment of magnetic structures is the Heisenberg hamiltonian:

$$H^{op} = -\sum_g \mu H . S_g - \sum_{g,f} J_{s.f}\ S_g . S_f \qquad \text{(VI.1)}$$

with g and f numbering over all lattice points. In this formula $\mu = \mu_B\, g_L$, g_L is the Landé g-factor, μ_B the Bohr magneton, H the external magnetic field, and S_g the spin vector of the g-th lattice site. However, the Heisenberg hamiltonian itself is an approximation based on the following assumptions[3]:

1) Localised spins. This means that one has a model consisting of N electrons with N different orthogonal states. Every state always contains one and only one electron and it is possible to count the states (lattice points) instead of the electrons. This is only justified in a non-conducting medium.
2) The exchange is between two electrons.
3) Complete isotropy. This assumption can be removed to a certain extent by introducing suitable anisotropy terms.

For a detailed discussion of the consequences of these approximations we refer to the paper by Anderson[3].

In the molecular field theory the second righthand term in equation (VI.1) is approximated by replacing all spins that interact with S_g by their average. The effective hamiltonian per spin can be written:

$$H_{eff} = - < S_g > \left[2 \sum_f J_{g,f} < S_f > + g_L\, \mu_B\, H \right] \qquad \text{(VI.2)}$$

A short calculation under assumption of Boltzmann statistics results in:

$$\langle S_g \rangle = s B_s \left(\frac{SH g_L \mu_B}{k_B T} \right) \qquad \text{(VI.3)}$$

with $B_s(x)$ the Brillouin function of x. For $s = \frac{1}{2}$ we have $B_{\frac{1}{2}}(x) \equiv \equiv \text{tgh } x$. This formalism has been extended to the case with orthorhombic anisotropy by Gorter and Haantjes[12] for T = 0 and by Gorter and van Peski - Tinbergen[13] for T > 0. We summarise their results without a derivation. For the derivations we refer to the original papers.

We assume a spin system with spin $s = \frac{1}{2}$ consisting of two sublattices 1 and 2 with antiferromagnetic interaction between spins in different sublattices and ferromagnetic interaction between spins in the same sublattice. The antiferromagnetic exchange is represented by coefficients α and the ferromagnetic exchange by coefficients γ. The exchange field H_{E_n} of the sublattices can be written:

$$\left.\begin{aligned} H_{E_1} &= -\alpha M_2 + \gamma M_1 \\ H_{E_2} &= -\alpha M_1 + \gamma M_2 \end{aligned}\right\} \qquad \text{(VI.4)}$$

with M_1 and M_2 the sublattice magnetisations.

To obtain an anisotropic exchange α and γ have to be replaced by tensors that we assume to contain only diagonal terms: α_i and γ_i.

$$\left.\begin{aligned} H^i_{E_1} &= -\alpha_i M^i_2 + \gamma_i M^i_1 \\ H^i_{E_2} &= -\alpha_i M^i_1 + \gamma_i M^i_2 \end{aligned}\right\} \qquad \text{(VI.5)}$$

The solution for the sublattice magnetisation leads to three stable solutions and the equilibrium state of the system is described by the solution that gives the lowest value of the thermodynamic potential. The three solutions correspond to three regions in the magnetic phase diagram, the antiferromagnetic a-state, the antiferromagnetic b-state, and the paramagnetic p-state (fig. VI.2).

In fig. VI.2 the drawn curves indicate qualitatively the phase boundaries as they are predicted by this theory while the dotted lines represent the mathematical extensions of the curves that have no physical significance. For the mathematical meaning of the curves we refer to the original paper.[13]

The boundary between the a- and b-phases has been found in a number of cases [26, 27, 28, 29, 34] and large parts of the phase diagram have been measured for $MnCl_2.2H_2O$[6], $MnBr_2.2H_2O$[6] (unpublished work by Schelleng and Friedberg mentioned in ref. [17]) and $CoCl_2.2H_2O$[42, 43]. (§ 6).

The curve that separates the b- and the p-phase determines $H_{b-p}(T)$ and is given by:

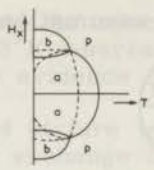

Fig. VI.2. Magnetic phase diagram of an orthorhombic antiferromagnet according to Gorter and Van Peski-Tinbergen[13].

$$H_{b-p}(x) = \frac{\alpha_x + \alpha_y - \gamma_x - \gamma_y}{\mu_x(\alpha_y + \gamma_y)} W' \qquad \text{(VI. 6.)}$$

for $H \parallel$ x-axis, with

$$W' = (\alpha_x + \gamma_y) \operatorname{tgh} \frac{W'}{kT} \qquad \text{(VI. 7)}$$

and $k_B T_N = \alpha_x + \gamma_x$ (VI. 8)

Similar expressions can be given for $H \parallel$ y-axis.

The values of α_i and γ_i have been determined by susceptibility measurements.[6]. Using these values one obtains:

$$\begin{aligned} H_x &= 210 \text{ kOe} \\ H_y &= 225 \text{ kOe} \\ T_N &= 7.64\,^{\circ}\text{K} \end{aligned} \qquad \text{(VI. 9)}$$

The slopes of $H_{b-p}(T)$ in the neighbourhood of $T = T_N$ and $T = 0$ are given implicitly by the expressions (VI. 6) and (VI. 7). Because it is not simple to find an analytical expression for $H_{b-p}(T)$ that is valid over the whole temperature range we have calculated $H_{b-p}(T)$ graphically and plotted in fig. VI. 10 (§ 7) together with the results of the measurements.

To estimate the slope of the experimental curve in the neighbourhood of $T = T_N$ we take the usual series expansion for $H_{b-p}(T)$ in the neighbourhood of $T = T_N$ in the molecular field model for $s = \frac{1}{2}$:

$$\frac{H_{b-p}(T)}{H_{b-p}(0)} = 3^{\frac{1}{2}} \left(1 - \frac{T}{T_N}\right)^{\frac{1}{2}}. \qquad \text{(VI. 10)}$$

and we vary the exponent of $(1 - \frac{T}{T_N})$ to find an optimal adaptation to the results of the measurements.

Finally we calculate the slope of the magnetisation as a function of the magnetic field for $T = 0$ in the antiferromagnetic b-phase. This follows directly from formula (14) of reference[13]:

$$M_{x1} = \frac{\mu_x^2 H_x}{\alpha_x + \alpha_y - \gamma_x + \gamma_y} \qquad \text{(VI. 11)}$$

and a similar expression for M_y.

It follows immediately that M_x depends linearly on H and that $\chi_{\parallel}$ is constant. The same applies to $\chi_{\perp}$, for $H > H_{a-b}$, giving a constant powder susceptibility χ_p.

§ 5. *The Heisenberg antiferromagnet.*

We start again from formula (VI.1) and for the antiferromagnetic case we introduce an explicit sign of the exchange integral in the second righthand term and we obtain

$$H^{op} = - g_{\perp} \mu_B H \sum_g S_g^z + \sum_{g,h} J_{g,h} S_g . S_h \qquad (VI.12)$$

The magnetic field is supposed to be directed in the z-direction.

The transition from the paramagnetic to the antiferromagnetic state can be defined by observing that the spin wave frequency in the paramagnetic state is lowered by decreasing the external magnetic field and becomes negative. A negative frequency gives an instable state and a transition occurs [17]. To calculate $H_{b-p}(T)$ one determines the spin wave energy spectrum in the paramagnetic state then find its minimum as a function of k and obtain the magnetic field that makes this minimum vanish. This approach is only valid if the spin wave concept is valid i.e. at relatively low temperatures. However, some authors extend the calculations to the Néel temperature in the case of antiferromagnetics as $CuCl_2.2H_2O$ which have a low Néel temperature [17,21].

The spin wave energy is given by:

$$\hbar \omega (k) = \mu H - S \left(J(o) - J(k) \right) \qquad (VI.13)$$

where $J(o)$ and $J(k)$ are the Fourier transforms of the exchange interaction. However, (VI.13) predicts a temperature independent H_{b-p}. This can be corrected by observing that the spin wave frequencies have to be renormalised by a factor R(T).

$$\hbar \omega (k) = \mu H - S \left[J(o) - J(k) \right] R(T) \qquad (VI.14)$$

giving

$$\mu H_{b-p}(T) = S \left[J(o) - J(k_{min}) \right] R(T) \qquad (VI.15)$$

This shows that from a measurement of $H_{b-p}(T)$ one obtains the behaviour of R(T) and it would be interesting to discuss the experimentally obtained temperature dependence of $H_{b-p}(T)$ in view of a theoretically calculated R(T). However, for the case of $CuCl_2.2H_2O$ this calculation seems not to be available in literature. The only calculations that have been done are the low field analysis of $CuCl_2.2H_2O$ by Hewson, ter Haar, and

Lines[21] and the calculation of the non linear behaviour of $\chi(H)$ of EuTe by Jacobs and Silverstein[30] which agrees qualitatively with the behaviour observed in $CuCl_2.2H_2O$.

Hewson, ter Haar and Lines[21] made a formal analysis of the spin hamiltonian

$$H^{op} = -g_L \mu_B H \sum_g S_g^z + \sum_{g,h} J_1(g-h)\, S_g . S_h - \sum_{g,f} J_2(g-f) S_g . S_f \qquad (VI.16)$$

The exchange integrals are supposed to depend only upon the distance between lattice points, g counting all lattice points. The first righthand term is the Zeeman term, the second righthand term the antiferromagnetic exchange, the third the ferromagnetic exchange. The antiferromagnetic exchange is supposed to exist between nearest neighbours h and the ferromagnetic exchange between next nearest neighbours f.

One of the approximations included is the omission of higher order terms, e.g. biquadratic exchange and the Moriya type interaction[31]. Biquadratic exchange is supposed to be unimportant in $CuCl_2.2H_2O$[21] and the influence of the Moriya interaction has been shown to be only of importance below the threshold field H_{a-b}[32]. The characteristic anisotropy in $CuCl_2.2H_2O$ is accounted for by the ferromagnetic exchange term. Magnetostrictive effects are not allowed as usual in this type of theories.

The crucial point in this type of analysis is the approximation which is made to solve the problem explicitly. As to the predictions that can be verified by the present research, only the slope of the $H_{b-p}(T)$ curve near $T = T_N$, $H_{b-p}(0)$ and the behaviour of $\chi(H)$ are important. The slope near $T = T_N$ does not differ from the molecular field predictions[17]. A short calculation based on equation (VI.16) gives

$$\mu H_{b-p}(0) = z_1 J_1 \qquad (VI.17)$$

with z_1 the number of nearest neighbours. Therefore a measurement of $H_{b-p}(0)$ verifies directly the value of J_1. Hewson, ter Haar, and Lines[21] calculate from susceptibility measurements $J_1 = 13.56\ k_B\,^{\circ}K$ and $J_2 = 1.78\ k_B\,^{\circ}K$.

As to the behaviour of $\chi(H)$ we outline the calculation by Jacobs and Silverstein[30] for EuTe. As far as we know a calculation for $CuCl_2.2H_2O$ is not available in the literature.

The susceptibility can be derived from the thermodynamic potential

$$\chi = \frac{\partial M}{\partial H} = -\left(\frac{\partial^2 G}{\partial H^2}\right)_T \qquad (VI.18)$$

For $s = \frac{1}{2}$ the thermodynamic potential can be written as

$$G = -\frac{3}{2} N J z - N \mu_B g_L \frac{H^2}{2 H_{b-p}} + \tfrac{1}{2} \hbar \sum_{\underline{k}} (\omega_{\underline{k}}^{+} + \omega_{\underline{k}}^{-}) \qquad \text{(VI.19)}$$

From the analysis of the antiferromagnetic b-state of a Heisenberg antiferromagnet by Wang and Callen [33] we have:

$$\hbar \omega_{\underline{k}}^{\pm} = \tfrac{1}{2} z J (1 \pm \gamma_{\underline{k}})^{\frac{1}{2}} \left\{ 1 \pm \gamma_{\underline{k}} \left(2 \frac{H^2}{H_{b-p}^2} - 1 \right) \right\}^{\frac{1}{2}} \qquad \text{(VI.20)}$$

with $\gamma_{\underline{k}} = z^{-1} \sum_{\underline{\delta}} \exp (i \underline{k} . \underline{\delta})$, $\underline{\delta}$ summing over nearest neighbours.

The differentiation of the second righthand term of (VI.19) yields the molecular field prediction:

$$\chi_{m.f} = \frac{N \mu^3}{z J} \qquad \text{(VI.21)}$$

The differentiation of the spin wave contribution gives:

$$\tfrac{1}{2} h \sum_{\underline{k}} \frac{z J}{H_{b-p}^2} \left[\gamma_{\underline{k}} (1 + \gamma_{\underline{k}})^{\frac{1}{2}} \left\{ 1 + \gamma_{\underline{k}} \left(2 \frac{H^2}{H_{b-p}^2} - 1 \right) \right\}^{-\frac{1}{2}} - \right. \qquad \text{(VI.22)}$$

$$\left. - \gamma_{\underline{k}} (1 - \gamma_{\underline{k}})^{\frac{1}{2}} \left\{ 1 - \gamma_{\underline{k}} \left(2 \frac{H^2}{H_{b-p}^2} - 1 \right) \right\}^{-\frac{1}{2}} \right]$$

For a quantitative evaluation the summation over $\underline{k}$ has to be carried out. Jacobs and Silverstein [30] did this for EuTe and their result is shown in fig. VI.3.

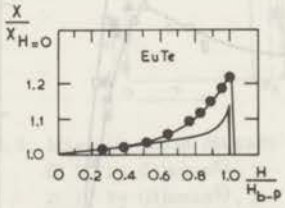

Fig. VI.3. Normalised susceptibility curve for EuTe [30].
experimental - calculated.

The difference between theory and experiment can be ascribed to magnetostrictive effects cf the last paragraphs of the next section.

In section 7 we give the experimental susceptibility of $CuCl_2.2H_2O$ as a function of the magnetic field.

§ 6. *Review of data on magnetic phase diagrams for some other antiferromagnetic materials.*

In this section we review some data from the literature on magnetic phase diagrams of other antiferromagnetic materials. We restrict ourselves to those materials the behaviour of which is analogous to that shown by $CuCl_2.2H_2O$.

Occasional data on one or some points of the phase diagram have been reported for many substances mainly in the low field region. The data on T_N occur by far the most frequently and the reader is referred to table works for this subject, e.g. Landolt und Börnstein or the Handbook of the American Institute of Physics.

The threshold field H_{a-b} has been measured in MnF_2[34] apart from the materials mentioned below whereas data on some chromium compounds are vailable from resonance measurements[35].

The only materials on which sufficient data are available to construct phase diagrams are $MnCl_2.2H_2O$ and $MnBr_2.2H_2O$. On the low field region of the $CoCl_2.6H_2O$ phase diagram some information is available, but there seems to be no detailed calculation of this diagram.

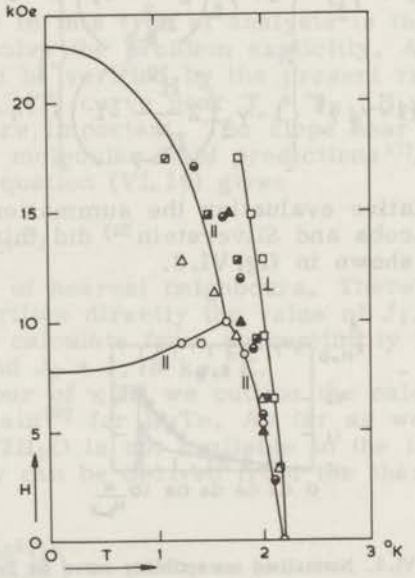

Fig. VI.4. Magnetic phase diagram for $MnBr_2.2H_2O$.
- ○ $H_{||}$ quoted by Anderson and Callen[17], c_v and optical.
- ▲ powder by Schelleng and Friedberg[36], c_v.
- □ $H_\perp$ by Gijsman[6], χ.
- △ $H_{||}$ by Gijsman[6], χ.
- ◪ powder estimated from Gijsman's results. χ.
- ◒ powder Henry[37], χ.
- —— molecular field prediction[17].

In fig. VI.4 we have compiled some observations by Gijsman[6], Schelleng and Friedberg[36], and Henry[37] both for single crystals and powder samples. The molecular field prediction, as calculated in the usual way from susceptibility measurements, has been copied from Anderson and Callen[17] for the external field parallel to the ground state spin direction and from Gijsman[6] for the external field perpendicular to the ground state spin direction. The transition field $H_{b-p}^{\perp}$ for the external field perpendicular to the ground state spin direction at zero temperature can be estimated from the susceptibility measurements by Gijsman[6] to be 35 kOe (molecular field prediction).

Because even the powder transition field H_{b-p}^{powder} can be estimated from the observations to be lower than the molecular field prediction for the transition field $H_{b-p}^{\parallel}$ at zero temperature we conclude that the prediction of $H_{b-p}(0)$ by molecular field theory is far too high.

The slope of $H_{b-p}(T)$ near to $T = T_N$ is about the same as that predicted by the molecular field theory.

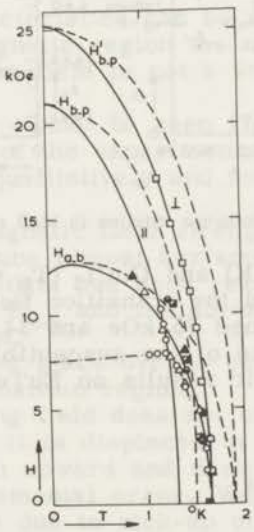

Fig. VI.5. Magnetic phase diagram for $MnCl_2.4H_2O$.
□ $H^{\perp}$ by Gijsman[6], χ.
△ $H^{\parallel}$ by Gijsman[6], χ.
▲ powder Gijsman[6], c_v.
◒ powder Henry[37], χ.
O resonance, quoted by Gijsman[6]. ∥.
◪ powder by Voorhoeve and Dokoupil[38], c_v.
---- molecular field prediction[6].
—— molecular field with Gijsman correction.
-.-.- adaptation to the results by Gijsman.

In fig. VI. 5 the observations on $MnCl_2.4H_2O$ by Gijsman[6], Henry[37], and Voorhoeve and Dokoupil[38] have been compiled. The observations for $H_{b-p}^{\perp}$ agree with the molecular field prediction, corrected by Gijsman[6] but both $H_{b-p}^{\parallel}$ and H_{b-p}^{powder} turn out to be lower than the theory predicts.

Because the temperature range in which measurements have been reported does not extend below 0.5 T_N no experimental estimate of the b-p transition field at T=0 can be made.

Biquadratic exchange has been shown to play an important role in the dependence on the temperature of the sublattice magnetisations of MnO and NiO[39]. However, this does not account for all deviations from molecular field predictions and lattice distortion is probably the important factor. Evidence on lattice distortion in antiferromagnetic materials upon cooling down through the Néel temperature has been obtained by Rodbell, Osika, and Lawrence[40] in MnO and EuTe by means of neutron diffraction. Their results are shown in fig. VI. 6.

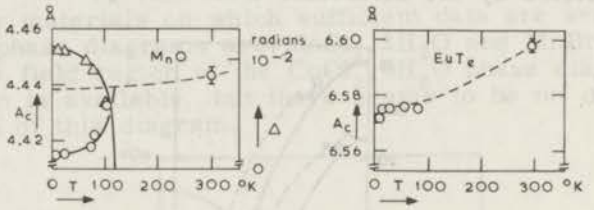

Fig. VI. 6. Exchange striction in MnO and EuTe[40].

For EuTe (T_N = 11°K) and $CoCl_2$ (T_N = 25°K) Jacobs and Silverstein[30] measured the transition field at 2.1°K and 4.2°K respectively and obtained 75 kOe and 34 kOe respectively. They obtained the dependence of the susceptibility on the external magnetic field and their results on EuTe have been shown in fig. VI. 3.

§ 7 *Measuring results.*

We carried out a measurement of H_{b-p} as a function of the temperature between 1°K and 4.3°K of $CuCl_2.2H_2O$.

The experiment consisted of measuring the magnetisation of a cylindrical powder sample in a pulsed magnetic field. The sample was 5mm long and had a diameter of 3mm. Because of the low susceptibility value the demagnetising factor can be omitted. The measuring method has been described in chapter V, § 4. The total systematic error of the experimental arrangement can be assumed to be less than 10 %, and the reproducibility between different samples better than a few percent. The precision near T_N is worse because of the steep fall of the H_{b-p} (T) curve near T_N.

A typical oscillogram showing the magnetisation as a function of the external magnetic field is shown in fig. VI. 7.

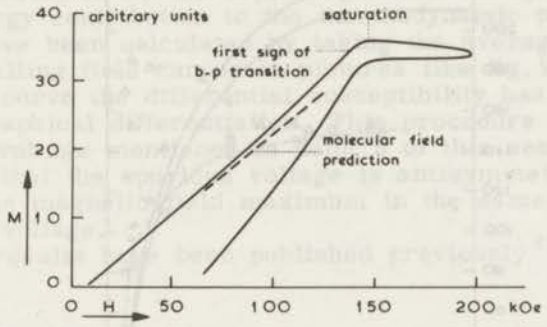

Fig. VI. 7. Oscillogram of the magnetisation of $CuCl_2.2H_2O$ as a function of the external magnetic field. T = 3°K.

The following characteristics can be noted.

1. In the antiferromagnetic region the magnetisation as a function of the magnetic field is not a straight line but it bends upwards.
2. The a-b transition cannot be seen (7 kOe [26]). This is caused by the field scale of the experiment. To reassure ourselves we determined it qualitatively and found it indeed at about 7 kOe.
3. When a certain magnetic field strength has been reached the curve bends and runs almost horizontally until the maximum magnetic field strength has been reached. We identify this bending point with H_{b-p} and the horizontal part with paramagnetic saturation.
4. The transition takes place over a certain region and this region we call transition region.
5. The curve at falling field does not coincide with the curve at rising field but it is displaced in vertical direction. The transition points in upward and downward curves are the same within experimental error. We ascribe the displacement to spurious effects due to pick-up or to motion of the sample in the magnetic field.

From all oscillograms of the type of fig. VI. 7 we have taken the upper and lower limits of the transition region and indicated them by triangles and circles in fig. VI. 8. The dotted lines indicate the phase diagram as we suggest it from these observations.

Furthermore we give in fig. VI. 8 the molecular field predictions for $H_\perp$ the spin direction and for $H_\parallel$ the spin direction as well as some observations by Gijsman [6] and by Poulis and Hardeman [24].

Through the circles a curve can be drawn that falls with rising temperature and shows a very steep descent as the tem-

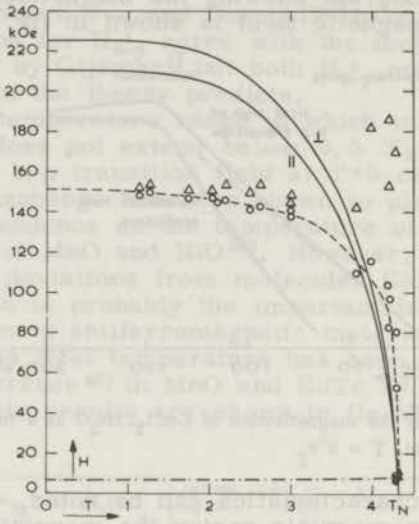

Fig. VI.8. Boundaries of the H_{b-p} transition region as a function of the temperature.
- ● $H^{\parallel}$ by Gijsman[6], $\chi_{\cdot}$
- ▲ $H^{\perp}$ by Gijsman[6], $\chi_{\cdot}$
- — · — curve through measuring points by Poulis and Hardeman[24], resonace.
- O this work, begin transition region.
- Δ this work, end transition region.
- —— molecular field prediction with Gijsman correction[6].
- – – – $H_{b=p}$ transition curve as suggested from this work.

perature approaches the Néel point indicated by a rectangle.

The curve that can be drawn through the triangles runs parallel to the curve through the circles at low temperature but rises again with rising temperatures over 3°K.

The circles are supposed to represent the transition field H_{b-p} and the triangles the apparent paramagnetic saturation field.

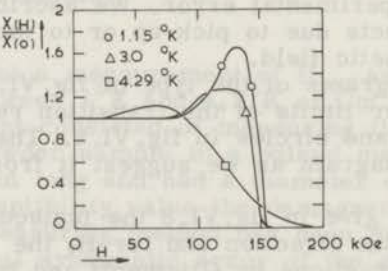

Fig. VI.9. Normalised susceptibility as a function of the magnetic field for three different temperatures.

In fig. VI. 9 we present for three temperatures the susceptibility as a function of the magnetic field strength. The picture shows the rise of the susceptibility as a consequence of the spin wave energy contribution to the thermodynamic potential. The curves have been calculated by taking the averages between rising and falling field curves in pictures like fig. VI. 7. From the resultant curve the differential susceptibility has been determined by graphical differentiation. This procedure corrects the spurious voltage mentioned in point 5 of this section under assumption that the spurious voltage is antisymmetrical with respect to the magnetic field maximum in the same way as the induction voltage.

These results have been published previously [41].

§ 8. *Discussion.*

a. *Quantitive results from the observations on* $CuCl_2.2H_2O$.

From the results presented in fig. VI. 8 we extrapolate the transition field $H_{b-p}^{powder}(T)$ to find $H_{b-p}^{powder}(0) = (150 \pm 10)$ kOe.

The molecular field theory predicts

$$H_{b-p}^{\parallel}(0) = 210 \text{ kOe.}$$

$$H_{b-p}^{\perp}(0) = 225 \text{ kOe.}$$

However, if we insert for $\alpha_x + \gamma_y$ the experimental value for T_N instead of the value calculated from susceptibility measurements we obtain

$$H_{b-p}^{\parallel}(0) = 165 \text{ kOe}$$

$$H_{b-p}^{\perp}(0) = 176 \text{ kOe.}$$

In this way the molecular field phase diagram is scaled down both along the H and the T axis, this in contrast to Gijsman's method in which an ad hoc temperature dependent factor is introduced to correct the temperature scale only [6] and no correction for the H axis is included.

A stil better agreement is obtained by introducing the correction for the spin wave contribution to the thermodynamic potential which we estimate to about 10 % from the calculation by Jacobs and Silverstein [30]. We obtain

$$H_{b=p}^{\parallel}(0) = 148 \text{ kOe}$$

$$H_{b=p}^{\perp}(0) = 158 \text{ kOe.}$$

and this yields a powder transition field within the limits of experimental error of our observations.

By equation (VI.17) the transition field of 150 kOe with $z_1 = 2$ gives an exchange constant

$$J_1/k_B = 10^{\circ}K$$

This has to be compared with the value derived from susceptibility measurements [21] of 13.56°K which is significantly higher.

From the paramagnetic Curie-Weiss constant one calculates an exchange constant of 10 k_B °K, by the molecular field formula.

The slope of the experimental curve near $T = T_N$ can be estimated from the approximation:

$$H_{b-p}(T) = H_{m.f.}(0)\, 3^{\frac{1}{2}} \left(1 - \frac{T}{T_N}\right)^{\alpha} \qquad \text{(VI.23)}$$

and this yields $\alpha = 0.37 \pm 0.05$ by graphical analysis. If one takes $H_{b-p}^{exp}(0)$ instead of $H_{b-p}^{m.f.}$ in the righthand side of (VI.23) one obtains $\alpha = 0.29 \pm 0.05$. Both results are in disagreement with the molecular field theory.

Fig. VI.9 shows that the behaviour of χ as a function of H and T is rather complicated. Qualitatively the low temperature behaviour is in agreement with the behaviour observed in EuTe by Jacobs and Silverstein[30], but the peak value is higher. An analysis of the temperature dependence of the peak value seems not to be available

b. *Conclusions.*

From the evidence presented in § 6 and § 7 we conclude that the molecular field theory gives no satisfactory quantitative description of the transition from the antiferromagnetic b-state to the paramagnetic state in a magnetic field, and that it is not probable that the correction from the spin wave contribution to the thermodynamic potential will be sufficient to obtain the experimental value for the transition field. These conclusions are valid for those orthorhombic antiferromagnets which have been studied sufficiently extensive to make a conclusion possible.

The inability of the molecular field theory to give a correct description of other details of the magnetic phase diagram has been discussed before [6,17] and the correction of the temperature scale by Gijsman[6] has been a way to obtain the correct value of the Néel temperature.

By scaling down the complete phase diagram for $CuCl_2.2H_2O$ both T_N and $H_{b-p}(0)$ can be adapted to the experimental value by the use of only one scaling parameter. However, the agreement for $H_{a-b}(0)$ is spoilt and the detailed shape of the diagram remains in disagreement with the observations. At present the scaling down of the phase diagram for $MnCl_2.4H_2O$ and for $MnBr_2.4H_2O$ cannot be done in the same way as for $CuCl_2.2H_2O$ because sufficient experimental data seem not to be available. However, a priori it is not clear that the correction for the deviations at zero magnetic field and near the Néel temperature and for high magnetic field and at zero temperature can be based on the same mechanism.

It is remarkable, that the exchange constant that can be obtained from our observations is significantly lower than the exchange constant that can be obtained from low field susceptibility measurements. For an explanation we point to the evi-

dence that many magnetic substances show changes in the lattice structure at the magnetic transitions. The possibility is not excluded that at high magnetic field a similar lattice deformation occurs as the deformation that has been shown to occur at the Néel temperature in EuTe and MnO[40]. However, no theory seems to be available which describes H_{b-p} and takes lattice deformation into account. These deformations should cause a field dependence in the exchange constant, and our observations give some evidence for this field dependence.

To obtain more data in connection with these problems it is necessary to have at disposal accurate measurements of the phase diagrams and of possible magnetostrictive phenomena for antiferromagnetic materials. Without further instrumental development this is possible for $MnCl_2.4H_2O$, $MnBr_2.4H_2O$, $CoCl_2$, $CoCl_2.6H_2O$ and EuTe. These measurements have to be extended down to about 0.2 T_N to be able to obtain a sufficiently accurate estimate of the behaviour at T = 0.

References.

1. T.Nagamiya, K.Yosida, and R.Kubo, Adv.Phys. 4 (1955), 1.
2. N.J.Poulis and C.J.Gorter, Progr.Low Temp.Phys.I, (1955), 251, ed.Gorter.
3. P.W.Anderson, Solid state physics, 14 (1963), ed.Seitz and Turnbull.
4. P.W.Anderson, Magnetism I, (1962), ed.Rado and Suhl.
5. J.Ubbink, Thesis, Leiden (1953), Comm.KOL 105 c (1953); Physica 19 (1953), 919.
6. H.M.Gijsman, Thesis, Leiden (1958).
7. W.Heisenberg, Z.Physik, 38 (1926). 411; ib. 49 (1928), 619.
8. P.A.M.Dirac, Proc.Roy.Soc. 123 (1929); 714.
9. L.Néel, Ann.Phys. (10) 18 (1932), 5.
10. F.Bitter, Phys.Rev. 54 (1938), 79.
11. J.H.Van Vleck, J.Chem.Phys. 9 (1941), 85.
12. C.J.Gorter and J.Haantjes, Physica 18 (1952), 285; Comm.KOL suppl. 104 b.
13. C.J.Gorter and T.van Peski Tinbergen, Physica 22 (1956), 273; Comm.KOL suppl. 110 b
14. L.R.Walker, Magnetism I, (1962), ed. Rado and Suhl.
15. Fu-Cho-Pu, Dokl.Fiz.Nauk 130 (1960), 1244; engl.transl. 5 (1960), 128 and 321.
16. S.V.Tyablikov, Ukr.Fiz.Zh. 11 (1961), 287.
17. F.B.Anderson and H.B.Callen, Phys.Rev. 127 (1964), A 1068.
18. R.A.Tahir-Kheli and D.ter Haar, Phys.Rev. 127 (1962) 88.
19. A.C.Hewson and D.ter Haar, Physica 30 (1964), 890.
20. M.E.Lines, Phys.Rev. 131 (1963), 540; 546.
21. A.C.Hewson, D.ter Haar, and M.E.Lines, Phys.Rev. 137 (1964) A 1465.
22. D.N.Zubarev, Usp.Fiz.Nauk, 71 (1960), 71; engl.transl. 3 (1960), 320.
23. Th.Ernst, Landolt und Börnstein, Bd I, Tl.4, p.153.
24. N.J.Poulis and G.E.G.Hardeman, Physica 18 (1952), 201; Comm.KOL 278a.
25. W.Marshall, J.Phys.Chem.Sol. 7 (1958), 159.
26. J.van den Handel, H.M.Gijsman, and N.J.Poulis, Physica 18 (1952), 862; Comm. KOL 290 c.
27. S.A.Friedberg, Physica 18 (1952), 714; Comm.KOL 289 d.
28. N.J.Poulis, Thesis, Leiden (1952).

29. N.J.Poulis, and G.E.G.Hardeman, Physica 18 (1952), 201; Comm.KOL 287a; Physica 18 (1952), 315; Comm.KOL. 288b; Physica 19 (1953); 391; Comm.KOL 291d; Physica 20 (1954), 7; Comm.KOL 294a.
30. I.S.Jacobs and S.D.Silverstein, Phys.Rev.Lett. 13 (1964), 272.
31. T.Moriya, Phys.Rev. 120 (1960), 91.
32. R.J.Joenk, Phys.Rev. 126 (1962), 565; err.ib. 127 (1962), 2287.
33. Yung Li-Wang and H.B.Callen, J.Phys.Chem. Sol. 25 (1964), 1459.
34. I.S.Jacobs, J.appl.Phys. 32 (1961), 61S.
35. S.Foner, High Magnetic Fields, New York 1961, p.489.
36. S.A.Friedberg and J.Schelleng, Proc.Int.Conf.Magn., Nottingham (1964), p.91.
37. W.A.Henry, Phys.Rev. 94 (1954), 1146.
38. W.H.M.Voorhoeve and Z.Dokoupil, Physica 27 (1961), 777; Comm.KOL 328b.
39. D.S.Rodbell, I.S.Jacobs, J.Owen and E.A.Harris, Phys.Rev.Lett. 11 (1963), 10.
40. D.S.Rodbell, L.M.Osika, and P.E.Lawrence, J.appl.Phys. 36 (1965), 666.
41. J.C.A.van der Sluijs, B.A.Zweers, and D.de Klerk, Phys.Lett. 24A (1967), 637.

VII. DAMPING AND RELAXATION PHENOMENA IN SOME SUPERCONDUCTING MATERIALS.

§ 1. *Introduction.*

Recently a number of papers have been published about the resistive transition of type II superconducting wires in pulsed magnetic fields.[1,2,3,4,5,6] A considerable dependence upon the rate of change of the magnetic field has been observed, especially for pulse durations of 1 msec and less.

In this chapter we describe some observations of the behaviour of Nb_3Sn ribbon and Nb 25 % Zr wire in pulsed magnetic fields. Part of the work has been published previously[1,2]. In contrast to some of the papers mentioned above[3,4,5,6] the present discussion covers the complete transition up to the field values where the normal resistance value has been reached. Furthermore we studied the Nb_3Sn on ribbon shaped samples.

After a short review of some properties of type II superconductors and a description of the results obtained both in the papers[3,4,5,6] and in our experiments we propose a tentative explanation of the phenomena.

The measuring apparatus has been described in chapter V, § 4.

§ 2. *A short review of some properties of type II superconductors.*

In this section we only speak about the properties we need for our discussions in the last section. Detailed reviews with literature references have been given a.o. by de Gennes[7] and by Goodman[8].

The characteristic properties of superconducting materials are the disappearance of the electrical resistance below a certain critical temperature T_c and the fact that, with the exception of the surface layer, no magnetic flux is present in the material for $T < T_c$ and the magnetic field below a certain critical value, that for type II superconductors is called H_{c1}. For Nb_3Sn $T_c = 18\ ^\circ K$ and for Nb25 % Zr $T_c = 11\ ^\circ K$.

For a type II superconductor if the external magnetic field exceeds H_{c1} flux starts to penetrate into the material and if the external magnetic field reaches a second critical value H_{c2} the magnetic flux density inside and outside the material is equal.

If in a current carrying sample of a type II superconductor in an external magnetic field $H_e < H_{c2}$ the transport current is increased above a certain critical value resistance appears.

However, if the external magnetic field is parallel to the surface of the material surface superconductivity can persist to a field strength $H_{c3} = 1.69\ H_{c2}$.

Usually H_{c1} is less than 1 kOe. H_{c2} can be quite large and for Nb_3Sn, V_3Si, and V_3Ga it is reported to exceed 200 kOe.

For $H_{c1} < H_e < H_{c2}$ the magnetic flux that has penetrated into the material is present as small filaments. These filaments consist of a core of normally conducting material with a diameter 2ξ and a region outside the core where the magnetic field strength decays with a characteristic length λ. The quantity ξ is called the coherence length and λ the penetration depth. The quantities ξ and λ have a far more general importance in the theory of superconductivity but this is not relevant for the present considerations. It can be shown that the value of the flux per filament is always equal to

$$\phi_o = \frac{c\,h}{2\,e} = 2 \times 10^{-7} \text{ Gauss cm}^2. \qquad \text{(VII.1)}$$

If a superconducting material contains a finite number n of filaments (vortex lines) per unit area it is said to be in the mixed state or vortex state. The magnetic induction inside the superconducting material is given by

$$B = n\,\phi_o \qquad \text{(VII.2)}$$

The vortex lines are arranged in a regular array by the forces that they exert on each other and the array is characterised by a specific distance d.

If a type II superconductor is in the mixed state and the external magnetic field H_e is directed perpendicularly to the transport current I energy dissipation is observed. The motion of the vortex lines that are driven by the transport current causes energy dissipation by the currents that are induced by the motion of the vortex lines in and around the vortex cores. This energy dissipation causes the material to become resistive and this resistance can be observed as a voltage over the sample.

Lattice defects tend to fix the vortex lines. This mechanism is called "pinning". If a transport current is present the vortex lines only move if the driving force exceeds the pinning force and a viscous flow results.

If $H_e \,/\!/\, I$ the vortex lines do not tend to move and no energy dissipation occurs in a stationary case. We shall discuss the dynamic case in section 6.

Strnad, Hempstead, and Kim[9] studied dissipation phenomena in Nb-Ta and Pb-In superconducting samples in the vortex state and they observed a dependence of the apparent resistance on the magnetic field strength that could be described by

$$\frac{\rho_s}{\rho_n} = a\,\frac{H}{H_{c2}} \qquad \text{(VII.3)}$$

up to the transition field and a sharp saturation of the resistance at the transition field. For $T/T_c \cong 0.35$, in Nb-Ta, $a \cong \cong 0.7$. The magnetic field was directed perpendicularly to the transport current.

They showed that a similar behaviour should be expected

when the resistance of the vortex cores is averaged over the total cross section of the superconducting material. Then

$$\frac{\rho_s}{\rho_n} \sim \frac{\xi^2}{d^2} = \frac{H}{H_{c2}} \qquad \text{(VII.4)}$$

if H_{c2} is taken to be the magnetic field that causes the vortex lines to touch.

§ 3. *Pulsed field measurements by other investigators.*

Pulsed field measurements of the resistive transition in Nb_3Sn wires have been reported by Cline, Kropschot, Arp, and Wilson[4] and by Hart, Jacobs, Kolbe, and Lawrence[3] while Flippen[6] makes some qualitative remarks about measurements on ribbon type material. In all investigations hairpin samples have been used with H parallel to the long dimension of the hairpin (fig. VII. 1a).

Cline, Kropschot, Arp, and Wilson[4] report a mixed state resistance in 0.5 mm wires. The resistance remains below the normal value up to fields well above 185 kOe. The fields have a pulse duration of about 20 msec. They measured with pulsed currents with a pulse duration that was short in comparison with the duration of the field pulse. They observed that the sample remained superconducting up to a field H_o where the first measurable resistance appeared. In pulsed fields H_o was considerably less than in constant fields. They were not able to extend their measurements to complete saturation.

Hart, Jacobs, Kolbe, and Lawrence[3] measured the resistive transition of 0.25 mm wires. Their field duration was 18 msec., their maximum field 198 kOe. They observed gradual or sharp transitions in identical experiments. The gradual transition tended to occur more frequently if the field rise time was decreased. These gradual transitions do not give an accurate criterion for the field strength H_o where the resistance starts to be significantly different from zero. The gradual transition looks somewhat similar to our observations on ribbon type Nb_3Sn but the resistance in the neighbourhood of the transition field is much smaller than in our case. The authors do not report on the saturation behaviour of the wires.

Weyl and Dietrich[5] studied the decrease of the magnetic field H_o that causes a significant resistance in Nb 40 % Ti, Nb 80 % Ti, and Nb 25 % Ti with pulsed currents as well as with pulsed fields. The field rise times ranged between 0.15 and 2.2 msec. They noted a considerable decrease of H_o at increasing field rates.

Flippen[6] studied the same effect on Nb 25 % Zr wires but with field rise times between 10 and 100 μsec. He noted also the decrease of the critical field for increasing field rates. He made some suggestions on thermal effects as a cause of the phenomena, but he did not obtain a satisfactory explanation.

§ 4. *Sample and sample mounting.*

The measurements have been done on ribbon type Nb_3Sn of make Supercon and RCA and on wire type Nb 25 % Zr make Supercon.

Nb_3Sn. 1. Supercon, type Niostan, $3.18 \times 75 \times 10^{-4}$ mm^2 (Nb_3Sn cross section as stated by the manufacturer). Thickness of the carrier ribbon 10^{-1} mm. This material can be obtained with and without copper plating. Most of our experiments have been done on copper plated samples with the copper layer removed between the voltage contacts by means of abrasive paper. To detect consequences of the removal of the copper layer the results obtained with our standard specimen have been compared with results obtained on copper plated and on non-copper plated material.

2. RCA, type R - 60214, $3.0 \times 64 \times 10^{-4}$ mm^2 (Nb_3Sn cross section as stated by the manufacturer). Thickness of the carrier ribbon 10^{-1} mm. This material has been purchased with silver plating. The silver plating has been removed between the voltage contacts by means of abrasive paper.

Nb 25 % Zr. Supercon, type A 25, 0.25 mm diameter. The material has been purchased with copper plating that has been removed between the voltage contacts by etching.

The Nb_3Sn samples have been mounted in several arrangements to detect the influence of different orientations of the transport current with respect to the external magnetic field. (fig. VII. 1)

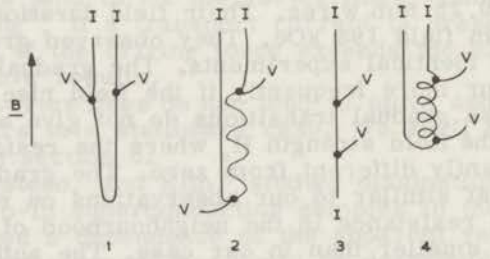

Fig. VII. 1. Sample shapes.
1. Hairpin: Niostan, RCA. 2. Transverse: Niostan.
3. Longitudinal: RCA. 4. Spiral: Nb 25 % Zr.

Most experiments have been made on the hairpin type arrangement. The zigzag arrangement is the best transverse arrangement we could mount in our 5 mm cryostat tail.

§ 5. *Measuring results.*

a. *Nb_3Sn ribbon.*

The transition has been measured for Supercon and for RCA material, with current densities from 2.5 A/mm^2 to 7.5 x 10^2 A/mm^2, calculated for the cross section of the superconducting layer. The pulsed field maximum ranged from 10 to 300 kOe, the temperatures from 1 to 4.2 °K and from 14 to 17°K.

The measurements between 14 and 17°K have been repeated in constant fields up to 80 kOe using the continuous field solenoid in our laboratory[10,11,12].

In fig. VII.2a the transition curves in pulsed fields are given for T = 1 and 4.2°K and for I = 10 A (J = 250 A/mm^2), in fig. VII.2b the transition curves in pulsed and constant fields at 63 A/mm^2 and 14°K.

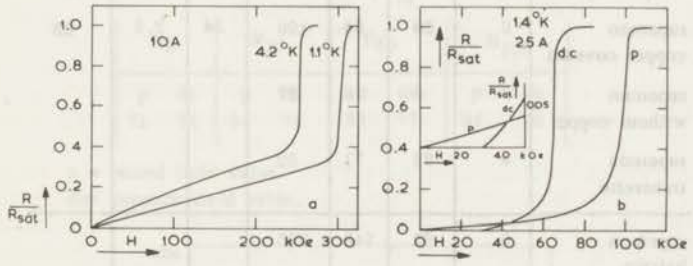

Fig. VII.2. Transition curves for Nb_3Sn ribbon.
a. J = 250 A/mm^2, T = 1 and 4.2°K and pulsed magnetic field.
b. J = 63 A/mm^2, T = 14°K, pulsed(p) and constant(d.c.) magnetic field.

The numerical values are compiled in the tables VII.1 and VII.2. The values indicate the fields where a first significant resistance has been measured (H_o), where 10 % of the resistance has been recovered (H_{10}), respectively 50 % (H_{50}), and 100 % (H_{100}). The values have not been corrected for the carrier resistance. A correction gives that for H_{10} 2 % of the layer resistance has been recovered and for H_{50} 25 %.

The accuracy of H_{10} is poor because the curve in the slowly rising region for low H is flat and small changes in the slope of the curve produce large changes in the transition field. For H_{50} and H_{100} a 10 % accuracy can be assumed.

The results show that the removal of the copper layer does not influence the results up to the field rates which cause eddy currents in the copper layer to obscure other effects.

In fig. VII.3 the temperature dependence of the saturation field is shown for J = 63 A/mm^2 and J = 250 A/mm^2. For clearity straight lines through the high temperature points have been drawn.

TABLE VII.1

sample	H_0 kOe	H_{10} kOe	H_{50} kOe	H_{100} kOe	T °K	I_m Amp	J_m A/mm^2
supercon hairpin	0	0	33	36			
supercon copper covered	0	0	28	40	17	2.5	63
supercon without copper	0	0	25	33			
supercon transverse	0	0	16	26			
supercon hairpin	0	71	88	95			
supercon copper covered	0	69	89	120	14	2.5	63
supercon without copper	0	0	76	87			
supercon transverse	0	28	71	92			
supercon hairpin	0	92	249	275			
supercon copper covered	1)	1)	1)	1)	4	10	250
supercon without copper	6 2)	91	-	-			
RCA hairpin	14 2)	85	188	225			
supercon hairpin	0	116	295	320	1.1	10	250
RCA hairpin	0	0	204	231			

1) Obscured by eddy current effects.
2) Value $\neq 0$ by a few measuring points, causing the average to deviate from zero.

Table VII.2.

1. Nb_3Sn supercon ribbon

I_m Amp	T °K	H_0 kOe		H_{10} kOe		H_{50} kOe		H_{100} kOe	
		p	dc	p	dc	p	dc	p	dc
1	15.5	0	17	35	34	61	42	66	48
2.5	15.5	0	11	32	28	57	37	60	44
1	14	0	38	64	64	93	72	101	81
2.5	14	0	26	71	55	88	65	95	71
5	14	0	15	55	38	86	52	90	64
10	14	0	9	48	23	74	38	81	47

2. Nb 25 % Zr wire. T = 4.2°K; I_m = 1 Amp.; H is given in kOe.

H_0		H_{10}		H_{50}		H_{100}	
p	dc	p	dc	p	dc	p	dc
71	74	84	76	89	77	94	82

p = pulsed field value.
dc= constant field value.

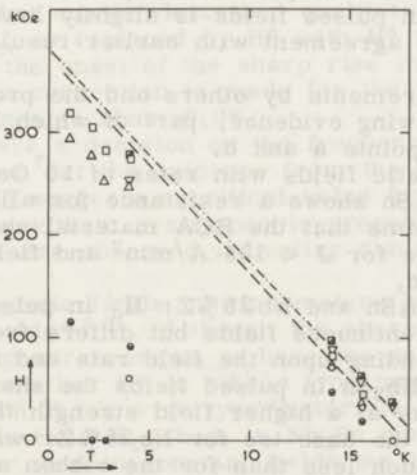

Fig. VII.3. Temperature dependence of H_{100} for Nb_3Sn ribbon.

	H_{10}	H_{50}	H_{100}
2.5 A	O	▽	□
10 A	◒	△	◪

—.—.— straight line through 2.5 A high temp. points.
– – – – straight line through 10 A high temp. points.

The relative shape of the transition curve in a rising field does not depend strongly upon the current density. This excludes Joule heating by the measuring current to be important for $H \ll H_{100}$.

b. *Nb 25% Zr wire.*

The transition has been measured in pulsed and in constant fields at 4.2 °K. The transition curves are shown in fig. VII. 4

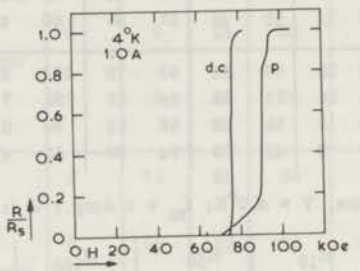

Fig. VII. 4. Transition curves for Nb25%Zr wire at 4.2 °K. p = pulsed field and d.c. = constant field.

The numerical values are given in table VII. 2.
The qualitative behaviour in pulsed and constant fields is the same. The low resistance part of the pulsed field curve is smeared out. H_o in pulsed fields is slightly lower than in constant fields this in agreement with earlier results [5,6].

From the measurements by others and the present author we obtain the following evidence, part of which has already been given in the points a and b.

1. In pulsed magnetic fields with rates of 10^7 Oe/sec and more, ribbon type Nb_3Sn shows a resistance for all field strengths. However, it seems that the RCA material shows a zero resistance range for $J < 125$ A/mm^2 and field rates lower than 10^7 Oe/sec.
2. In wire type Nb_3Sn and Nb 25% Zr H_o in pulsed fields is lower than in continuous fields but differs from zero with an amount depending upon the field rate and the material. [4,6]
3. In ribbon type Nb_3Sn in pulsed fields the sharp rise in the resistance starts at a higher field strength than in constant fields. This is the case too for Nb 25% Zr wire but the difference is much less than for the ribbon sample.
4. In ribbon type Nb_3Sn in pulsed fields the field strength that makes the resistance saturate at its normal value (H_{100}) is much higher than in constant fields. This is also the case for Nb25% Zr wire but the difference is much less than for the ribbon sample. For Nb_3Sn wire this information is not available.

5. In pulsed fields Nb_3Sn ribbon type RCA and Nb 25% Zr show jumps in the voltage over the sample if a transport current is present and $H < H_o$.
6. The phenomena described in the points 1 to 5 were not different for the different orientations with respect to the magnetic field that we used.
7. The possibility of measuring purely inductive pick up is eliminated by the compensation loop, described in chapter V, § 4. The compensation has been adjusted to give a zero signal if a magnetic field was generated with no measuring current present.

§ 6. *Discussion.*

From the evidence given in points 1 to 7 of the preceding section we come to the following assertions.

a. Because of the exclusion of the inductive effects we measure a true resistance. This resistance appears not to depend on the orientation of the sample with respect to the magnetic field. This excludes the driving force on the vortex lines to be caused by the transport current. We assume that the driving force that is caused by the eddy currents induced in the sample by the rising magnetic field brings the sample in a resistive state.
b. In ribbon type Nb_3Sn in pulsed magnetic fields a resistance is observed that can be described qualitatively by equation (VII.3). If H_{c2} is replaced by H* with H* the field strength which marks the onset of the sharp rise in the transition curve and if a correction is made for the resistance of the carrier ribbon a is about 0.06.
We cannot make a decision on the frequency dependence of the phenomenon but the evidence from the RCA material (§ 5, point 1) suggests a critical value for dH/dt below which a range without resistance is present. In this range voltage jumps are observed indicating discrete changes in the material.
c. In pulsed magnetic fields in wire materials H_o is lower than in constant fields [4,5,6]. Although the sharp rise in resistance in ribbons and wires seems to have the same character it is not clear whether H* in ribbon type materials has some connection with H_o in wire type materials.
d. The saturation field H_{100} both in Nb_3Sn ribbon and in Nb25%Zr wire is higher than in constant fields but in Nb_3Sn ribbon the relative effect is larger than in Nb25% Zr wire. We observed that for each material the duration of the sharp transition is largely independent of the pulse height. We noted 3 msec for the duration of the transition in the Supercon material, 2 msec in the RCA material, and 0.5 msec in the Nb 25 % Zr wire. Sometimes the saturation of the

resistance is reached after the maximum of the pulse and in that case these times are longer. This gives strong evidence for a relaxation phenomenon. The quantitative values should be considered with some care because of the small interval of field rates at our disposal.

For a tentative explanation of our observations we consider the rapidly rising external magnetic field. If an external magnetic field is present outside a piece of superconducting material a shielding current flows at the surface of the sample. The magnetic field generated by the shielding current cancels the magnetic field that would be present in the interior of the sample without shielding current. If the current density exceeds the critical current density the surface layer becomes resistive permitting flux to penetrate into the material. In a type II superconductor this flux penetrates in discrete quantities as vortex lines. In the stationary state without transport current an equilibrium density gradient of vortex lines is maintained, due to pinning, keeping the volume currents corresponding to this gradient just subcritical.

For complete shielding the shielding current density J_{sh} is determined by the external magnetic induction B_e by

$$L\, I_{sh} = B_e S$$

with L the self-inductance and S the area of the shielding current (I_{sh}) loop. From this expression one obtains

$$J_{sh} = \frac{B}{\mu_o \lambda} \qquad \text{(VII.5)}$$

supposing that the shielding currents are running in a surface layer of thickness λ. For $B = 0.1$ W/m^2 and $\lambda = 10^{-8}$ m, we obtain $J_{sh} = 8 \times 10^{12}$ A/m^2, exceding the critical current density of Nb_3Sn, J_{cr}, that is of the order of magnitude of 3×10^9 A/m^2 in low magnetic fields. So shielding is not maintained and flux flows into the material with a velocity v_ϕ.

If the external field keeps rising rapidly no equilibrium is established and eddy currents cause a flow of vortex lines. The velocity of the vortex lines can be calculated from the current density:

$$v_\phi = \frac{\rho J}{B} \qquad \text{(VII.6)}$$

Now we take for the resistivity ρ that is generated by the eddy currents the assumption by Strnad, Hempstead, and Kim[9] that it is proportional to the resistivity of the vortex cores, averaged over the total cross section of the sample. The number of vortex lines is taken to be the number that would be present in the material at a flux density B in the stationary state (see section 2).

$$\rho = a \frac{B}{B_{c2}} \rho_n \sim \frac{\xi^2}{d^2} \qquad \text{(VII. 7)}$$

From (VII. 6) and (VII. 7) we obtain:

$$v_\phi = a \rho_n \frac{J}{B_{c2}} \qquad \text{(VII. 8)}$$

It is possible to estimate the vortex line velocity in our experiment in the following way. Suppose we have a ribbon sample consisting of a carrier ribbon of normally conducting material with a superconducting surface layer (fig. VII. 5).

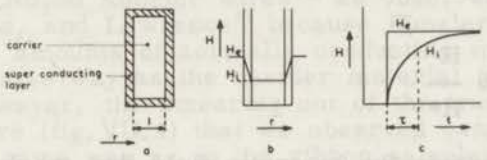

Fig. VII. 5. Geometry and field pattern of ribbon sample.
a. geometry ribbon sample.
b. stationary field distribution for $H_{c1} < H_e < H_{c2}$.
c. assumed response of H_i to square H_e pulse.

We estimate the average vortex line velocity v_ϕ by equating the change of flux in the carrier material to the flux transported by the vortex lines.

The result will be the velocity of the vortex lines that is necessary to maintain the equilibrium field distribution.

$$n \bar{v}_\phi \phi_o = \frac{1}{2} \frac{dB}{dt}$$

giving

$$\bar{v}_\phi = \frac{1}{2B} \frac{dB}{dt} \qquad \text{(VII. 9)}$$

If B is harmonic with frequency ω we obtain

$$\bar{v}_\phi = \tfrac{1}{2} \omega l \operatorname{cotg} \omega t \qquad \text{(VII. 10)}$$

For $t = 0$ this expression diverges but this has no physical significance because at $B = 0$ no vortex lines are present. At a relatively low field larger than the field where the first vortex lines penetrate, e.g. $H_e = H_{max}/400$, and with $\omega = 150$ and $l = 10^{-4}$m we obtain from equation (VII. 8) that a current density of 6×10^9 A/m^2 is necessary to maintain the vortex line velocity of 3 m/sec.

For higher fields v_ϕ decreases rapidly but by the high initial velocities the sample temperature has been increased and the heat flow to the helium bath can be neglected for these short times.

We conclude that in our case everywhere in the sample eddy currents are running with more than the critical current density causing a resistivity and we assume this resistivity to be proportional to the total resistivity of the vortex cores[9]. To explain the observations from our measurements we assume that the transport current experiences this resistance.

In a ribbon sample with the geometry shown in fig. VII.5 the vortex line velocity is high everywhere in the superconducting layer and if a transport current is present a macroscopic resistance is observed. In our experiment we observe a resistance

$$\frac{\rho_s}{\rho_n} = 0.06 \frac{H}{H^*}$$

where H* represents the magnetic field that marks the onset of the sharp rise in the resistance. Thus we have a value 0.06 for a in equation (VII.7) too.

A priori it cannot be said how the transport current experiences resistance caused by the eddy currents and does not run through superconducting short circuits. It is possible to think of a smearing out of the rapidly moving vortices in such a way that 6 % of the core resistance is observed.

In a wire sample in a rapidly rising external magnetic field the vortex line velocity in the inner part of the wire is always small, decreasing to zero in the geometrical center of the wire. Thus the resistive surface layer is short circuited by the inner part of the wire and no macroscopic resistance is observed. The high vortex line velocities manifest themselves by the heat which the corresponding eddy currents produce. This heat makes the sample temperature rise and this explains the decrease of H_o.

The lowering of H_o will be a rising function of the vortex line velocity, thus of $H^{-1}\, dH/dt$, by equation (VII.9). Actually it has been observed by Flippen[6] that H_o is not decreased by increasing H_{max} and thus dH/dt for a constant pulse time but only by decreasing the pulse time i.e. by increasing ω in equation (VII.10) and this is in agreement with the present model.

We did not measure the sample temperature but the temperature rise should be observable. The appearance of voltage jumps (§ 5, point 5) can also be attributed to this heating effect. It would be of interest to measure the sample temperature during the experiment.

The increase of the saturation field H_{100} can be ascribed to a relaxation time τ that would be measured exactly if one used

a square field pulse $H_e > H_{c2}$. The carrier space has to be filled with flux through a magnetically resistive wall giving again the first order differential equation (VII.9) and a relaxation time (fig. VII. 5c)

$$\tau = \frac{1}{2 v_\phi} \qquad \text{(VII.11)}$$

We observed that the sharp transition between H* and H_{100} gives a relaxation time τ of about 1 msec for Supercon ribbon, giving a v_ϕ of 5 cm/sec in the high field region. This is in the same order of magnitude as the velocities in the high field region derivable from equation (VII.10).

The above mechanism can also be used to explain the gradual transition in Nb_3Sn Kunzler wires[13] as observed by Hart, Jacobs, Kolbe, and Lawrence[4] because Kunzler wires always contain large amounts of normally conducting material that acts in the same way as the carrier material in our ribbon samples. However, the smearing out of the transition in the Nb25%Zr wire (fig. VII.4) that we observed cannot be understood in the same way as in the ribbon samples because Nb25%Zr is a homogeneous material and because the transition occurs when in the center of the wire the critical current density is reached. Either the Nb25%Zr wire is not quite homogeneous or there is another mechanism present that we do not understand.

The above mentioned resistance effect should be observable in an experiment in which one measures the resistance of a superconducting tube in an a.c. magnetic field superposed on a d.c. field sufficiently high to bring the sample into the mixed state. It would be of interest to study this effect in more detail experimentally e.g. the dependence on the relative orientation of the magnetic field and the transport current in order to supply data for a theoretical description.

We acknowledge with thanks mr. H. van Beelen for valuable discussions, mr. W. Metselaar for cooperation in the experiments in the constant fields, dr. W. J. Huiskamp for giving us the RCA ribbon material, and Supercon, inc. for giving us the Supercon ribbon material.

References.

1. J.C.A. van der Sluijs, H.R. de Beun, B.A. Zweers, and D. de Klerk, Bull. Belg. Phys. Soc. V, no 2-3, (1966), 165.
2. J.C.A. van der Sluijs, H.R. de Beun, B.A. Zweers, and D. de Klerk, Proceedings of the conference on high magnetic fields, Grenoble, 1966, 429.
3. H.R. Hart, I.S. Jacobs, C.L. Kolbe, and P.E. Lawrence, High magnetic fields, New York, 1961, p. 584.

4. D.Cline, R.H.Kropschot, V.Arp, and J.H.Wilson, High magnetic fields, New York, 1961, p.580.
5. R.Weyl and I.Dietrich, Phys.Lett. 18 (1965), 96.
6. R.B.Flippen, Phys.Rev. 137 (1965), A 1822.
7. P.G.de Gennes, Superconductivity of metals and alloys, New York 1966.
8. B.Goodman, Rep.Progress in Phys. 29 (1966), 445.
9. A.R.Strnad, C.F.Hempstead, and Y.B.Kim, Phys.Rev.Lett. 13 (1964), 794.
10. D.de Klerk, High magnetic fields, New York, 1961, p.412.
11. D.de Klerk, The construction of electromagnets, Newport Pagnell 1965.
12. W.Metselaar and D.de Klerk, Proceedings of the conference on high magnetic fields, Grenoble, 1966, 79.
13. J.E.Kunzler, Rev.Mod.Phys. 33 (1961), 501.

SAMENVATTING.

In dit proefschrift geven wij een beschrijving van een opstelling voor het opwekken van sterke gepulste magneetvelden, en enige experimenten, die wij in deze magneetvelden hebben gedaan.

Wij hebben magneetvelden opgewekt met een maximum van 420 kOe in een ruimte van enkele kubieke centimeters. De vorm van de puls als functie van de tijd is ongeveer een halve sinus met een pulsduur van 20 msec.

Naast de besturing van een installatie met een energie van 180 kJoule (hoofdstuk IV) vormt de constructie van de magneetspoelen een interessant probleem (hoofdstukken II en III).

Het thermische gedrag van de pulsmagneten kan vrij goed kwantitatief beschreven worden, hoewel het opstellen van een volledige energie-balans voor hoge velden niet meer mogelijk is. Bij hoge velden wordt een aanmerkelijk deel van de energie gebruikt voor de elastische en plastische deformatie van de pulsmagneet. De deformatie is niet te voorspellen bij gebrek aan kwantitatieve gegevens over de mechanische eigenschappen van de spoelmaterialen. Uit de experimentele bepaling van het rendement volgt een schatting van de genoemde deformatie energie (hoofdstuk II, § 2 en 3).

De analyse van de krachten in een pulsmagneet toont aan, dat een stationaire benadering slechts tot matige veldsterkte is toegestaan. Een demonstratie van dynamische effecten is gegeven (hoofdstuk II, § 7).

De gebruikelijke berekening van de statische krachten in een pulsmagneet is gebaseerd op het behandelen van de randvoorwaarden met het principe van Saint Venant. Wij bespreken de toepasbaarheid van dit principe bij berekeningen aan magneetspoelen met in de practijk gebruikelijke afmetingen. Wij geven, door hetzelfde principe op een iets andere manier te gebruiken, een analyse, die, behalve met de normale spanningen, die doorgaans uitgerekend worden, ook met de torsiespanning rekening houdt en het blijkt dat deze in sommige gevallen niet verwaarloosbaar is.

In de verkregen magneetvelden onderzochten wij de faseovergang van antiferromagnetisme naar paramagnetisme aan een poederpreparaat van $CuCl_2.2H_2O$ (hoofdstuk VI) en de weerstandsovergang van de harde supergeleider Nb_3Sn in bandvorm (hoofdstuk VII).

De resultaten verkregen aan $CuCl_2.2H_2O$-poeder tonen aan, dat de bestaande berekeningen over $CuCl_2.2H_2O$ en verwante materialen bij deze veldsterkten geen goede benadering van de verschijnselen geven. Als mogelijke oorzaak geven wij aan, dat de kristalconstanten onder invloed van het magneetveld zouden kunnen veranderen, hetgeen aanleiding geeft tot een veldafhankelijke exchange constante. De waarnemingen geven een

aanwijzing ten gunste van deze veldafhankelijkheid.

De verschijnselen die wij gemeten hebben in het Nb_3Sn-band kunnen worden toegeschreven aan warmteproductie en relaxatie-effecten. Wij geven een eenvoudig model aan, dat de verschijnselen kwalitatief goed beschrijft. Een bezwaar van het model is, dat het moeilijk tot vergelijkbare verschijnselen in homogene draadmaterialen kan worden uitgebreid.

Hoofdstuk V geeft een algemeen overzicht van de tot dusverre ontwikkelde meetmethoden in pulsvelden met een literatuur overzicht en een analyse van de specifieke problemen die optreden bij het gebruik van meetmethoden met lage meetfrequentie in pulsvelden.

Teneinde te voldoen aan het verzoek van de Faculteit der Wiskunde en Natuurwetenschappen volgt hieronder een overzicht van mijn studie.

Na de lagere school in mijn geboorteplaats te hebben bezocht, volgde ik het onderwijs aan het Christelijk Lyceum te Zwolle. Deze periode beëindigde ik in 1953 met het afleggen van het eindexamen gymnasium β. Daarna studeerde ik aan de afdeling Natuurkunde van de Technische Hogeschool te Delft. Deze studie werd mogelijk gemaakt onder meer door de hulp van ir. W. H. Oosten. Het voor het ingenieursexamen vereiste wetenschappelijke onderzoek deed ik onder leiding van professor dr B. S. Blaisse, en wel over de dubbele breking van helium kristallen. Het onderzoek leidde tot een mededeling op het congres over de natuurkunde in het gebied van de lage temperaturen, dat in 1960 in Toronto werd gehouden. Gedurende het laatste jaar van mijn studie genoot ik een toelage van het Delfts Hogeschool Fonds.

Sinds 1960 ben ik aan het Kamerlingh Onnes Laboratorium verbonden geweest, en wel als wetenschappelijk medewerker van de Stichting voor Fundamenteel Onderzoek van de Materie. In deze tijd construeerde ik de in dit proefschrift beschreven apparatuur en maakte ik een begin met onderzoekingen met behulp van deze apparatuur. De stootstroomgenerator kwam tot stand in samenwerking met de firma's N. V. Philips Gloeilampenfabrieken, te Eindhoven, N. V. de Nederlandse Siemensmaatschappij, te Den Haag, N. V. Willem Smit Transformatorenfabrieken, te Nijmegen, en N. V. Gebroeders van Swaaij, te Den Haag. De laatste firma verzorgde het contact met de leverancier van de condensatoren, E. Haefely, A. G., te Basel. In het bijzonder spreek ik mijn erkentelijkheid uit voor de adviezen, die ik ontving van de heren ir G. Hess, van Philips, ir J. Lisser, van Smit, en de heer W. A. Hansen, van de Rijksgebouwendienst.

Het contact met de firma van Swaaij leidde tot een bezoek aan de firma's Haefely te Basel en Oerlikon te Zürich over eventuele aankopen.

Over de resultaten van het werk heb ik gerapporteerd op de conferenties over sterke magneetvelden in Cambridge (Mass.) in 1961, in Oxford in 1963, in Leuven in 1966 en in Grenoble in 1966. Behalve de mededeling in Oxford werden alle voordrachten gepubliceerd. In 1967 werd een korte mededeling in Physics Letters gepubliceerd.

Gedurende de curcus 1962 - 1963 assisteerde ik dr J. C. Verstelle bij de leiding van het electronisch practicum. Van 1963 tot 1967 nam ik een gedeelte van het college van dr D. de Klerk waar, over vectoranalyse en over de toepassing van de complexe rekenmethode bij het analyseren van eenvoudige wisselstroomnetwerken. Over de stof nam ik tentamens af.

Een belangrijke bijdrage tot het onderzoek vormde het regelmatig contact met dr D. de Klerk. Van veel nut waren ook de discussies in onze werkgroep, met name met dr S. H. Goedemoed.

Assistentie werd verleend door drs H.R.de Beun, drs J.B.Ubbink en de heren M.Lebret, B.A.Zweers en A.K.Boerema, candidaten in de Natuurkunde. De technische medewerking werd gegeven door de heren J.Dunsbergen, T.Oosterbaan, P.van Ieperen en de hoofden van de werkplaatsen, onder wie ik met name de heren H.M.Nater, J.M.Verbeek en E.S.Prins noem. Het benodigde glaswerk werd vervaardigd onder leiding van de heren A.R.B.Gerritsen en C.J.van Klink, terwijl ook in het algemeen de medewerking, die ik ondervond van de dames en heren van de wetenschappelijke, technische, administratieve en huishoudelijke staf van het Kamerlingh Onnes Laboratorium genoemd moet worden.

De tekeningen werden verzorgd door de heer W.F.Tegelaar. De engelse tekst werd gecorrigeerd door dr T.W.Spriggs en mevrouw F.Janson-Oosterhagen.

STELLINGEN,
behorende bij het proefschrift van J.C.A. van der Sluijs.

1. In de artikelen van Kuznetsov en van Hord worden bij de berekening van de mechanische spanningen in magneetspoelen van gebruikelijke afmetingen de gevolgen van de toepassing van het principe van Saint Venant ten onrechte niet besproken.

   A.A. Kuznetsov, Zh. Tekhn. Fiz. 30 (1960), 592.
   J.N. Hord, J. Res. Nat. Bur. Stand. 69C (1965), 287.

2. Het verdient aanbeveling in araldiet en verwante impregneerharsen tussen 77°K en kamertemperatuur het dempingsgedrag bij compressie te onderzoeken.

   Dit proefschrift, hoofdstuk II.

3. Hoewel het fasediagram van $CuCl_2.2H_2O$, zoals dit met de theorie van het moleculaire veld wordt berekend, met behulp van één parameter zo kan worden gereduceerd, dat zowel het overgangsveld naar verzadigd paramagnetisme bij temperatuur nul als de Néel temperatuur met het experiment overeenkomen, moet men betwijfelen of deze procedure theoretisch kan worden gemotiveerd.

   Dit proefschrift, hoofdstuk VI.

4. Het abnormale gedrag van supergeleidend niobium-tin band in gepulste magneetvelden moet aan geometrische oorzaken worden toegeschreven.

   R.B. Flippen, Phys. Rev. 137 (1965), A 1822.

5. Het verdient aanbeveling het gedrag van de roosterconstanten van antiferromagnetische stoffen niet alleen als functie van de temperatuur, maar ook als functie van het magneetveld te onderzoeken.

   D.S. Rodbell, L.M. Osika, and P.E. Lawrence, J. appl. Phys. 36 (1965), 666.

6. Het is onjuist om in stoffen met een exchange wisselwerking die veel groter is dan de dipool-dipool wisselwerking aan te nemen, dat het verloop in de tijd van de correlatiefunctie van de fluctuaties van de spins met behulp van een Gauss-functie kan worden beschreven.

   V. Jaccarino, Magnetism II A, ed. Rado and Suhl (1965), p. 335.

7. De vereenvoudigde berekeningen van de viscositeitscoefficient van binaire gasmengsels volgens Strunk, Custead en Stevenson zijn niet alleen minder nauwkeurig, maar ook bewerkelijker dan soortgelijke berekeningen met behulp van de theorie van Chapman en Enskog.

M.R. Strunk, W.G. Custead, and G.L. Stevenson, A.I.Ch.E. Journal, 10 (1964), 483.

8. Bij de berekeningen van Raff over de omzetting van energie van rotatie in energie van translatie in mengsels van waterstof en helium is aan een belangrijke voorwaarde voor het zinvol gebruiken van electronische rekenmachines niet voldaan.

L.M. Raff, J. Chem. Phys. 46 (1967), 520.

9. Aangezien de theorie van Löwdin voor de cohesie van alkali-halogeniden uitgaat van een volledige ionogeen kristal-model, is de toepassing van deze theorie op magnesium-oxyde door Calais, Mansikka, Petterson en Vallin onjuist.

J.L. Calais, K. Mansikka, G. Petterson and J. Vallin, Arkiv för Fysik, 34 (1967), 361.

10. De grondwettelijke aanspraak, die een ieder in Nederland kan maken op bescherming van persoon en goederen, wordt op de openbare weg niet voldoende gehonoreerd. In verband hiermee verdient het aanbeveling het voeren van een preventief gericht verkeersveiligheidsbeleid te overwegen.

De Grondwet, artikel 4.

11. In sommige filosofische beschouwingen van natuurkundigen komen schijnbaar rationele begrippen voor, waarvan de functie analoog is aan een van de functies van het godsbegrip in oudere cultuurvormen.

P.A.M. Dirac, Scientific American, 208 (1963), 53.

12. In de gevolgtrekkingen, die van Buren maakt uit zijn betoog over de toepassing van de filosofie van Wittgenstein op de bijbel gebruikt hij soms stilzwijgend traditioneelkerkelijke argumenten.

P. van Buren, The secular meaning of the gospel, Hfdst. VIII, London, 1965.